

INFORMATION TO USERS

This manuscript has been reproduced from the microfilm master. UMI films the text directly from the original or copy submitted. Thus, some thesis and dissertation copies are in typewriter face, while others may be from any type of computer printer.

The quality of this reproduction is dependent upon the quality of the copy submitted. Broken or indistinct print, colored or poor quality illustrations and photographs, print bleedthrough, substandard margins, and improper alignment can adversely affect reproduction.

In the unlikely event that the author did not send UMI a complete manuscript and there are missing pages, these will be noted. Also, if unauthorized copyright material had to be removed, a note will indicate the deletion.

Oversize materials (e.g., maps, drawings, charts) are reproduced by sectioning the original, beginning at the upper left-hand corner and continuing from left to right in equal sections with small overlaps.

Photographs included in the original manuscript have been reproduced xerographically in this copy. Higher quality 6" x 9" black and white photographic prints are available for any photographs or illustrations appearing in this copy for an additional charge. Contact UMI directly to order.

Bell & Howell Information and Learning
300 North Zeeb Road, Ann Arbor, MI 48106-1346 USA

UMI[®]
800-521-0600

UNIVERSITY OF ALBERTA

**HYBRID COAXIAL CAVITY
DIELECTROMETER**

BY

TIMOTHY BLAYNE REEVES



**A thesis submitted to the Faculty of Graduate Studies and Research in partial fulfillment of
the requirements for the degree of Master of Science.**

DEPARTMENT OF ELECTRICAL AND COMPUTER ENGINEERING

EDMONTON, ALBERTA

FALL, 1999



National Library
of Canada

Acquisitions and
Bibliographic Services

395 Wellington Street
Ottawa ON K1A 0N4
Canada

Bibliothèque nationale
du Canada

Acquisitions et
services bibliographiques

395, rue Wellington
Ottawa ON K1A 0N4
Canada

Your file *Votre référence*

Our file *Notre référence*

The author has granted a non-exclusive licence allowing the National Library of Canada to reproduce, loan, distribute or sell copies of this thesis in microform, paper or electronic formats.

The author retains ownership of the copyright in this thesis. Neither the thesis nor substantial extracts from it may be printed or otherwise reproduced without the author's permission.

L'auteur a accordé une licence non exclusive permettant à la Bibliothèque nationale du Canada de reproduire, prêter, distribuer ou vendre des copies de cette thèse sous la forme de microfiche/film, de reproduction sur papier ou sur format électronique.

L'auteur conserve la propriété du droit d'auteur qui protège cette thèse. Ni la thèse ni des extraits substantiels de celle-ci ne doivent être imprimés ou autrement reproduits sans son autorisation.

0-612-47087-3

UNIVERSITY OF ALBERTA

Library Release Form

NAME OF AUTHOR: TIMOTHY BLAYNE REEVES

TITLE OF THESIS: HYBRID COAXIAL CAVITY DIELECTROMETER

DEGREE: MASTER OF SCIENCE

YEAR THIS DEGREE GRANTED: 1999

Permission is hereby granted to the University of Alberta Library to reproduce single copies of this thesis and to lend or sell such copies for private, scholarly, or scientific research purposes only.

The author reserves all other publication and other rights in association with the copyright in the thesis, and except in hereinbefore provided, neither the thesis nor any substantial portion thereof may be printed or otherwise reproduced in any material form whatever without the author's prior written permission.



3864 Cedar Ridge Road, #1B

Indianapolis, Indiana

46236

Date: July 31, 1999

UNIVERSITY OF ALBERTA

FACULTY OF GRADUATE STUDIES AND RESEARCH

The undersigned certify that they have read, and recommend to the Faculty of Graduate Studies and Research for acceptance, a thesis entitled, Hybrid Coaxial Cavity Dielectrometer submitted by Timothy Blayne Reeves in partial fulfillment of the requirements for the degree of Master of Science in Electrical Engineering.



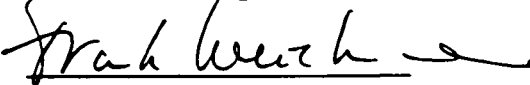
Dr. W.R. Tinga



Dr. F.E. Vermeulen



Dr. D. Routledge



Dr. F. Weichman

Date: April 22, 1999

ABSTRACT

Previously described dielectric measurement techniques that utilize a perturbation technique via a resonant test cavity have a loss tangent measurement range that is limited to two to three orders of magnitude. A new resonant cavity method is presented that extends the loss tangent measurement range to four orders of magnitude, and is suitable for obtaining dielectric data required for curing certain rubber materials whose loss tangents vary by four orders of magnitude.

A modified resonant coaxial cavity has been designed and is used as the test cavity. A quasi-TEM mode, at about 2.45 GHz, is used for measuring the dielectric properties of materials. This method utilizes two measurement modes. One mode, the *contact mode*, is used for measuring the properties of low loss materials, while properties of high loss materials are measured using the *partial contact mode*. In the partial contact mode, a fixed air gap is introduced above the test specimen that reduces resonator sample loading, thereby extending the measurable loss tangent range for lossy dielectrics.

Cavity field solutions are found using a two-dimensional finite difference frequency domain (FDFD) technique. Simulated resonant frequency, Q-factor and loading factor provide data for three theoretical calibration curves that are used for dielectric determination.

An automatic measuring and heating system is implemented that utilizes the test cavity, a reflectometer and an analog controller. The frequency response

of the test cavity is obtained by use of the reflectometer. An analog circuit controls the temperature of the test specimen. A small cylindrical test specimen contained within the resonant cavity can be heated and tested simultaneously via a computer data acquisition program.

The dynamic range for measuring relative dielectric constant is $1.03 < \epsilon_r' < 30$ while for measuring loss tangent the range is $0.0001 < \tan\delta < 1.63$. Uncertainty sources in the dielectric determination are examined. Room temperature complex dielectric constant measurements obtained from a number of commercial materials are compared with the manufacturer's specified data, showing a good agreement between the two. Finally, dielectric properties of five rubber materials were measured from room temperature to 120°C and their complex dielectric constant versus temperature behavior is discussed.

ACKNOWLEDGEMENT

I acknowledge the financial support provided by the Natural Science and Engineering Research Council of Canada and the Department of Electrical Engineering of the University of Alberta.

This project was carried out with excellent support from the machine shop at in the Department of Electrical Engineering. I would also like to thank Andrey Detkov, Jim Fearn and Don Preskarchuk for technical assistance with project software and hardware.

I thank Dr. W.R. Tinga and Dr. F.E. Vermeulen for taking me on as a graduate student. I also thank Dr. D.R. Routledge, Dr. A.M. Robinson and Dr. F. Weichman for serving on the examination committee and reviewing the thesis.

Finally, I am grateful to my family and close friends for their support and encouragement. Their encouragement is especially remembered when my spirits were lowest during the project.

TABLE OF CONTENTS

Chapter 1	INTRODUCTION	1
	1.1 Thesis Objective	1
	1.2 Application	1
	1.3 Thesis Content Overview	2
Chapter 2	THEORETICAL BACKGROUND AND LITERATURE REVIEW	4
	2.1 Introduction	4
	2.2 Theoretical Background	4
	2.3 Literature Review	8
Chapter 3	DIELECTROMETER DESIGN	14
	3.1 Introduction	14
	3.2 Cavity Design	15
	3.2.1 Design Considerations	15
	3.2.2 Design of the Cavity	18
	A. Cavity Radius	18
	B. Inner Conductor Length	19
	C. Plate Separation of the Cylindrical Parallel Plate Waveguide	19
	D. Low Impedance Coaxial Transmission Line	20
	E. Test Specimen Dimensions and Position	21
	F. Coupling Loop	22
	3.3 Temperature Controller Design	22

	3.3.1 Temperature Control Circuit Design	23
	3.4 Reflectometer Interface	24
Chapter 4	DIELECTRIC CONSTANT DETERMINATION USING A FINITE DIFFERENCE FREQUENCY DOMAIN METHOD	26
	4.1 Introduction	26
	4.2 Relating Dielectric Constant to Cavity Field Perturbations	27
	4.3 HERZ Program	29
	4.4 Algorithms for Finding Resonant Frequency and Q-factor of a Circular Cylindrical Resonant Cavity	32
	4.4.1 Algorithm for Calculating Electric and Magnetic Mean Stored Energies	33
	4.4.2 Algorithm for Calculating Power Dissipation	34
	4.5 Grid Structure for the Problem Domain	36
	4.6 A Simple Test of the Algorithm for Finding Resonant Frequency	38
	4.7 Conclusion	40
Chapter 5	MICROWAVE CHARACTERISTICS OF THE EMPTY CAVITY AND LOADED CAVITY	43
	5.1 Introduction	43
	5.2 Cavity Field Solution	43
	5.2.1 Half Wavelength Coaxial Section	44
	5.2.2 Cylindrical Parallel Plate Waveguide Section	44
	5.2.3 Low Impedance Transmission Line and Surrounding Region	45
	5.2.4 Loaded Cavity Field Solution	46

5.3	Empty Cavity Q-factor and Resonant Frequency	54
5.4	Equations for Dielectric Determination	56
5.5	Conclusion	61
Chapter 6	DYNAMIC MEASUREMENT RANGE OF THE DIELECTROMETER	63
6.1	Introduction	63
6.2	Relative Dielectric Constant Measurement Range	63
6.3	Loss Factor or Loss Tangent Measurement Range	65
6.3.1	Minimum Measurable Loss Tangent	65
6.3.2	Maximum Measurable Loss Tangent	68
6.3.3	Discussion	73
6.4	Conclusion	74
Chapter 7	MEASUREMENT PROCEDURES AND RESULTS	75
7.1	Introduction	75
7.2	Measuring Cavity Frequency Response	75
7.2.1	Resonant Frequency and Q-factor Determination	76
7.3	Test Specimen and Dielectrometer Calibration	79
7.3.1	Test specimen size	79
7.3.2	HPBASIC Calibration Programs	79
7.3.3	Dielectrometer Calibration	80
7.4	Verification of Dielectric Measurement Technique	83
7.5	Elevated Temperature Permittivity Measurement Procedure	84
7.6	Elevated Temperature Dielectric Measurements	85

	7.6.1 Cavity Heating and Changes in Empty Cavity Frequency Response	85
	7.6.2 Experimental Results and Discussion	90
	7.7 Conclusions	92
Chapter 8	UNCERTAINTY ANALYSIS OF THE REFLECTOMETER AND EFFECTS ON DIELECTRIC MEASUREMENT ACCURACY	95
	8.1 Introduction	95
	8.2 Analysis of Reflectometer Uncertainty upon the Dielectric Measurement Accuracy	95
	8.2.1 Relative Dielectric Constant Measurement Uncertainty Analysis	95
	8.2.2 Loss Tangent Measurement Uncertainty Analysis	97
	8.3 Overall Effect of Reflectometer Uncertainty on Dielectric Measurement Accuracy	100
	8.4 Conclusions	101
Chapter 9	CONCLUSION	102
	References	106
Appendix 1	THE HERZ SIMULATION PROGRAM	114
	A1.1 HERZ Program	114
Appendix 2	EVALUATION OF Q-MEASUREMENT AND LOSS TANGENT UNCERTAINTY	153
	A2.1 Uncertainty of Measured Q-factor	153
	A2.2 Uncertainties in the Loss Tangent Measurement	157
Appendix 3	MEASUREMENT UNCERTAINTY ATTRIBUTABLE TO THE TEST SPECIMEN AND CAVITY HEATING	163
	A3.1 Variation in Test Specimen Dimensions	163

LIST OF TABLES

Table 4.1	Comparison between analytically calculated and numerically calculated parameters for a resonant empty short-circuited $\frac{\lambda}{2}$ coaxial resonator.	40
Table 5.1	Numerically calculated power dissipation and unloaded Q-factor values for both the unloaded contact and partial contact cavity configurations.	55
Table 5.2	Numerically calculated and measured resonant frequencies for both the unloaded contact and partial contact cavity configurations.	55
Table 5.3	Coefficients of the calibration equations for the contact mode.	57
Table 5.4	Coefficients of the calibration equations for the partial contact mode.	58
Table 6.1	Filling factor as a function of relative dielectric constant for both the contact and partial contact modes.	67
Table 6.2	Loss tangent limits as a function of relative dielectric constant.	73
Table 7.1	Power reflection ratios utilized in calculating cavity Q-factor.	77
Table 7.2	Dielectric data for Eccosorb HiK500 materials measured using the contact mode and dielectric data specified by the manufacturer.	83
Table 7.3	Dielectric data for Eccosorb HiK500 materials measured using the partial contact mode and dielectric data specified by the manufacturer.	83
Table 7.4	Measured room temperature dielectric properties of five Royalene rubber materials.	90
Table 7.5	Chemical constituent levels of each of the five Royalene rubber materials tested.	91
Table 8.1	Uncertainty in measured relative dielectric constant for the contact mode.	97

Table 8.2	Uncertainty in measured relative dielectric constant for the partial contact mode.	97
Table 8.3	Uncertainty in measured loss tangent for the contact mode, as a function of directivity and relative dielectric constant.	98
Table 8.4	Uncertainty in measured loss tangent for the partial contact mode, as a function of directivity and relative dielectric constant.	98
Table 8.5	Uncertainty in measured loss tangent attributable to uncertainty in measured dielectric constant for the contact mode, as a function of directivity and relative dielectric constant.	100
Table 8.6	Uncertainty in measured loss tangent attributable to uncertainty in measured dielectric constant for the partial contact mode, as a function of directivity and relative dielectric constant.	100
Table 8.7	Overall reflectometer uncertainty in the measurement of dielectric constant and loss tangent (contact mode).	101
Table 8.8	Overall reflectometer uncertainty in the measurement of dielectric constant and loss tangent (partial contact mode).	101
Table A3.1	Uncertainty in relative dielectric constant as a function of temperature (per °C), contact mode.	167
Table A3.2	Uncertainty in relative dielectric constant as a function of temperature (per °C), partial contact mode.	167
Table A3.3	Temperature dependent loss tangent measurement uncertainty (per °C) listed as a function of directivity and relative dielectric constant, contact mode.	170
Table A3.4	Temperature dependent loss tangent measurement uncertainty (per °C) listed as a function of directivity and relative dielectric constant, partial contact mode.	170

LIST OF FIGURES

Figure 3.1	Experimental dielectrometer for elevated temperature dielectric measurements.	14
Figure 3.2	Cross-section of the cavity structure of the dielectrometer.	17
Figure 3.3	Circuit schematic for the analog controller.	24
Figure 4.1	The finite difference grid structure used in HERZ.	31
Figure 4.2	A two-dimensional (r, z) plot of the magnitude of the radial electric field distribution, E_r , within a resonant empty short-circuited $\frac{\lambda}{2}$ coaxial cavity.	41
Figure 4.3	A two-dimensional (r, z) plot of the magnitude of the azimuthal magnetic field distribution, H_ϕ , within a resonant empty short-circuited $\frac{\lambda}{2}$ coaxial cavity.	42
Figure 5.1	A two-dimensional (r, z) plot of the magnitude of the radial electric field distribution, E_r , within the empty hybrid coaxial cavity displayed along side a half cavity cross-section.	48
Figure 5.2	A two-dimensional (r, z) plot of the magnitude of the axial electric field distribution, E_z , within the empty hybrid coaxial cavity displayed along side a half cavity cross-section.	49
Figure 5.3	A two-dimensional (r, z) plot of the magnitude of the azimuthal magnetic field distribution, H_ϕ , within the empty hybrid coaxial cavity displayed along side a half cavity cross-section.	50
Figure 5.4	A two dimensional (r, z) plot of the magnitude of the radial electric field distribution, E_r , within the loaded cavity operating in the contact mode containing a material with a relative dielectric constant of $\epsilon_r' = 10$ displayed along side a half cavity cross-section.	51

Figure 5.5	A two dimensional (r, z) plot of the magnitude of the axial electric field distribution, E_z , within the loaded cavity operating in the contact mode containing a material with a relative dielectric constant of $\epsilon_r' = 10$ displayed along side a half cavity cross-section.	52
Figure 5.6	A two dimensional (r, z) plot of the magnitude of the azimuthal magnetic field distribution, H_ϕ , within the loaded cavity operating in the contact mode containing a material with a relative dielectric constant of $\epsilon_r' = 10$ displayed along side a half cavity cross-section.	53
Figure 5.7	Calibration curve for determining relative dielectric constant of a test specimen while the cavity is operated in the contact mode.	58
Figure 5.8	Calibration curve for determining relative dielectric constant of a test specimen while the cavity is operated in the partial contact mode.	59
Figure 5.9	Calibration curve for determining the inverse cavity filling factor while the cavity is operated in the contact mode.	59
Figure 5.10	Calibration curve for determining the inverse cavity filling factor while the cavity is operated in the partial contact mode.	60
Figure 5.11	Calibration curve for determining cavity Q-factor while testing is performed in the contact mode.	60
Figure 5.12	Calibration curve for determining cavity Q-factor while testing is performed in the partial contact mode.	61
Figure 6.1	Relative error in measured Q-factor versus the reflection coefficient, $ \Gamma_0 $, at the resonant frequency for a reflectometer directivity of $D = 30$ and 40 dB.	68
Figure 7.1	Decrease in empty cavity resonant frequency when heating the test cavity from 20°C to 125°C (contact mode).	88
Figure 7.2	Decrease in empty cavity resonant frequency when heating the test cavity from 20°C to 125°C (partial contact mode).	88

Figure 7.3	Decrease in empty cavity Q-factor when heating the test cavity from 20°C to 125°C (contact mode).	89
Figure 7.4	Decrease in empty cavity Q-factor when heating the test cavity from 20°C to 125°C (partial contact mode).	89
Figure 7.5	Measured relative dielectric constants of the Royalene rubber materials, A - E, at 2.45GHz, as functions of temperature.	93
Figure 7.6	Measured loss tangents of the Royalene rubber materials, A -E, at 2.45GHz, as functions of temperature, presented in a semi-log format.	94
Figure A2.1	Relative uncertainty in measured Q-factor versus the bandwidth reflection coefficient, $ \Gamma_{pp} $, for various resonant frequency reflection coefficient values, $ \Gamma_0 $ when reflectometer directivity is $D = 30$ dB.	156
Figure A2.2	Error transfer function, i.e., the relative error in the loss tangent measurement resulting from an error of $\Delta\epsilon_r' = 1.00$ in the measured relative dielectric constant for the contact mode.	161
Figure A2.3	Error transfer function, i.e., the relative error in the loss tangent measurement resulting from an error of $\Delta\epsilon_r' = 1.00$ in the measured relative dielectric constant for the partial contact mode.	161
Figure A3.1	Relative uncertainty in measured dielectric constant for a test specimen with a thickness uncertainty of 0.5% and of radius $r = 5.0$ mm (contact mode).	165
Figure A3.2	Relative uncertainty in measured dielectric constant for a test specimen with a thickness uncertainty of 0.5% and of radius $r = 5.0$ mm (partial contact mode).	165

LIST OF SYMBOLS AND ABBREVIATIONS

a_1, a_2, \dots	polynomial coefficients of the calibration curve for determining the relative dielectric constant (Ch.5)
$a_{i,j}, b_{i,j}, c_{i,j}, d_{i,j}, e_{i,j}$	coefficients of the linear equations used to find field values in the HERZ program
A	cross sectional surface area of a material
A_0	amplitude of the peak axial electric field in the cylindrical parallel plate waveguide
$A_{i,j}, B_{i,j}, C_{i,j}, D_{i,j}, E_{i,j}$	coefficients of the linear equations used to find H'_i in the HERZ program
b_0, b_1, b_2, \dots	polynomial coefficients of the calibration curve for determining filling factor, F_i
B_1	coefficient of the first and second order Bessel function of the first kind for the region outside the dielectric material (Ch.5)
BJT	bipolar junction transistor
c_0, c_1, c_2, \dots	polynomial coefficients of the calibration curve for determining the cavity Q-factor, Q_c
c_D	specific heat of the test material $\left(\frac{J}{g^\circ C} \right)$
C	coupling coefficient of a directional coupler
C_1	coefficient of the first and second order Bessel function of the second kind for the region outside the dielectric test specimen (Ch.5)
CPM	cavity perturbation method
d	gap width; material thickness (Ch.2)
D	directivity of a directional coupler
DUT	device under test

E	electric field intensity
f	frequency
FDFD	finite difference frequency domain
F_i	the ratio of the mean stored electrical energy in the test specimen to that in the cavity, commonly referred to as cavity filling factor
H	magnetic field intensity
H'	product of magnetic field intensity and radial distance
H''	magnetic field intensity at a conductor boundary
HERZ	acronym for <u>H</u>-field, <u>E</u>-field, <u>r</u>-<u>z</u> geometry
i	radial grid block integer number
I	total number of grid block divisions in the radial direction
I₀	TEM current in the coaxial cavity
ISM	industrial, scientific and medical
j	axial grid block integer number
J	total number of grid block divisions in the axial direction
J₀, J₁	the first and second order Bessel function of the first kind
K	Kelvin temperature scale
L	cavity length; inductance (Ch.6)
n	weighting factor
N	total number of grid blocks used in the HERZ program
P_D	power density within the dielectric
P_D	electric power dissipated in a dielectric
P_{in}	input power supplied to heat a dielectric material

Q'	heat generation within a material
Q	quality factor (of empty or loaded cavity)
Q_C	cavity Q-factor resulting from only conductor losses when a perfectly lossless dielectric is situated within the test cavity
Q_D	cavity Q-factor resulting from only the test material's dielectric loss
Q_{EXT}	transmission line Q-factor
Q_L	Q-factor of a loaded cavity
Q_{LC}	Q-factor of loaded cavity along with transmission line feeding the cavity
Q_m	measured Q-factor
Q_0	Q-factor of an empty cavity
Q_w	cavity Q-factor only considering wall losses (Ch.6)
r	radial distance in a cylindrical coordinate system
r_1	radius of center conductor
r_2	radius of outer conductor
r_3	radius of low impedance transmission line
r_4	radius of test specimen
\bar{R}	normalized input resistance
R_D	resistance of dielectric material, Chapter 6
R_s	surface resistivity
RL	return loss in dB
s	second
t	time; thickness

$\tan \delta$	loss tangent, i.e. $\frac{\epsilon'}{\epsilon''}$
T	temperature
TE	transverse electric
TEM	transverse electromagnetic
TM	transverse magnetic
V	voltage
V_C	cavity volume
V_D	test specimen volume
V_{therm}	voltage corresponding to test material plate temperature
W	power (Watts)
W_D	total mean electric energy stored in a dielectric
W_E	total mean electric energy stored in a cavity
W_M	total mean magnetic energy stored in a cavity
x	optimum power reflection ratio (Ch.7)
Y_0, Y_1	the first and the second order Bessel function of the second kind
z	axial position in a cylindrical coordinate system
Z	impedance
Z_{in}	input impedance of the transmission line
Z_L	impedance of an external load connected to a transmission line
Z_0	characteristic impedance of a transmission line
α	bandwidth parameter (Ch.7)
β	axial wave number

Δf	bandwidth
Δf_0	cavity resonant frequency shift resulting from test specimen insertion
ΔQ_0	variation in the cavity Q-factor resulting from test specimen insertion
$\Delta\left(\frac{1}{Q_0}\right)$	variation in the inverse of the cavity Q-factor resulting from test material insertion
Δr	radial width of a grid block in the HERZ program
Δz	axial length of a grid block in the HERZ program
ϵ^*	complex relative dielectric constant or permittivity of a material
ϵ'	dielectric constant or permittivity of a material
ϵ''	loss factor of a dielectric material
ϵ_r'	relative dielectric constant of a material
ϵ_r''	relative loss factor of a material
ϵ_0	permittivity of free space ($\approx 8.85 \times 10^{-12}$ F/m)
ϕ	angle in a cylindrical coordinate system
Γ	(amplitude of) reflection coefficient
η_0	intrinsic impedance of free space 377Ω
κ	thermal conductivity of a material
λ	wavelength
λ_0	resonant wavelength
μ	permeability
μ_0	permeability of free space ($4\pi \times 10^{-7}$ A/m)
ρ_D	material density

σ	electrical conductivity
Ω	$\omega + j\frac{\omega}{2Q}$, complex resonant frequency; ohms
ω	angular frequency
ζ	error transfer function (Appendix 2)

CHAPTER 1

INTRODUCTION

1.1 Thesis Objective

Knowledge of a material's dielectric properties is required in order to design and to control its microwave heating process within a given temperature and frequency range. The material's dielectric properties are measured with a dielectrometer. With the addition of heating hardware, the dielectrometer can also be used for controlling the temperature of the test specimen and hence can be used for determining dielectric properties of a material as a function of both frequency and temperature.

This thesis is devoted to designing a dielectrometer that has an extended dielectric loss measurement range. The dielectrometer will be used to measure the dielectric properties of high loss uncured rubber sheets that are commercially cured using a microwave heating process.

1.2 Application

The use of microwaves to cure rubber has greatly increased during the past 30 years. Microwave energy is used to cure hundreds of millions of pounds of rubber a year [1]. The merits of this process are a fast curing time, an enhanced rubber product and an efficient curing process [1-3].

1.3 Thesis Content Overview

Chapter 2 begins with a brief summary of the subject of material heating via microwave energy. Then, a literature review is presented that describes a number of dielectric measurement techniques.

In Chapter 3 an outline of the dielectrometer design constraints is given. The resonant cavity design follows and then the design of the heater is described. Finally, the interface between the reflectometer and the resonant cavity is described.

In Chapter 4 the procedure for determining a material's complex dielectric constant with the dielectrometer is given. First the perturbation technique for a dielectrically loaded resonant cavity is described. Then, an analytical relationship between the complex dielectric constant of a test specimen and the change in the cavity's resonant frequency and Q-factor is developed. A finite difference frequency domain (FDFD) method is introduced to numerically calculate the empty and loaded cavity's electric and magnetic fields, and to determine a test specimen's complex dielectric constant.

In Chapter 5 the microwave characteristics of the empty and loaded cavities are described, including field configurations and a comparison of the measured and simulated resonant frequencies for the two modes of cavity operation. Then, numerically calculated calibration curves for determining a material's complex dielectric constant are given in both a graphical and a polynomial format.

In Chapter 6 the limits of the dynamic range of the dielectrometer are evaluated. Their dependence upon measurement sensitivity and accuracy of test equipment is described.

In Chapter 7 a description of the algorithms used in the data acquisition computer program are given. Calibration and measurement procedures are described. Measured dielectric properties of four commercial materials are tabulated alongside the manufacturer's specified values in order to verify the dielectric measurement method proposed. Finally, new dielectric data for five Royalene rubber materials is presented and discussed.

In Chapter 8 the measurement accuracy of the reflectometer is analyzed in order to predict uncertainty in the dielectric measurements.

Relevant conclusions are presented in Chapter 9. The limitations of the dielectrometer that has been developed are discussed and suggestions for improvements are made.

CHAPTER 2

THEORETICAL BACKGROUND AND LITERATURE REVIEW

2.1 Introduction

In this chapter the theory for microwave heating is presented. A literature review is then necessary so as to determine an appropriate method of measuring the dielectric properties of the rubber sheets. A number of dielectric measurement techniques are described.

2.2 Theoretical Background

In the literature a great deal of work has been reported in regard to deriving heating rate models for materials heated via microwave energy at both the macroscopic and microscopic levels [4-5]. An introduction to the subject of microwave heating of materials is given at the macroscopic level. To this end, the power dissipation, P_D , corresponding to an electric field intensity, E_i , along with a dielectric material's complex dielectric constant, $\epsilon^* = \epsilon' - j\epsilon''$, are related to the total input microwave power, P_{inv} corresponding to an electric field intensity, E_0 , delivered to the dielectric material.

The time rate of temperature change of a material is calculated using the heat conduction equation [5] given by

$$\frac{\partial T}{\partial t} = \frac{1}{C\rho}(Q' + \kappa\nabla^2 T) \quad (2.1)$$

where T is temperature ($^{\circ}\text{C}$), t is time (s), Q' is the heat generation term ($\text{W}\cdot\text{m}^{-3}$), ρ is the material density ($\text{kg}\cdot\text{m}^{-3}$), C is its specific heat ($\text{J}\cdot\text{kg}^{-1}\cdot^{\circ}\text{C}^{-1}$) and κ is the material's thermal conductivity ($\text{J}\cdot(\text{m}\cdot\text{s})^{-1}\cdot^{\circ}\text{C}^{-1}$). Assuming a uniform temperature profile throughout the heated material, the following simplification can be made

$$\kappa\nabla^2 T = 0 \quad (2.2)$$

and Eq. (2.1) can be re-written as

$$\frac{dT}{dt} = \frac{Q'}{C\rho} \quad (2.3)$$

In the case of microwave heating of a material, Q' represents the internal heat generation at a point. For non-magnetic materials, the time-average power dissipated in a material volume, V , resulting from molecular mass mechanisms [4] is given by

$$P_D = \frac{1}{2} \int_V \mathbf{E}_i \cdot \mathbf{J} \, dV = \frac{1}{2} \int_V \sigma |\mathbf{E}_i|^2 \, dV = \frac{1}{2} \int_V \omega \varepsilon'' |\mathbf{E}_i|^2 \, dV \quad (2.4)$$

where $E_i = E_i(x, y, z, f, \varepsilon^*)$ is the peak electric field at the point of interest and σ and ε'' are the total effective conductivity and loss factor respectively and $\omega = 2\pi f$. Re-writing Eq.(2.4) in point form gives the time average power density at a point as

$$\frac{dP_D}{dV_D} = p_D = \frac{1}{2} \omega \varepsilon'' |\mathbf{E}_i|^2 \quad (2.5)$$

which, incidentally, represents the internal heat generation term described previously, i.e., $Q' = \frac{dP_D}{dV_D}$.

Now, Eq.(2.3) can be re-written in terms of the electric field intensity, E_i , within the material and its complex dielectric constant, $\epsilon' - j\epsilon''$, i.e.

$$\frac{dT}{dt} = \frac{1}{C_D \rho_D} \left((\pi f) \epsilon'' |E_i|^2 \right) = \frac{1}{C_D \rho_D} \left((\pi f) \epsilon' (\tan \delta) |E_i|^2 \right) \quad (2.6)$$

where $\tan \delta = \frac{\epsilon''}{\epsilon'}$.

The electric field intensity, E_i , within a material is not explicitly known. For simple material shapes, E_i is found using the value of the material's relative dielectric constant, ϵ_r' , along with either the known electric field, E_0 , of the incident wave striking the material interface or the corresponding input microwave power, P_{in} . Some simple cases that relate these quantities are outlined. If the electric field, E_0 , strikes parallel to the interface, the electric field, E_i , inside the material is given by [8]

$$E_i = \frac{2}{1 + \sqrt{\epsilon_r'}} E_0 \quad (2.7).$$

Conversely if the electric field, E_0 , is perpendicular to the interface, then the electric field, E_i , is [8]

$$E_i = \frac{1}{\sqrt{\epsilon_r'}} E_0 \quad (2.8).$$

For the case when a uniform plane wave is propagating in an infinite, lossless material, the input power, P_{in} , and electric field intensity, E_i , are related by [9]

$$|E_i|^2 = \frac{2\eta_0 P_{in}}{A\sqrt{\epsilon_r'}} \quad (2.9)$$

where A is the cross-sectional area transverse to the direction of propagation, η_0 is the free space wave impedance ($\eta_0 = 377\Omega$), and P_{in} is the total power in Watts delivered through area A , into a volume of material of thickness, d . In practice the assumption can be made that a finite lossy material with volume Ad retains a near uniform electric field intensity, E_i . Re-writing Eq.(2.6) utilizing Eq. (2.9) results in

$$\frac{dT}{dt} = \frac{2\pi f \eta_0 \epsilon_0}{A} \frac{\epsilon''(T)P_{in}}{C_D(T)\rho_D(T)\sqrt{\epsilon_r'}} \quad (2.10)$$

where ϵ_0 is the permittivity of free space ($\approx 8.85 \times 10^{-12}$ F/m).

For the general case, the electric field intensity, E_i , within a material is found from the Helmholtz equation [8]

$$\nabla^2 E_i + \omega\mu\epsilon^* E_i = 0 \quad (2.11)$$

where μ is the material's permeability. In this equation, the complex dielectric constant, ϵ^* , is the only parameter that describes the electric behavior of the material. Apparently in order to solve Eq.(2.11) and hence Eq.(2.6), the temperature dependent dielectric properties of a material are required. These quantities are only found via measurement within a given temperature and frequency range.

For this thesis project, the dielectric measurement technique utilized must meet the following conditions. Complex dielectric constant must be measured at a frequency of $f_0 = 2.45$ GHz. The temperature range of interest is $20\text{ }^\circ\text{C} < T < 120\text{ }^\circ\text{C}$. Loss tangents of the materials vary between $0.001 \leq \tan \delta \leq 1.0$, while their relative dielectric constants vary between $3.0 < \epsilon_r' < 30.0$. Test material thickness is $t \approx 2.0$ mm.

2.3 Literature Review

Since the late 1940's a large number of dielectric measurement techniques have been developed. Short and open circuited waveguide techniques are used for measuring a material's dielectric properties over a wide range of frequencies [10-13]. Many scientists have used various cavity perturbation techniques for testing relatively small test specimens with a large range of loss tangents and dielectric constants [14-31]. At millimeter and sub-millimeter wavelengths, open resonators are utilized for measuring dielectric properties of materials used in ray-optic applications [32-33]. Open-ended coaxial probes are commonly used in broadband dielectric measurements of liquids [34-42].

One of the earliest developed and most practical dielectric measurement methods is the short circuited waveguide technique [10-11, 43]. In this method, a material completely fills a short-circuited section of waveguide and the material's dielectric properties are determined from the loaded waveguide's

measured complex reflection coefficient. One of the requirements of this method is that the test specimen thickness must be approximately $t \approx \frac{\lambda}{4}$, where λ is the wavelength of the microwave test signal fed to the loaded waveguide [43]. Utilizing this technique, a large range of loss tangents, $0.001 \leq \tan \delta \leq 1.0$ and relative dielectric constants, $2.00 \leq \epsilon_r' \leq 100.0$, can be measured over a broad range of temperatures $20^\circ\text{C} < T < 500^\circ\text{C}$ and frequencies, $0.30 \text{ GHz} < f < 24.0 \text{ GHz}$. Von Hippel characterized the dielectric properties of many materials as a function of frequency and temperature utilizing this technique [10].

An open circuited waveguide is used for measuring the dielectric properties of a material completely covering the open and flanged end of a waveguide. Complex dielectric constant of a material is found from the measured input admittance of the waveguide [12-13]. As with the short-circuited waveguide method, a large range of loss tangents, $0.001 \leq \tan \delta \leq 1.0$ and relative dielectric constants, $2.00 \leq \epsilon_r' \leq 100.0$ can be measured over a broad range of frequencies, $0.30 \text{ GHz} < f < 24.0 \text{ GHz}$.

At the Industrial, Scientific and Medical (ISM) frequencies of $f = 915 \text{ MHz}$ and $f = 2450 \text{ MHz}$, relatively large test specimens are required if either a short or open circuit waveguide dielectric measurement technique is employed. Comparable measurement results are achieved utilizing a resonant cavity perturbation technique that requires a much smaller test specimen [14-31]. For this technique, the dielectric properties of a test specimen are determined by

measuring the changes in the resonant cavity's resonant frequency and Q-factor after test specimen insertion into the resonant cavity [14-31].

Many different implementations of the cavity perturbation technique have been reported [14-31]. Some implementations offer the advantage of the resonant cavity being used for both heating the test specimen at a particular cavity resonant frequency or mode while being used to measure the specimen's dielectric properties at a second cavity resonant frequency or mode [17-19, 22, 23, 28]. This has the advantage of maintaining the resonant cavity at room temperature while heating the test specimen to high temperatures thus achieving quite favorable accuracy in the dielectric measurements [17-19, 22, 23, 28].

Utilizing the cavity perturbation technique, a loss tangent and dielectric constant measurement range that covers two orders of magnitude is achieved [14-31]. The dielectric constant measurement range is limited by the perturbation condition that states the relative shift in the cavity's resonant frequency can not exceed $\left| \frac{\Delta f_0}{f_0} \right| < 1\%$. For resonant frequency shifts that exceed $\left| \frac{\Delta f_0}{f_0} \right| > 1\%$, the perturbation formula breaks down when determining a test specimen's relative dielectric constant. Loss tangent measurement range is limited to two orders of magnitude since Q-factor measurement uncertainty at both the minimum and maximum measurable loss tangent values approaches critical values [8].

At millimeter and sub-millimeter wavelengths the physical size and Q-factor of a resonant cavity operating in a low order mode may be too small to be

useful [44]. One way to avoid these difficulties is to remove the sidewalls of a cavity resonator thus leaving two parallel metal plates [32-33, 44]. A more stable configuration utilizes either spherical or parabolic-shaped reflecting mirrors to focus and confine the energy to a stable mode pattern.

One common application of these devices is dielectric measurements of materials at optical frequencies. For this measurement method, a dielectric specimen is placed at the location, between the two mirrors where the beam-width of the microwave signal is minimum. A material's dielectric properties are found by using ray-optic analysis where the measured changes in the resonator's resonant frequency and Q-factor are again utilized along with the measured mirror separation and radius of curvature of the mirrors used [32-33]. This method is used for finding the dielectric properties of low loss dielectric materials used in both short-millimeter wave circuit components and quasi-optical elements such as windows, lenses, beam-splitters and substrates. Low loss measurements of $\tan\delta \approx 5 \times 10^{-6}$ have been reported for these devices [33]. Afsar et al. [32] reported a loss tangent measurement range of $5 \times 10^{-5} < \tan\delta < 1.36 \times 10^{-3}$. An upper loss tangent value of $\tan\delta \approx 0.01$ should be achievable using an open resonator.

Although cavity perturbation techniques are used for measuring the dielectric properties of high loss liquids [8, 16], an open coaxial probe technique permits measurement of a liquid's dielectric properties over a broadband of frequencies and the test setup required is quite simple [34-42]. An open-ended

probe consists of a truncated section of coaxial line, with an optional extension of a ground plane [42]. In this method, the material under test is placed flush with the probe and values of the complex permittivity are then determined from the measurement of the input impedance of the probe [42]. One critical criterion for this technique is that good contact between the probe and the material under test is maintained [42]. In the literature relative loss factor measurement ranges of $0.1 < \epsilon_r'' < 250$ and relative dielectric constant measurement ranges of $2.0 < \epsilon_r' < 110$ have been reported utilizing this technique [34-42]. One drawback of this technique is that it does not provide accurate results for low permittivity and low loss materials [36].

The short-circuit waveguide, the open-circuit waveguide, open resonator and open coaxial probe dielectric measurement techniques are not suitable for our problem based upon the following reasoning. For the short-circuited waveguide technique, a relatively large test specimen volume is required at a frequency of $f_0 = 2.45$ GHz. In addition, the test specimen has to be machined to precisely fit the waveguide. Neither of these requirements is practical. Major foreseeable problems with an open waveguide technique include maintaining a uniform waveguide to test specimen contact and a uniform temperature profile throughout the test specimen volume when heated. At a frequency of $f_0 = 2.45$ GHz, the required physical size of an open resonator and test specimen makes it impractical to pursue this type of dielectric measurement technique. A major drawback of the open ended coaxial probe technique is that when the probe is

heated the outer conductor of the coaxial probe heats faster than the inner conductor [42]. This causes the outer conductor to expand more than the inner conductor, producing an air gap between the inner conductor and a solid material under test [42]. This air gap can lead to errors as high as 300% in the relative loss factor measurement [42].

Instead, a cavity perturbation technique is selected to fulfill the measurement requirements of this project. This technique is very conducive to performing dielectric measurements at a frequency of $f_0 = 2.45$ GHz. All of the conditions outlined at the beginning of this section, apart from the loss tangent measurement range, are achievable using a standard cavity perturbation technique. With test equipment available the measurement and data acquisition process are easily automated permitting good repeatability in measured results if "averaging" techniques are utilized. Using a cavity perturbation technique allows for a uniform temperature profile to be maintained throughout a small test specimen. The only major technical issue to overcome is extending the loss tangent measurement range beyond two orders of magnitude. In the following chapters, the design, simulated and measured operation of a resonant cavity that has a loss tangent measurement range that covers four orders of magnitude is described.

CHAPTER 3

DIELECTROMETER DESIGN

3.1 Introduction

In order to make elevated temperature dielectric measurements, an experimental dielectrometer was implemented as shown in the block diagram of Figure 3.1. The reflectometer measures the frequency response of the test cavity at approximately 2.45 GHz. The temperature of the cavity and test specimen was monitored by two thermocouples. The heater, consisting of two power resistors controlled by an analog temperature controller, was used to heat the insulated cavity and test specimen.

Design details of this dielectrometer consisting of a hybrid coaxial cavity, a reflectometer, a temperature controlled heater and thermometer are presented.

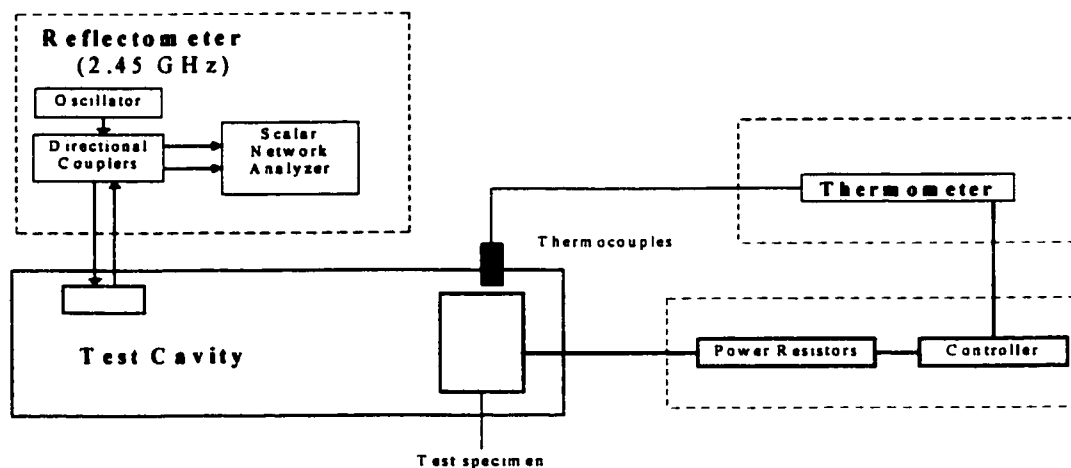


Figure 3.1 Experimental dielectrometer for elevated temperature dielectric measurements.

3.2 Cavity Design

3.2.1 Design Considerations

Four technical criteria must be met by the design of this test cavity. First, the resonant frequency of this cavity is $f_0 \approx 2.45$ GHz. Second, the magnitude of the unloaded cavity Q-factor must be large enough to allow for adequate loss tangent measurement resolution. Third, in order to achieve maximum frequency sensitivity to load variation, the test specimen must be placed in a strong electric field region. Finally, since any dielectric loading of the test cavity degrades its input impedance match, the input impedance of the empty test cavity must be well matched to its feed line so as to realize a loss tangent measurement range of $0.001 \leq \tan \delta \leq 1.0$.

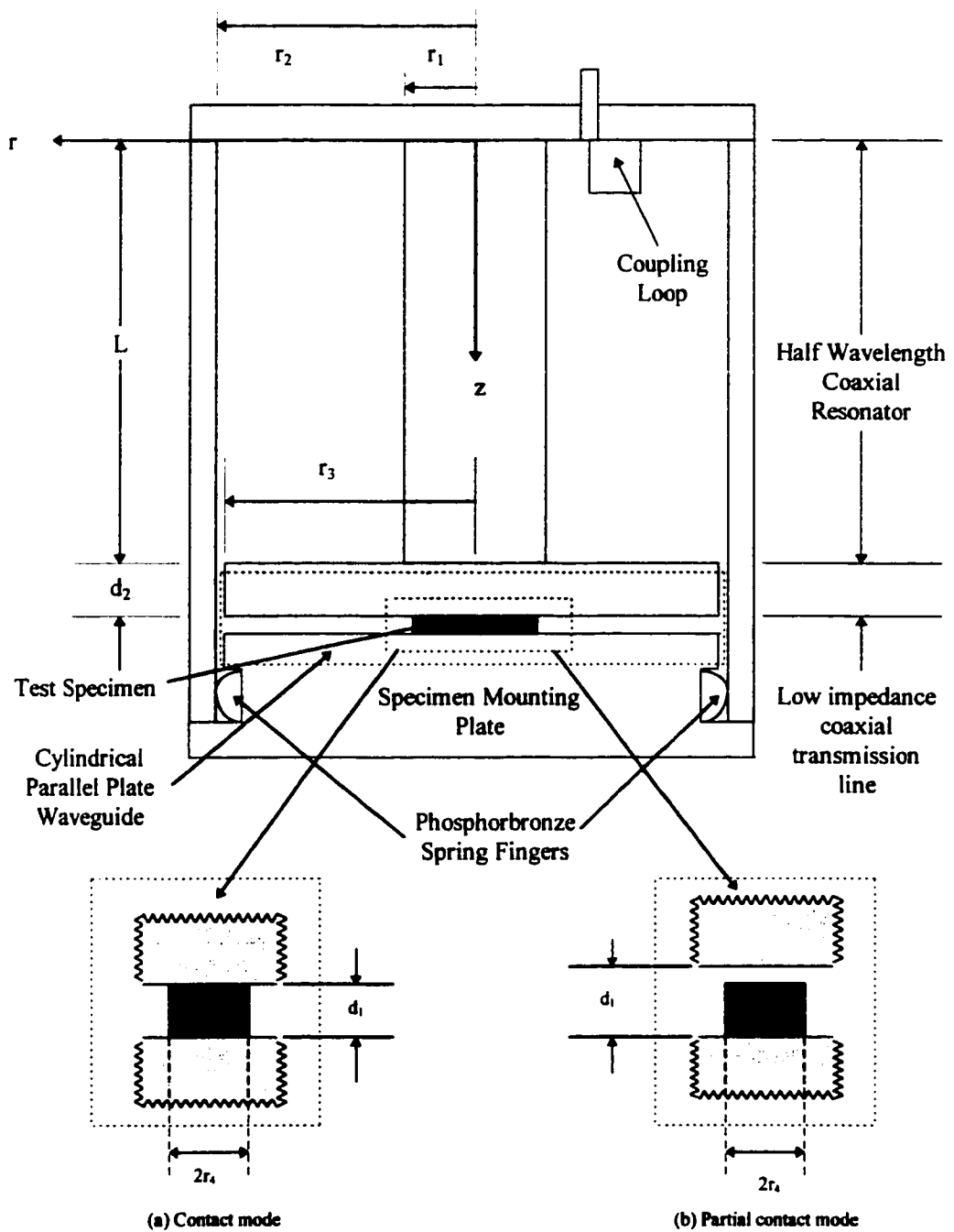
To maintain reasonable accuracy in the dielectric measurements, the test specimen loading on the cavity must satisfy the following two perturbation assumptions: the relative shift in resonant frequency is $\left| \frac{\Delta f_0}{f_0} \right| \leq 1\%$, and the loaded cavity Q-factor is $Q_1 \geq \frac{Q_0}{3}$.

To achieve these technical criteria and measurement accuracy conditions a resonator as shown in Figure 3.2 was used. The resonator consists of four parts: a half-wavelength coaxial resonator, a cylindrical parallel plate waveguide section, a low impedance coaxial transmission line and a coupling loop. A resonant frequency of $f_0 \approx 2.45$ GHz and a Q-factor of approximately $Q_0 \approx 2900$ is initially

set by the half wavelength coaxial resonator. Dielectric test specimens lie at the center of the cylindrical parallel plate waveguide, a strong electric field region. A transmission line extending from $z = L$ to $z = L + d_2$ (see Figure 3.2) permits energy to be coupled via the magnetic field from the coaxial resonator to the cylindrical parallel plate waveguide. A wire loop, situated within the test cavity, connected to the microwave feed line through the cavity's input port excites electric and magnetic fields within the test cavity as well as setting the cavity's input impedance.

In order to insert a dielectric within the cavity, the coaxial resonator is separated from the specimen mounting plate as shown in Figure 3.2. Electrical contact between the coaxial resonator and the test specimen mount is maintained via phosphorbronze spring fingers on the specimen mounting plate.

To cover a large loss tangent range, the resonant cavity is used in either a "contact" or a "partial contact" mode. In the contact mode the test specimen contacts both plates of the parallel plate waveguide, as shown in illustration a) of Figure 3.2. Conversely for the partial contact mode, the length of the center conductor of the coaxial resonator is reduced. This causes a corresponding increase in the spacing between the plates of the parallel plate waveguide, so that the test specimen now contacts only the lower plate of the parallel plate waveguide as shown in illustration b) of Figure 3.2. This causes a reduction in the field energy within the test specimen, thereby, maintaining reasonable Q-factors while permitting higher loss materials to be measured. Use of the two test



Cavity Dimensions: $r_1 = 7.0$ mm, $r_2 = 28.0$ mm, $r_3 = 27.0$ mm, $r_a = 5.0$ mm,
 $L = 60.3$ mm (contact mode), 59.3 mm (partial contact mode), $d_1 = 2.0$ mm
 (contact mode), 3.0 mm (partial contact mode) and $d_2 = 3.1$ mm.

Figure 3.2 Cross-section of the cavity structure of the dielectrometer.

modes allows for a loss tangent measurement range that covers $0.0001 \leq \tan\delta \leq 1.6$.

3.2.2 Design of the Cavity

A. Cavity Radius

At a given resonant frequency, the unloaded Q-factor of a coaxial cavity is proportional to the radius of its inner and outer conductor, r_1 and r_2 . The unloaded Q-factor is a maximum value when $\frac{r_2}{r_1} = 3.58$ [37]. A ratio of $\frac{r_2}{r_1} = 4.0$ was chosen to simplify the dimensioning in the FDFD model. This cavity radius ratio causes the unloaded cavity Q-factor to be reduced by approximately 5% as compared to the Q-factor of a cavity that has the optimum radius ratio. The radial cavity dimensions were chosen to be $r_1 = 7.0\text{mm}$ and $r_2 = 28.0\text{mm}$.

To insure that this design prevents higher order modes to propagate within this cavity at $f = 2.45$ GHz, the cut-off frequency of the lowest order transverse mode has been calculated. For a cylindrical coaxial line with $r_1 = 7.0\text{mm}$ and $r_2 = 28.0\text{mm}$ the TE_{11} mode has a cut-off frequency of $f_c \approx 2.728$ GHz [37]. Thus, no transverse modes will exist at the desired resonant frequency of $f_o \approx 2.45$ GHz.

B. Inner Conductor Length

The half wavelength coaxial section sets the approximate resonant frequency to $f = c/2L$ where L is the length of the center conductor and f is the resonant frequency [44]. Since the parallel plate waveguide is capacitive, the length of the center conductor must be slightly shorter than $L = \frac{\lambda_0}{2}$, where λ_0 is the resonant wavelength, in order to set the cavity's resonant frequency properly. The length of the half wavelength coaxial section should be between $60.0\text{mm} < L < 62.5\text{mm}$ in order to obtain a cavity resonant frequency of approximately $f_0 \approx 2.45$ GHz.

C. Plate Separation of the Cylindrical Parallel Plate Waveguide

Optimum plate separation of the cylindrical parallel plate waveguide was determined by the test specimen's thickness and dielectric loss. Since low loss materials do not increase cavity losses significantly, low loss specimens are tested in the contact mode. This test mode is characterized by the plate separation being equivalent to the available test specimen thickness, $d_2 = t = 2.0$ mm. On the other hand, high loss dielectrics increase cavity losses excessively if tested using the contact mode. Thus to reduce specimen loading on the cavity an air gap between the test specimen and the top plate of the parallel plate waveguide was introduced. This causes a corresponding increase in the plate separation, a key factor in setting the loaded cavity Q-factor for the partial

contact mode. In order to maintain the measurement condition that states that $Q_1 \geq \frac{Q_0}{3}$ a loaded cavity Q-factor that exceeds $Q_1 = 1000$ is necessary for all testing conditions. Via results obtained from a numerical simulation technique, the plate separation was selected to be $d_2 = 3.0$ mm.

D. Low Impedance Coaxial Transmission Line

To optimize energy coupling between the coaxial resonant structure and the parallel plate waveguide structure, a transmission line impedance matched to both structures is required. The impedance's of the coaxial resonator at $z = L$ and the cylindrical parallel plate waveguide at $z = L + d_2$ are $Z \approx 0$. To achieve an impedance match at both of these planes, the input impedance of the transmission line as seen by both microwave structures must be $Z_{in} \approx 0$. The characteristic impedance of this section of air-filled transmission line [46-47] is given by

$$Z_0 = \frac{60}{\sqrt{\epsilon_r}} \ln\left(\frac{r_2}{r_3}\right) \quad (3.1).$$

To obtain a characteristic line impedance that approaches $Z_0 \approx 0$, the radius of the transmission line, r_3 , should be between $r_2 > r_3 > 0.95r_2$. For a short section of a low impedance transmission line, input impedance as seen by either the resonant coaxial section or the parallel plate waveguide is approximately given by

$$Z_{in} = Z_1 + jZ_0\beta l \quad (3.2)$$

where Z_0 is the characteristic impedance of the transmission line, β is the propagation constant of the microwave signal, l is the length of the transmission line and Z_1 is the impedance of either the resonant coaxial section at $z = L$ or the parallel plate waveguide at $z = L + d_2$ depending at which reference plane Z_{in} is being evaluated. Thus to obtain an impedance match between the microwave networks the transmission line length, d_2 , should be $d_2 \ll \frac{\lambda_0}{8}$. A low impedance transmission line matched to the coaxial resonator at $z = L$ and the parallel plate waveguide at $z = L + d_2$ is realized with a transmission line that has a radius of $r_3 = 27.0$ mm and a length of $d_2 = 3.1$ mm.

E. Test Specimen Dimensions and Position

Since the cavity fields are axially symmetric, the specimen shape is selected to be cylindrical. The cylindrical dimensions of the test specimen are dependent on both the electric field's radial distribution within the cylindrical parallel plate waveguide and the dimensions of the raw materials to be tested. Within the cylindrical parallel plate waveguide the electric field's radial distribution is proportional to the first order Bessel function of the first kind. To maintain a relatively uniform electric field distribution throughout the test specimen while achieving maximum frequency sensitivity to load variation, a test specimen diameter of $2r_4 = 10.0$ mm is chosen.

F. Coupling Loop

A wire loop, commonly referred to as a coupling loop, excites electric and magnetic fields within the test cavity, as well as setting the cavity's input impedance. The coupling loop is connected to the cavity's input port and is terminated at the boundary $z = 0$ (see Figure 3.2). Current flowing on the coupling loop excites evanescent TE and TM modes in the vicinity of the coupling loop, while a resonant quasi-TEM mode is excited in the rest of the cavity structure when the frequency of the exciting signal is at or near the cavity's resonant frequency. The impedance of the coupling loop and hence the input impedance of the cavity is set by the effective cross sectional area of the coupling loop with respect to the $r - z$ plane [48].

3.3 Temperature Controller Design

A temperature-controlled heater is designed for heating test specimens contained within the resonator from 20°C to 120°C . An analog electronic circuit monitors the specimen and cavity temperatures by thermocouples and a digital thermometer while it controls two power resistors that heat both the test specimen and the resonant cavity.

3.3.1 Temperature Control Circuit Design

An analog controller regulates the temperature of the test specimen. The control circuit consists of a voltage amplifier, a comparator, a BJT transistor and a relay switch. A system diagram, with component values, is presented in Figure 3.3. A non-inverting amplifier with a gain of $A_v \approx 57$ converts the D.C. thermocouple voltage of the test specimen mount from the millivolt range to the 0 to 15 D.C. Volt range [49]. This amplified thermocouple voltage provides one input signal to a comparator, while the other input is a user-controlled voltage that corresponds to a desired test specimen temperature setpoint. While the amplified thermocouple voltage is less than the user controlled voltage, the comparator's output is approximately $V_O \approx +15V$ thus saturating Q_1 and causes the power relay to close [50-51]. When the amplified thermocouple voltage is equal to or greater than the setpoint voltage, the comparator's output is $V_O \approx -15V$ causing the transistor to turn off which opens the relay coil. The relay box provides 120 V at 15 A, AC to two 300Ω power resistors connected in parallel producing 96 W of power for heating the test specimen mount. The temperature of the test specimen and its mount are monitored by a digital thermometer connected to two thermocouples that have an overall temperature measurement uncertainty of $\Delta T = \pm 2.2 \text{ }^\circ\text{C}$ [52].

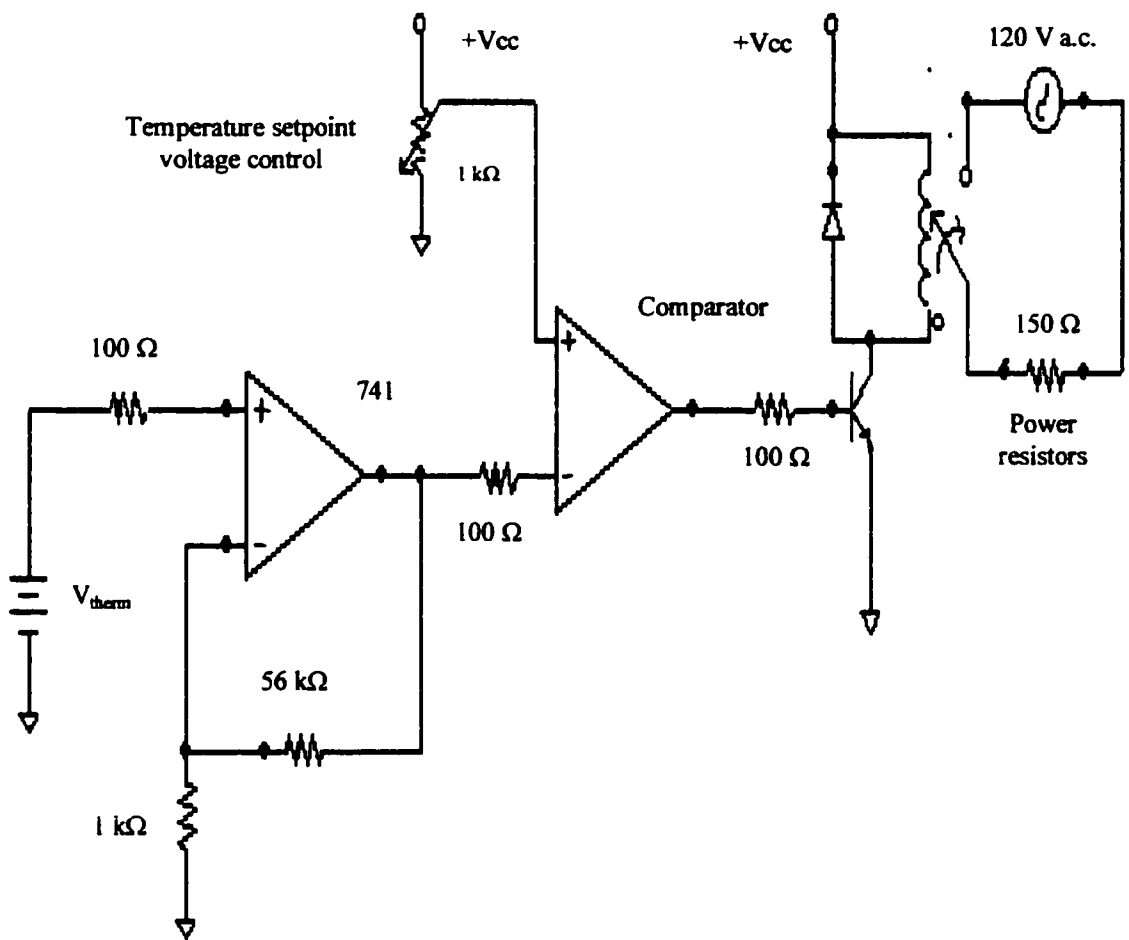


Figure 3.3 Circuit schematic for the analog controller.

3.4 Reflectometer Interface

A reflectometer provides a swept microwave test signal to the test cavity and monitors the cavity's frequency response. A synthesized sweep oscillator, model number HP 83752A, provides the swept frequency microwave signal. The range of the frequency sweep is set by the user. A scalar network analyzer, model number HP 8757D, monitors the reflection coefficient of the cavity's input

port over the same user defined frequency sweep range via two directional couplers and two diode detectors. The directional couplers, (Waveline Incorporated, serial numbers 5714 and 5715) have a coupling factor of 20 dB and 30 dB directivity and sample both the incident and reflected signals supplied by the sweep oscillator and reflected by the test cavity respectively. The sampled signals, modulated 30 kHz square waves, are demodulated using diode detectors connected to the directional couplers and their output is sent to the scalar network analyzer. From the reflection coefficient spectrum, the cavity's resonant frequency is determined and the cavity Q-factor is calculated from five different power bandwidths.

CHAPTER 4

DIELECTRIC CONSTANT DETERMINATION USING A FINITE DIFFERENCE FREQUENCY DOMAIN METHOD

4.1 Introduction

The relative dielectric constant and loss factor, ϵ_r' and ϵ_r'' , of a material can be found by measuring the perturbation of a resonant cavity that occurs upon insertion of the material. Relative dielectric constant, ϵ_r' , is obtained by measuring the shift in resonant frequency of the cavity, Δf_0 , and the relative loss factor, ϵ_r'' is obtained by measuring the change in the Q-factor, ΔQ_0 . Relative dielectric constant and loss factor are related to shift in resonant frequency and change in Q-factor, respectively, through the perturbation formula. Application of the perturbation formula requires knowledge of the electric and magnetic fields in the perturbed cavity. These fields are calculated numerically with a finite difference frequency domain method.

The FDFD numerical algorithm and problem solving approach are presented first. Following this, procedures for calculating mean electric stored energy, mean magnetic stored energy and power dissipation in the cavity are developed. These quantities are necessary to determine the resonant frequency, f_0 , and Q-factor, Q of the cylindrical cavity. Guidelines for selecting the grid structure for the problem domain are given. The known fields in a simple short-

circuited coaxial resonator of length $L = \frac{\lambda}{2}$ are then computed to verify the algorithms employed. Analytically calculated and numerically computed resonances are compared. The electromagnetic field solutions for the $\frac{\lambda}{2}$ coaxial resonator are then presented in graphical format.

4.2 Relating Dielectric Constant to Cavity Field Perturbations

The complex resonant frequency, Ω_0 , of a resonator is defined as

$$\Omega_0 = \omega_0 + j\frac{\omega_0}{2Q} \quad (4.1)$$

where ω_0 is the angular resonant frequency and Q is the quality factor of the cavity.

When a small, non-magnetic, dielectric specimen is inserted into the test cavity the relative change in the cavity's complex resonant frequency, $\frac{\Delta\Omega_0}{\Omega_0}$, [44]

is given by

$$\frac{\Omega_2 - \Omega_1}{\Omega_2} = \frac{- \int_{V_D} (\epsilon_{r2}^* - \epsilon_{r1}^*) \epsilon_0 E_1^* \cdot E_2 dv}{\int_{V_C} (\epsilon_{r1}^* \epsilon_0 E_1^* \cdot E_2 + \mu_0 H_1^* \cdot H_2) dv} \quad (4.2)$$

where μ_0 is the permeability of free space ($4\pi \times 10^{-7} \text{ A/m}$), E is the electric field intensity, H is the magnetic field intensity, and V_C and V_D are the cavity and test material volumes. Subscripts 1 and 2 designate values before and after test

material insertion and an asterisk denotes the complex conjugate. Re-writing Eq.(4.2) in terms of Q and f [44] results in

$$\frac{\Omega_2 - \Omega_1}{\Omega_1} \approx \frac{f_2 - f_1}{f_1} + j \left(\frac{1}{2Q_2} - \frac{1}{2Q_1} \right) = \frac{\Delta f_1}{f_1} + j \Delta \left(\frac{1}{2Q_1} \right) \quad (4.3),$$

provided that $\left(\frac{1}{2Q_1} \right) \ll 1$, and $\frac{|f_2 - f_1|}{f_2} \ll 1$.

Here $f = \frac{\omega}{2\pi}$ is the frequency in Hertz and Δf is the resonant frequency shift of the cavity caused by test specimen insertion. Combining Eq.(4.2) and (4.3) we get

$$\frac{\Delta f_1}{f_1} + j \Delta \left(\frac{1}{2Q_1} \right) \approx \frac{- \int_{v_D} (\varepsilon_{r2}^* - \varepsilon_{r1}^*) \varepsilon_0 E_1^* \cdot E_2 dv}{\int_{v_C} (\varepsilon_0 E_1^* \cdot E_2 + \mu_0 H_1^* \cdot H_2) dv} \quad (4.4).$$

It is useful to separate Eq.(4.4) into its real and imaginary parts

$$\frac{\Delta f_1}{f_1} \approx - \frac{(\varepsilon_r' - 1) \varepsilon_0 \int_{v_D} E_1^* \cdot E_2 dv}{\int_{v_C} (\varepsilon_0 E_1^* \cdot E_2 + \mu_0 H_1^* \cdot H_2) dv} \quad (4.5)$$

$$\Delta \left(\frac{1}{2Q_1} \right) \approx \frac{\varepsilon_r'' \varepsilon_0 \int_{v_D} E_1^* \cdot E_2 dv}{\int_{v_C} (\varepsilon_0 E_1^* \cdot E_2 + \mu_0 H_1^* \cdot H_2) dv} \quad (4.6).$$

At this point, it is necessary to evaluate the integrals on the right hand side of Eqs.(4.5) and (4.6). Following the perturbation assumptions stated in the previous chapter, when the integrals in Eqs. (4.5) and (4.6) are evaluated, the quantities yielded are real. For simple resonant structures, the loaded cavity fields E_2 and H_2 are approximately equal to the empty cavity fields E_1 and H_1

[53-55]. However, since the hybrid coaxial cavity is a complex geometric structure, the cavity fields E_2 and H_2 are not equivalent to the empty cavity fields E_1 and H_1 . A numerical computation of the cavity fields E_2 and H_2 within the test cavity is necessary to evaluate the integrals in Eqs.(4.5) and (4.6).

These calculated field solutions are also used to determine the mean stored electric and magnetic energies and the wall losses in the cavity. The Q-factor of the cavity can thus be determined. Calculation of mean electric and magnetic stored energy also provides the basis for determining the resonant frequency. Indeed, the frequency of excitation is progressively incremented until the computed mean electric and magnetic stored energies are equal, at which point the cavity is deemed to be at resonance.

4.3 HERZ Program

HERZ (H-field, E-field, r-z geometry) [56] is a FDFD numerical simulator that models cylindrically symmetric electromagnetic field problems for which the electric fields have radial and axial components (r,z) while the magnetic fields have only an azimuthal component (ϕ).

Time-harmonic solutions for such problems are of the form

$$\hat{\mathbf{E}} = E_r(r,z) + E_z(r,z) \quad (4.7)$$

$$\hat{\mathbf{H}} = H_\phi(r,z) \quad (4.8)$$

Assuming an $e^{j\omega t}$ time dependence, the integral form of Maxwell's equations can be expressed as

$$\oint \vec{E} \cdot d\vec{l} = -j\omega\mu \iint \vec{H} \cdot d\vec{s} \quad (4.9)$$

$$\oint \vec{H} \cdot d\vec{l} = (\sigma + j\omega\epsilon) \iint \vec{E} \cdot d\vec{s} \quad (4.10)$$

The finite difference algorithm is applied on the rectangular grid structure shown in Figure 4.1. By discretization of Eq.(4.9) the azimuthal field component, H_ϕ , is computed at the center of every grid block [56]. The resulting linear equations are of the form

$$a_{i,j}E_{z_{i,j}} + b_{i,j}E_{r_{i,j}} + c_{i,j}E_{z_{i+1,j}} + d_{i,j}E_{r_{i,j}} = e_{i,j}H_{\phi_i} \quad (4.11)$$

where $a_{i,j}$ through $e_{i,j}$ depend on the grid dimensions Δr_i and Δz_j . We now set

$$rH_\phi = H'_\phi \quad (4.12)$$

where r is the radial distance from the axis of symmetry to the center of an individual grid block [56].

By discretization of Eq.(4.10) each of the electric field components appearing in Eq.(4.11) are now written in terms of the magnetic fields at the center of each of the adjacent grid blocks. The resulting equations are of the form

$$A_{i,j}H'_{\phi_{i,j}} + B_{i,j}H'_{\phi_{i-1,j}} + C_{i,j}H'_{\phi_{i+1,j}} + D_{i,j}H'_{\phi_{i,j-1}} + E_{i,j}H'_{\phi_{i,j+1}} = 0 \quad (4.13)$$

where the coefficients $A_{i,j}$ to $E_{i,j}$ are given in terms of the angular frequency, ω , the electrical properties, σ , ϵ_r and μ , and the radial locations, r_i , and dimensions of the pertinent grid blocks, Δr_i and Δz_j , [57]. Each of the N grid

blocks referred to by indices i, j may have distinct electrical properties σ , ϵ_r and μ and is described by an equation of the form of Equation (4.13). The N equations are solved by Gaussian elimination for all values of H'_z , and hence H_z .

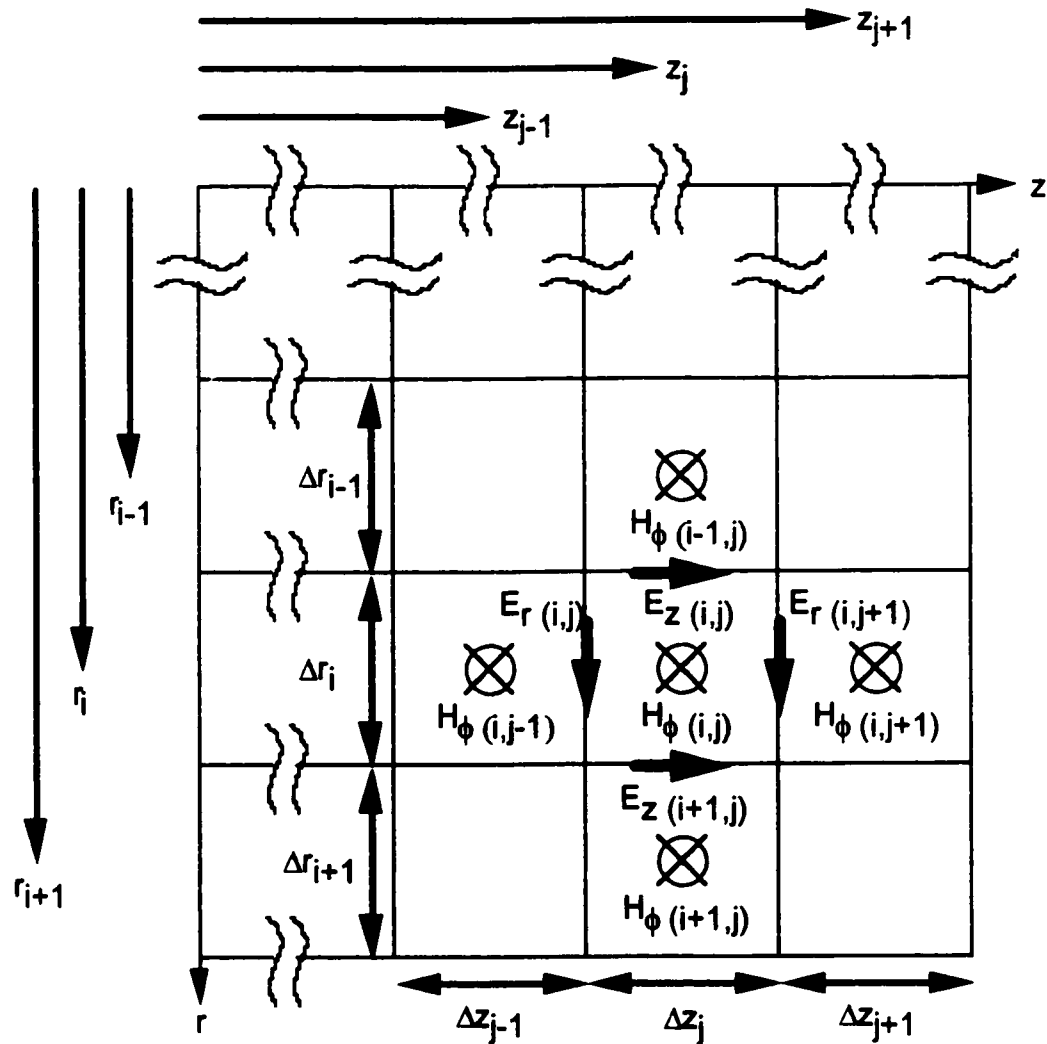


FIGURE 4.1 The finite difference grid structure used in HERZ. All magnetic field components are azimuthally directed and are computed at the grid centers, while the electric field components are computed on the grid boundaries.

Problem excitation may be both or either magnetic and electric. Electric field excitation may be specified on the perimeter of the problem domain only. At all other locations in the problem domain the electric field excitation is set to zero. Magnetic field excitation may be specified at the center of any grid block in the problem domain. Both magnitude and phase of the electric and magnetic field vectors must be specified.

Except at the location where the electric field excitation is specified, the perimeter of the problem domain is taken to be a perfect conductor, and where, hence, $E_{\text{tangential}}$ is set to zero [56].

4.4 Algorithms for Finding Resonant Frequency and Q-Factor of a Circular Cylindrical Resonant Cavity

To permit calculation of the resonant frequency, f_0 , and Q-factor, Q_0 , of the empty cavity, two subroutines were added to the existing program HERZ. One subroutine calculates the mean electric and magnetic stored energies within the cavity for a range of frequencies. The frequency at which these quantities are equal is taken to be the resonant frequency of the cavity. The other subroutine calculates power dissipation in the cavity walls and the test specimen and is used to determine the empty and loaded cavity Q-factors.

4.4.1 Algorithm for Calculating Electric and Magnetic Mean Stored Energies

The mean magnetic and electric stored energies are calculated for each grid block within the cavity. These energies are then summed. The mean electrical stored energy, $dW_{E_{i,j}}$, stored in grid block i, j , at co-ordinates r, z , is given by

$$dW_{E_{i,j}} = \frac{1}{2} \left(|E_{r_{i,j}}|^2 + |E_{z_{i,j}}|^2 \right) \epsilon'_{r_{i,j}} \epsilon_0 \pi r_i \Delta r_i \Delta z_j, \quad (4.14)$$

where $|E_{r_{i,j}}|$ and $|E_{z_{i,j}}|$ are the magnitudes of the peak radial and axial electric field components, $\epsilon'_{r_{i,j}}$ is the grid block's relative dielectric constant, r_i is the radial position and Δr_i is the radial thickness and Δz_j is the axial thickness of grid block i, j . The mean stored magnetic energy, $dW_{M_{i,j}}$, in grid block i, j is

$$dW_{M_{i,j}} = \frac{1}{2} |H_{\phi_{i,j}}|^2 \mu_0 \pi r_i \Delta r_i \Delta z_j \quad (4.15)$$

where $|H_{\phi_{i,j}}|$ is the magnitude of the peak azimuthal magnetic field of grid block i, j .

The total mean electric stored energy W_E is

$$W_E = \sum_{i=1}^I \sum_{j=1}^J dW_{E_{i,j}} \quad (4.16)$$

and the total mean magnetic stored energy W_M is

$$W_M = \sum_{i=1}^I \sum_{j=1}^J dW_{M_{i,j}} \quad (4.17)$$

where I and J are the total number of axial and radial grid blocks respectively.

The resonant frequency shift is the difference between the resonant frequency of the loaded cavity and that of the empty cavity. Calculating the resonant frequency shifts that occur when the cavity is loaded with a dielectric whose relative dielectric constant is given a large range of different values, permits one to establish a relationship between the relative dielectric constant of a test specimen and the resonant frequency shift it produces when inserted into the test cavity.

4.4.2 Algorithm for Calculating Power Dissipation

To determine the loss factor, ϵ_r'' , of a test specimen, the change in Q-factor, ΔQ_0 , of the cavity that occurs when the specimen is introduced must be calculated. As previously stated, the loaded cavity Q-factor is defined as

$$Q_L = \omega \frac{2W_E}{P_W + P_D} \quad (4.18)$$

The mean electric stored energy, W_E , is calculated from Eqs.(4.14) and (4.16). The calculation of cavity wall losses, P_W , and dielectric losses, P_D , is described below.

Conductor losses in the cavity, P_W , are calculated at the surface of each grid block adjacent to a cavity wall. Four cases must be considered in order to calculate the total power dissipation per grid block. With reference to Figure 4.1 the four cases are:

- (1). If grid block $i-1, j$ is a conductor then the power dissipation, $dP_{W_{ij}}$, at the inner most boundary of grid block i, j is

$$dP_{w_{ij}} = \sqrt{\frac{\omega\mu_o}{2\sigma_{i-1,j}}} |H''_{\phi,i}|^2 \pi \left(r_i - \frac{\Delta r_i}{2} \right) \Delta z_j \quad (4.19)$$

(2). If grid block $i+1, j$ is a conductor then the power dissipation,

$dP_{w_{ij}}$, on the outer most boundary of grid block i, j is

$$dP_{w_{ij}} = \sqrt{\frac{\omega\mu_o}{2\sigma_{i+1,j}}} |H''_{\phi,i}|^2 \pi \left(r_i + \frac{\Delta r_i}{2} \right) \Delta z_j \quad (4.20)$$

(3). If grid block $i, j-1$ is a conductor then the power dissipation,

$dP_{w_{ij}}$, on the left boundary of grid block i, j is

$$dP_{w_{ij}} = \sqrt{\frac{\omega\mu_o}{2\sigma_{i,j-1}}} |H''_{\phi,i}|^2 \pi r_i \Delta r_i \quad (4.21)$$

(4). If grid block $i, j+1$ is a conductor then the power dissipation,

$dP_{w_{ij}}$, on the right boundary of grid block i, j is

$$dP_{w_{ij}} = \sqrt{\frac{\omega\mu_o}{2\sigma_{i,j+1}}} |H''_{\phi,i}|^2 \pi r_i \Delta r_i \quad (4.22).$$

Here $|H''_{\phi,i}|$ is the magnitude of the azimuthal magnetic field extrapolated from the center of grid block i, j , to its boundary, and the conductivity, σ , of the grid block boundary is the conductivity of the cavity wall. The total power dissipation at the cavity walls adjacent to grid block i, j , is the sum of the RHS of Equations (4.16) through (4.22). The total power dissipation caused by all wall losses, P_w , is

$$P_w = \sum_{i=1}^I \sum_{j=1}^J dP_{w_{ij}} \quad (4.23).$$

Power dissipation in the i, j subvolume of the perturbing specimen is

$$dP_{D_{i,j}} = \sigma_{i,j} \left(|E_{r_{i,j}}|^2 + |E_{z_{i,j}}|^2 \right) \pi r_i \Delta r_i \Delta z_j \quad (4.24)$$

where $\sigma_{i,j}$ is the conductivity of the dielectric and is defined by

$$\sigma_{i,j} = \omega (\tan \delta)_{i,j} \epsilon'_{r_{i,j}} \epsilon_0 \quad (4.25).$$

The total power losses, P_D , in the dielectric perturbing specimen are

$$P_D = \sum_{i=1}^I \sum_{j=1}^J dP_{D_{i,j}} \quad (4.26).$$

With W_E , P_W and P_D known, Q_L can be calculated from Eq.(4.18). Calculating the changes in Q factor of the resonant cavity that occur when the cavity is loaded with a dielectric whose $\tan \delta$ is given a large range of different values, permits one to establish a relationship between the $\tan \delta$ of a test specimen and the change in Q-factor it produces when inserted into the test cavity.

The results of the foregoing numerical calculations permit one to deduce the relative dielectric constant ϵ'_r and loss tangent $\tan \delta$ of a test specimen from the experimentally measured shifts in resonant frequency and Q factor of the test cavity.

4.5 Grid Structure for the Problem Domain

To achieve results within 0.5% uncertainty, it was found during the course of repeated numerical simulations that no grid block dimensions should

be larger than $\lambda/15$. As well, the problem domain should utilize a large number of grid blocks.

The size of grid blocks used within subdomains, such as the test specimen and in regions where the electromagnetic fields change rapidly in space, should be at least five times smaller than would be the case if a uniform grid block size were employed throughout the problem domain. Generally, grid block dimensions at media interfaces that yielded satisfactory results, were, in the radial direction less than 0.04% of the wavelength, and in the axial direction, less than 0.01% of the wavelength.

The available computer memory permits a maximum of 5999 grid blocks. The test cavity nominally contains 85 grid blocks in the axial direction and 70 grid blocks in the radial direction, for a total of 5950 grid blocks. This total includes the dielectric specimen, 10.0 mm in diameter and 2.0 mm in thickness, which occupies 506 grid blocks in the contact mode, 23 in the radial direction and 22 in the axial direction. While for the partial contact mode, the dielectric specimen occupies 460 grid blocks, 23 in the radial direction and 20 in the axial direction.

A large number of grid blocks are required to represent the cylindrical parallel plate waveguide region since energy storage within the dielectric, which is located in this region, must be calculated very accurately. A large number of grid blocks are also required to represent the low impedance transmission line. Together these two regions occupy less than 4% of the cavity volume but require

approximately 20% of the total number of grid blocks used. In the cylindrical parallel plate waveguide region there are typically 2170 grid blocks (70 radial and 31 axial) for the partial contact mode and 1470 grid blocks (70 radial and 21 axial) for the contact mode. The low impedance coaxial transmission line is typically represented by 180 grid blocks (18 radial and 10 axial).

For the cavity Q-factor calculation, the conductivity of the brass walls is taken to be $1.1 \times 10^7 (\Omega m)^{-1}$. Finally, the cavity is excited by specifying a peak magnetic field of 0.5 A/m at a phase of 0° at the center of the grid block adjacent to the surface of the inner conductor of the coaxial section and the short circuit boundary of the resonator wall at $z = 0$.

4.6 A Simple Test of the Algorithm for Finding Resonant Frequency

A simple example is presented for testing the algorithm on a simple cylindrically symmetric short-circuited $\frac{\lambda}{2}$ coaxial resonator. The frequency of excitation is continuously incremented until the computed mean stored electric energy equals the computed mean stored magnetic energy, at which point the cavity is deemed to be resonant. The general time harmonic field solutions are [53]

$$\begin{cases} H_\phi = \frac{I_0}{2\pi r} \cos\left(\frac{2\pi}{\lambda_0} z\right) \\ E_r = \frac{60I_0}{r} \sin\left(\frac{2\pi}{\lambda_0} z\right) \end{cases} \quad (4.27)$$

where I_0 is the peak TEM current, λ_0 is the resonant wavelength, r is the radial position, and z is the axial position. Given these field solutions, the mean stored electric and magnetic energies, and power dissipation in the cavity walls can be analytically calculated at resonance. These results can then be compared to the corresponding numerical results obtained with HERZ.

The cavity dimensions will be similar to those of the coaxial portion of the hybrid coaxial dielectrometer. Cavity length is $L = 6.075$ cm, yielding a theoretical resonant frequency of $f_0 = 2.469$ GHz. The inner conductor radius is 7.00 mm and the outer conductor radius is 28.00 mm. 70 grid blocks in the radial direction, and 69 grid blocks in the axial direction represent the coaxial cavity. The inner conductor occupies 37 grid blocks in the radial direction. The magnetic field excitation of 0.5 A/m at a phase of 0° and the conductivity of the brass walls is $1.1 \times 10^7 (\Omega\text{m})^{-1}$, as for the cavity described in the previous section.

The results presented in Table 4.1 indicate that there is excellent agreement between analytically calculated values and those calculated numerically with the HERZ program. These results give confidence that HERZ can accurately model cylindrically symmetric resonators. Figures 4.2 and 4.3 display the electric and magnetic field distributions described by Eq.(4.27). These distributions may be compared to the numerically calculated field distributions for the hybrid coaxial cavity shown in Figures 5.1, 5.3, 5.4 and 5.6.

Table 4.1 Comparison between analytically calculated and numerically calculated parameters for a resonant empty short-circuited $\frac{\lambda}{2}$ coaxial resonator.

	Analytically Calculated	Numerically Calculated with HERZ	Magnitude of difference (%)
Resonant frequency (GHz)	2.469	2.468	0.057
Mean magnetic stored energy (10^{-12} J)	1.018	1.018	0.0
Mean electric stored energy (10^{-12} J)	1.018	1.018	0.0
Power dissipated (10^{-6} W)	9.390	9.395	0.054
Q-factor	3364	3361	0.097

4.7 Conclusion

The numerical procedures presented in this chapter lead to the empty and loaded cavity field solutions of the hybrid coaxial cavity. These field solutions, in conjunction with the perturbation formula along with measured resonant frequency shift and Q-factor shift are used to determine the complex relative dielectric constant of a test specimen contained within the hybrid coaxial cavity dielectrometer.

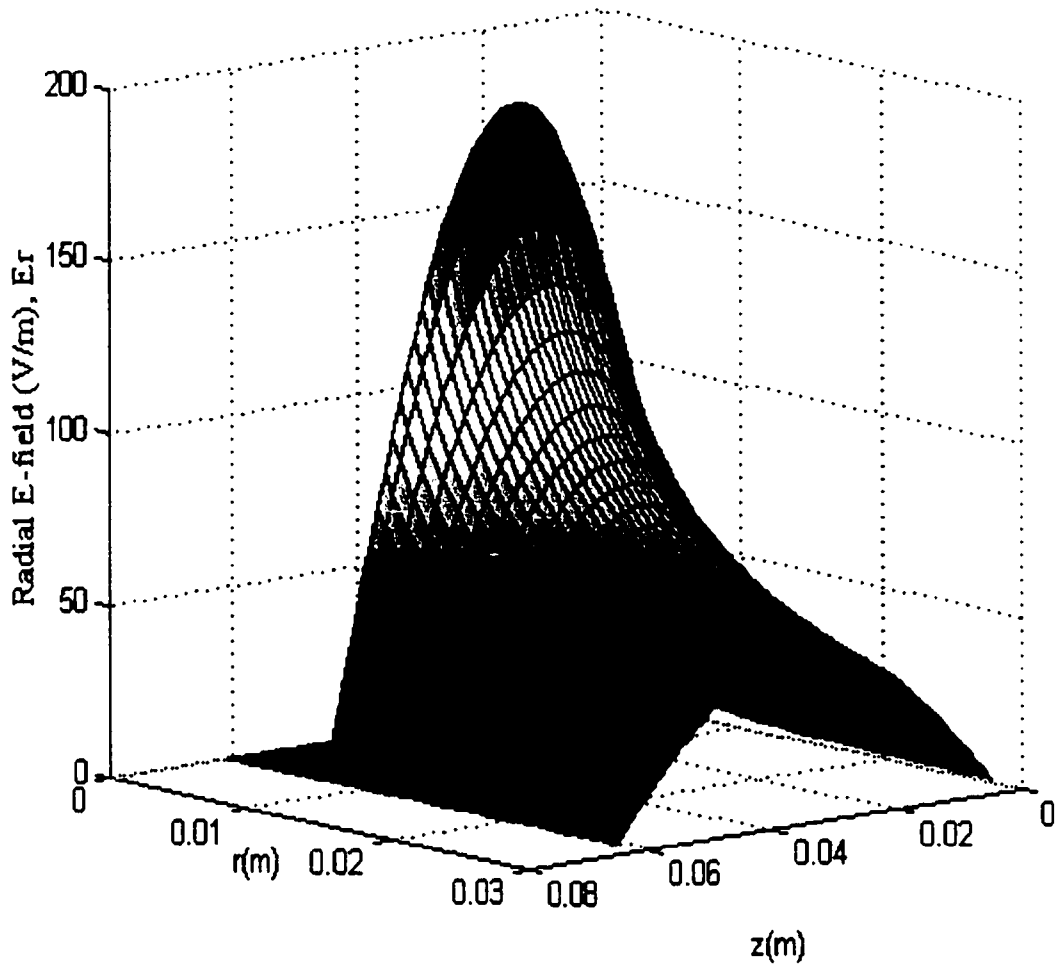


Figure 4.2 A two-dimensional (r, z) plot of the magnitude of the radial electric field distribution, E_r , within a resonant empty short-circuited $\frac{\lambda}{2}$ coaxial cavity. The inner conductor extends from $z = 0$ cm to $z \approx 6.08$ cm and $r = 0$ cm to $r \approx 0.7$ cm. The half wavelength is measured along the z -direction. The resonant frequency is $f_0 \approx 2.469$ GHz. Note the zero tangential electrical field intensity at the cavity end walls, and the maximum electric field intensity at the cavity mid plane.

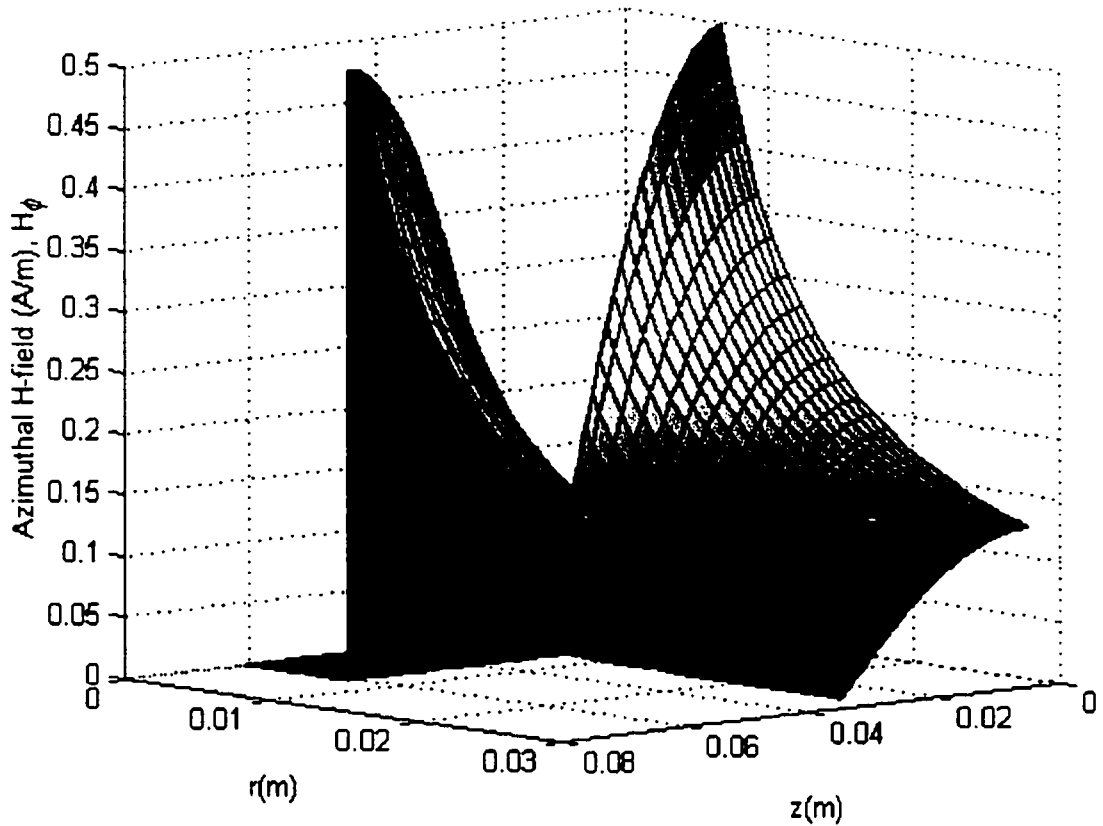


Figure 4.3 A two-dimensional (r, z) plot of the magnitude of the azimuthal magnetic field distribution, H_ϕ , within a resonant empty short-circuited $\frac{\lambda}{2}$ coaxial cavity. The inner conductor extends from $z = 0$ cm to $z \approx 6.08$ cm and $r = 0$ cm to $r \approx 0.7$ cm. The half wavelength is measured along the z -direction. The resonant frequency is $f_0 \approx 2.469$ GHz. Note the maximum tangential magnetic field intensity at the cavity end walls, and the zero magnetic field intensity at the cavity mid plane.

CHAPTER 5

MICROWAVE CHARACTERISTICS OF THE EMPTY AND LOADED CAVITY

5.1 Introduction

In this chapter the hybrid coaxial cavity's analytic, simulated and measured electromagnetic characteristics at resonance are described. The analytical field solutions for the regions within the two primary microwave structures are described. As well, the field solution for the dielectrically loaded cavity is supplied. Numerically calculated field solutions are displayed graphically for the empty cavity as well as the cavity loaded with a lossless specimen whose relative dielectric constant is $\epsilon_r' = 10$. Then numerically calculated Q-factors are presented for both the contact and partial contact modes. The empty cavity's measured resonant frequency is then compared to the numerically computed value. Finally, polynomial relationships are established that relate ϵ_r' to Δf_0 and $\tan\delta$ to ΔQ_0 for both cavity configurations.

5.2 Cavity Field Solution

A simple analytic field solution for the cavity does not exist since a low impedance transmission line is used for coupling the two primary microwave structures. However, for both the main coaxial resonator and the cylindrical parallel plate waveguide section analytic field solutions do exist and are

presented below. Solutions obtained from the FDFD program, HERZ, for this cavity structure are verified against these analytical results.

5.2.1. Half Wavelength Coaxial Section

As previously stated, the hybrid coaxial cavity's resonant frequency and Q-factor are mainly determined by the resonant coaxial section. Recalling that the field solutions for a half-wavelength resonant coaxial cavity [54] are given by

$$\begin{cases} H_{\phi} = \frac{I_0}{2\pi r} \cos\left(\frac{2\pi}{\lambda_0} z\right) \\ E_r = -\frac{60I_0}{r} \sin\left(\frac{2\pi}{\lambda_0} z\right) \end{cases} \quad (5.1).$$

a similar field pattern should be observed within the resonant coaxial section of the hybrid coaxial cavity. If one was to graph the solutions of Eq.(5.1) assuming that $I_0 \approx 22.0$ mA, $\lambda_0 \approx 12.24$ cm, and 0.7 cm $< r < 2.8$ cm and $0 < z < 6.03$ cm and compare those plots to the numerical solutions displayed in Figures 5.1 and 5.2 for $0 < z < 6.03$ cm and 0.7 cm $< r < 2.8$ cm, essentially identical plotted results would be observed between the numeric and analytic solutions.

5.2.2. Cylindrical Parallel Plate Waveguide Section

When the frequency of the electromagnetic fields within this structure is below the cutoff frequency of the TE_{11} mode, the structure acts as a radial transmission line [58]. Since this geometric structure does not have a TEM

resonance, its field solutions, for all frequencies below the cutoff frequency of the TE_{11} mode [58], are described by:

$$\begin{cases} H_{\phi} = \frac{A_0}{\eta_0} J_1\left(\frac{2\pi}{\lambda_0} r\right) \\ E_z = A_0 J_0\left(\frac{2\pi}{\lambda_0} r\right) \end{cases} \quad (5.2)$$

where η_0 is the intrinsic impedance of free space, J_0 and J_1 are the first and second order Bessel functions of the first kind and A_0 is the amplitude of the axial electric field at $r = 0$. The analytical solutions described above are only valid for $0 < r < 2.4$ cm (see Figure 3.2) because the radial discontinuity between 2.7 cm $< r < 2.8$ cm (see Figure 3.2) causes multiple higher order mode reflections in and around this boundary. For Eq.(5.2), it is assumed that $\lambda_0 \approx 12.24$ cm, $0 < r < 2.4$ cm and A_0 is determined from the numerically calculated solution.

5.2.3 Low Impedance Transmission Line and Surrounding Region

A simple analytic solution similar to those given in Eqs.(5.1) and (5.2) does not exist for the low impedance transmission line coupling the two other structures. One of the short falls of the finite difference and finite element numerical techniques is accurately predicting field solutions in and around cavity discontinuities [8]. Indeed, the mode matching technique is best suited for modeling cavity field solutions in regions around discontinuities [59]. However, mode matching analysis of the axial discontinuity at $r = r_3$ was beyond the scope

of this thesis. However, it should be pointed out that reactive evanescent TM_{0n} modes exist in the region near this radial discontinuity around $z = L$ and $z = L + d_2$, causing multiple reflections at this transmission line boundary [59]. Since a finite difference technique was used, the numerical solutions shown in Figures 5.1 - 5.6 are not correct for $6.03 \text{ cm} < z < 6.38 \text{ cm}$. However because of the relatively small volume, surface area and length of this transmission line in comparison to the overall cavity structure, numerical results provided by the FDFD program, HERZ, are deemed acceptable for the hybrid coaxial cavity.

5.2.4 Loaded Cavity Field Solution

When a dielectric specimen of radius, r_4 (see Figure 3.2), is placed in the cylindrical parallel plate waveguide, the waveguide's field patterns are described by [58]

for $0 \leq r \leq r_4$

$$\begin{cases} H_\phi = \frac{A_0}{\eta_0} \sqrt{\epsilon'} J_1 \left(\frac{2\pi}{\lambda_0} \sqrt{\epsilon'} r \right) \\ E_z = A_0 J_0 \left(\frac{2\pi}{\lambda_0} \sqrt{\epsilon'} r \right) \end{cases} \quad (5.3)$$

for $2.4 \text{ cm} > r > r_4$

$$\begin{cases} H_{\phi} = \frac{B_0}{\eta_0} J_1\left(\frac{2\pi}{\lambda_0} r\right) + \frac{C_0}{\eta_0} Y_1\left(\frac{2\pi}{\lambda_0} r\right) \\ E_z = B_0 J_0\left(\frac{2\pi}{\lambda_0} r\right) + C_0 Y_0\left(\frac{2\pi}{\lambda_0} r\right) \end{cases} \quad (5.4)$$

where Y_0 and Y_1 are the first and second order Bessel functions of the second kind and B_0 and C_0 are the coefficients of the first and second order Bessel functions. Their values are found by equating the respective field solutions of Eqs.(5.3) and (5.4) at $r = r_4$.

If one was to graph the solutions of Eqs.(5.3) and (5.4) assuming $\lambda_0 \approx 12.24$ cm, $0 < r < 2.4$ cm, $6.6\text{cm} > z > 6.4\text{cm}$, and A_0 , B_0 , and C_0 are calculated utilizing the numerical solution at the boundary $r = 0.5$ cm, essentially identical results would be observed between the numerical and analytic solutions. Similar results would be observed when the numerical results of Figures 5.4 and 5.6 for $0.7\text{cm} < r < 2.8\text{cm}$ and $0 < z < 6.03$ cm are compared to a graphical representation of Eq.(5.1) for $0.7\text{cm} < r < 2.8\text{cm}$, $0 < z < 6.03\text{cm}$, provided that $I_0 \approx 22.0\text{mA}$, and $\lambda_0 \approx 12.24$ cm.

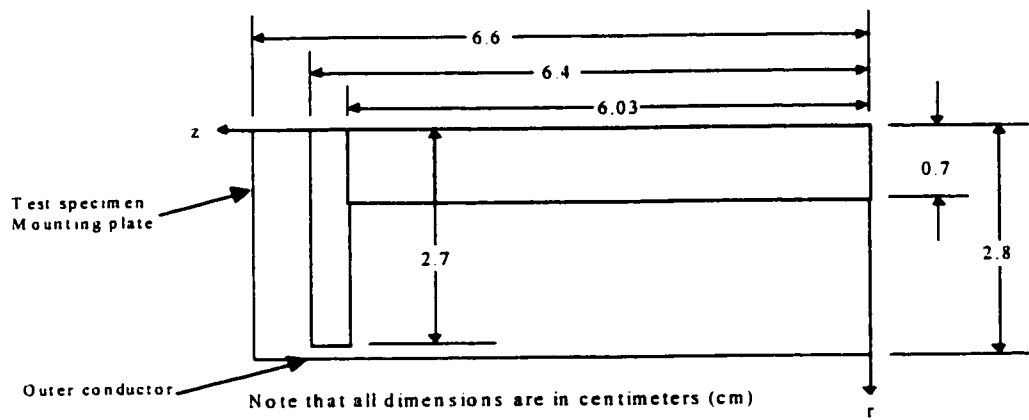
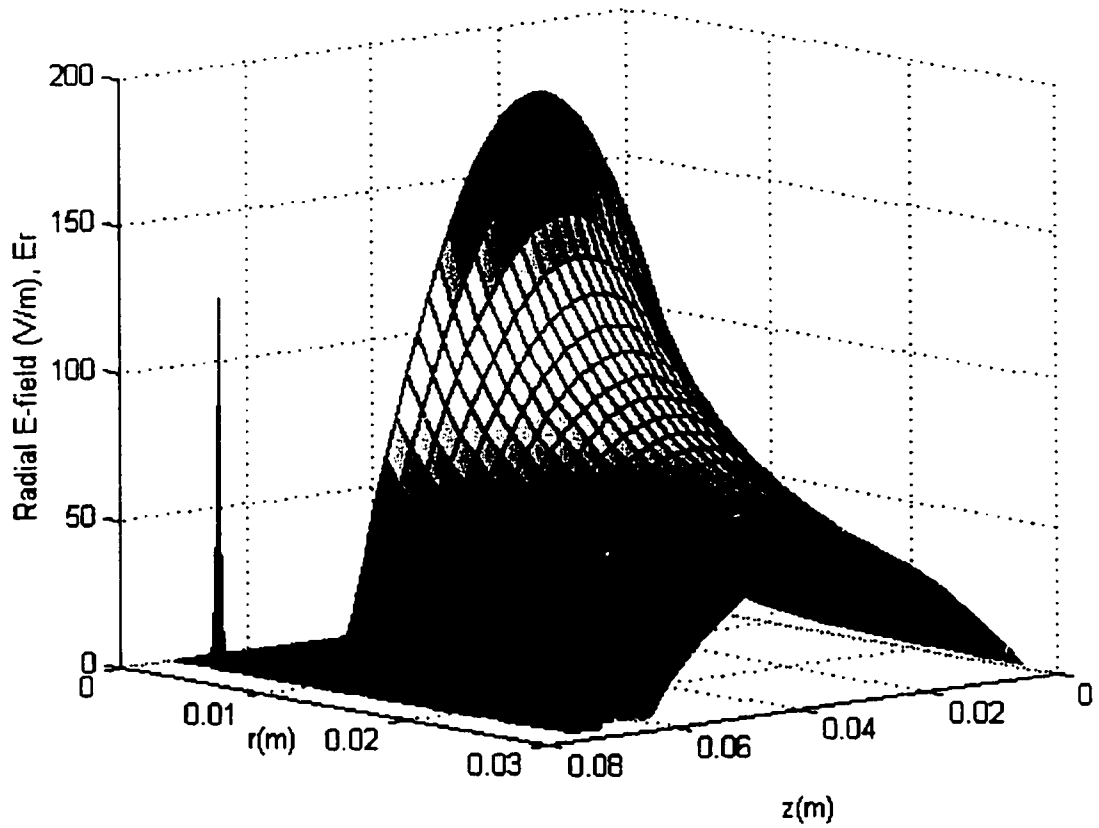


Figure 5.1 A two-dimensional (r, z) plot of the magnitude of the radial electric field distribution, E_r , within the empty hybrid coaxial cavity displayed along side a half cavity cross-section.

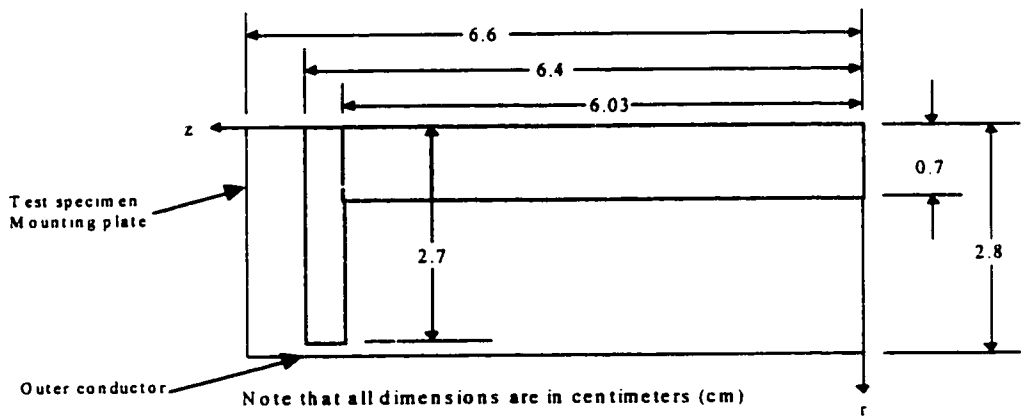
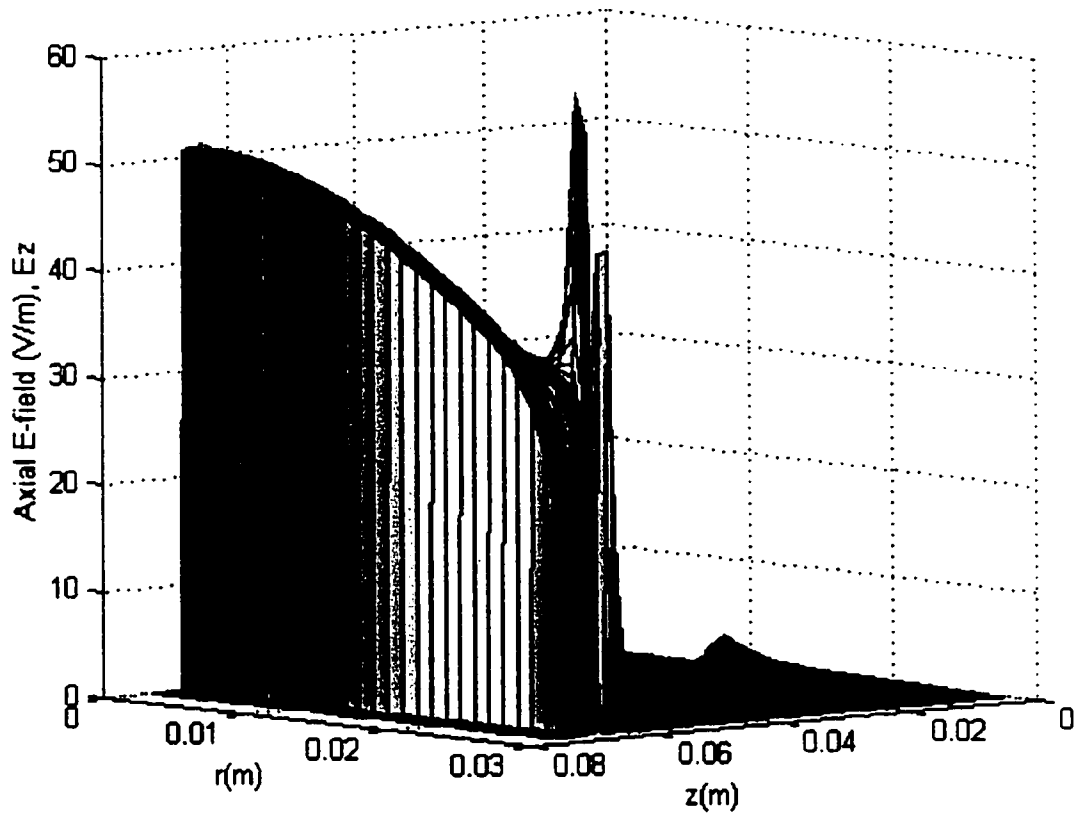


Figure 5.2 A two-dimensional (r, z) plot of the magnitude of the axial electric field distribution, E_z , within the empty hybrid coaxial cavity displayed along side a half cavity cross-section.

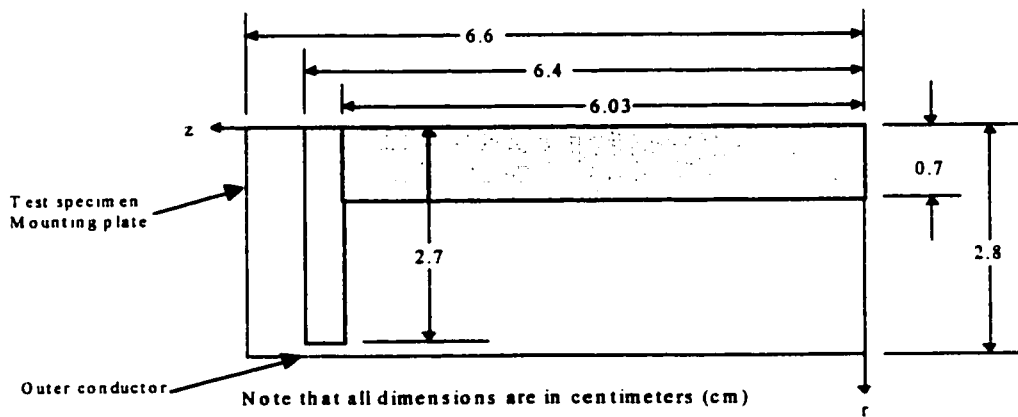
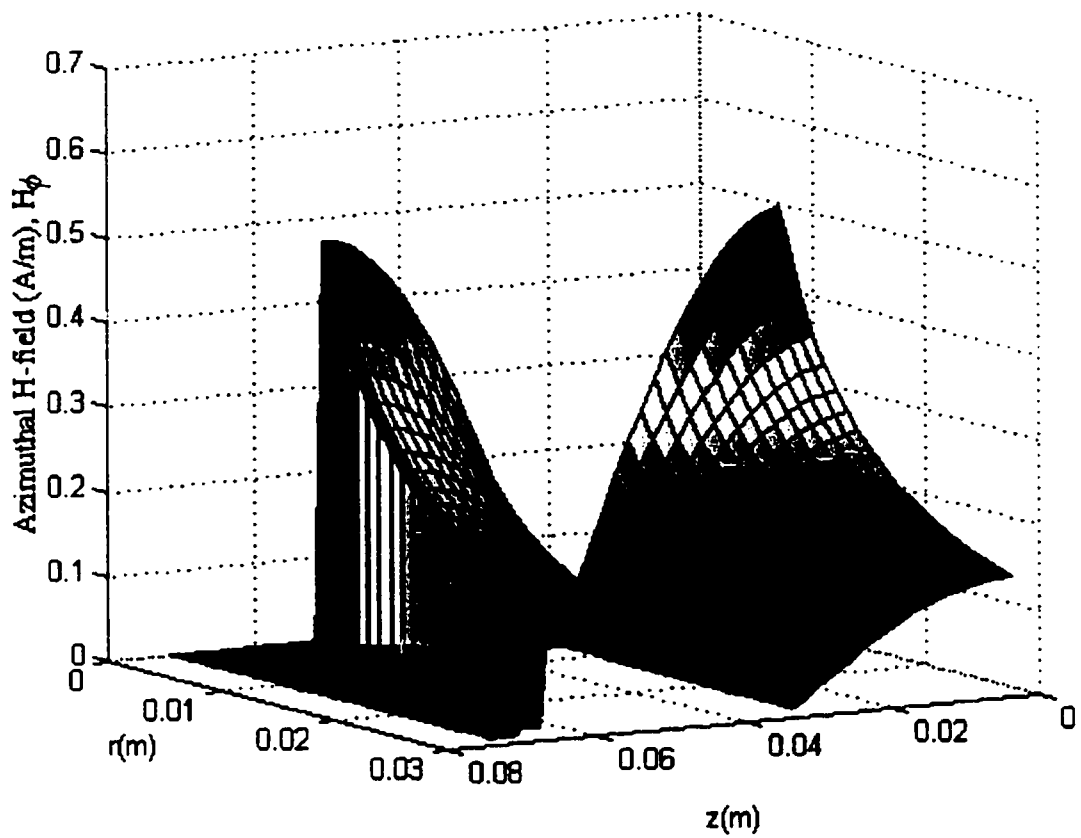


Figure 5.3 A two-dimensional (r, z) plot of the magnitude of the azimuthal magnetic field distribution, H_ϕ , within the empty hybrid coaxial cavity displayed along side a half cavity cross section.

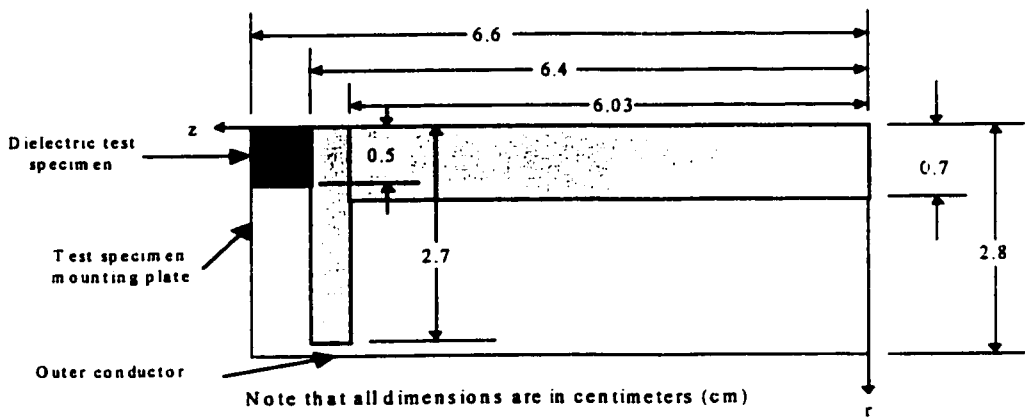
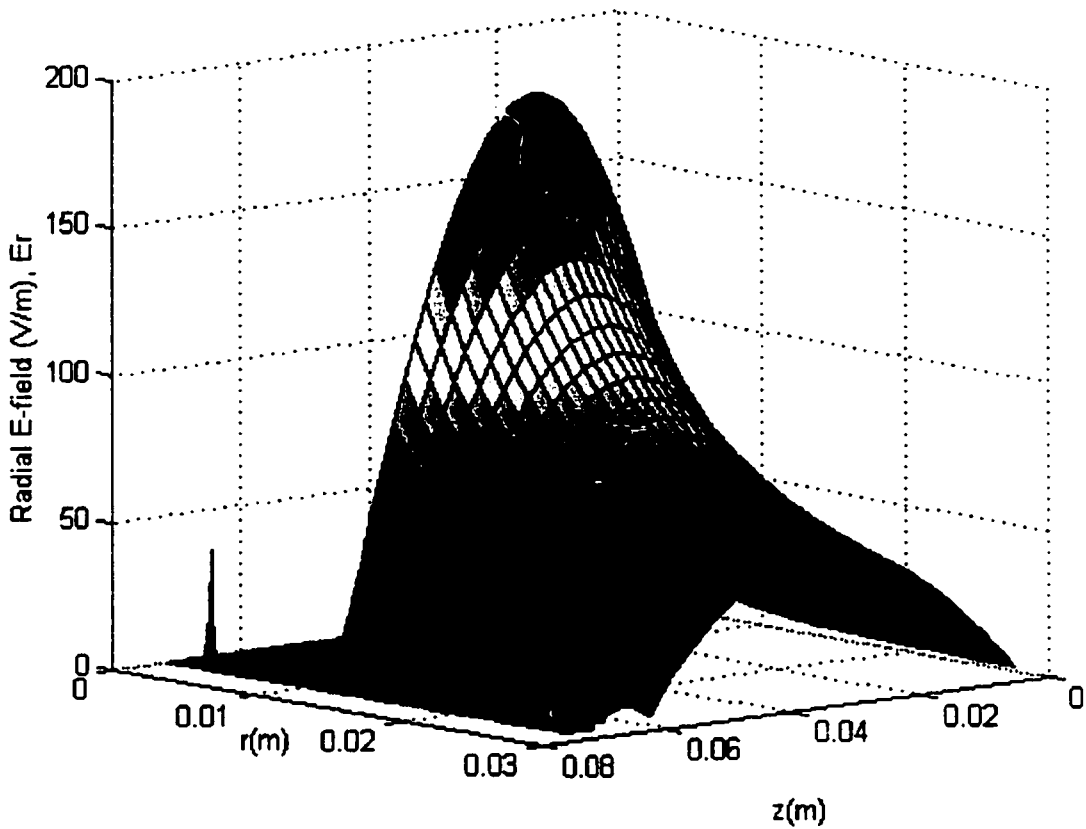


Figure 5.4 A two dimensional (r, z) magnitude plot of the radial electric field distribution, E_r , within the loaded cavity operating in the contact mode containing a material with a relative dielectric constant of $\epsilon_r' = 10$ displayed alongside a half cavity cross-section.

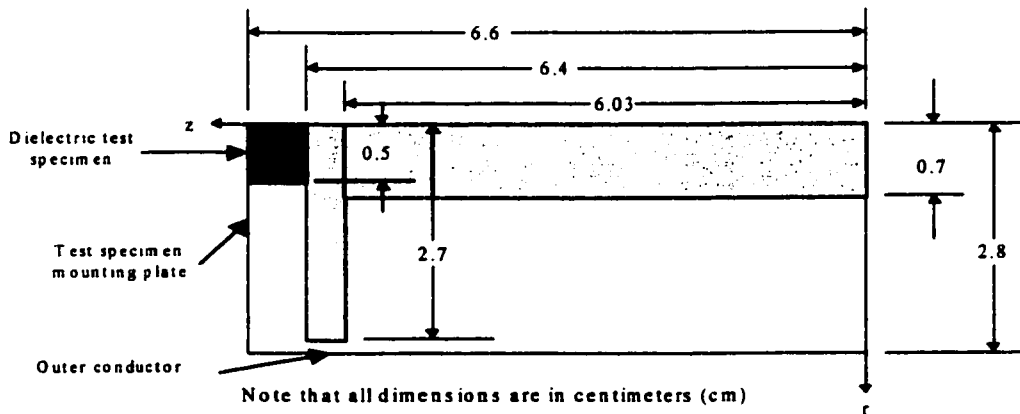
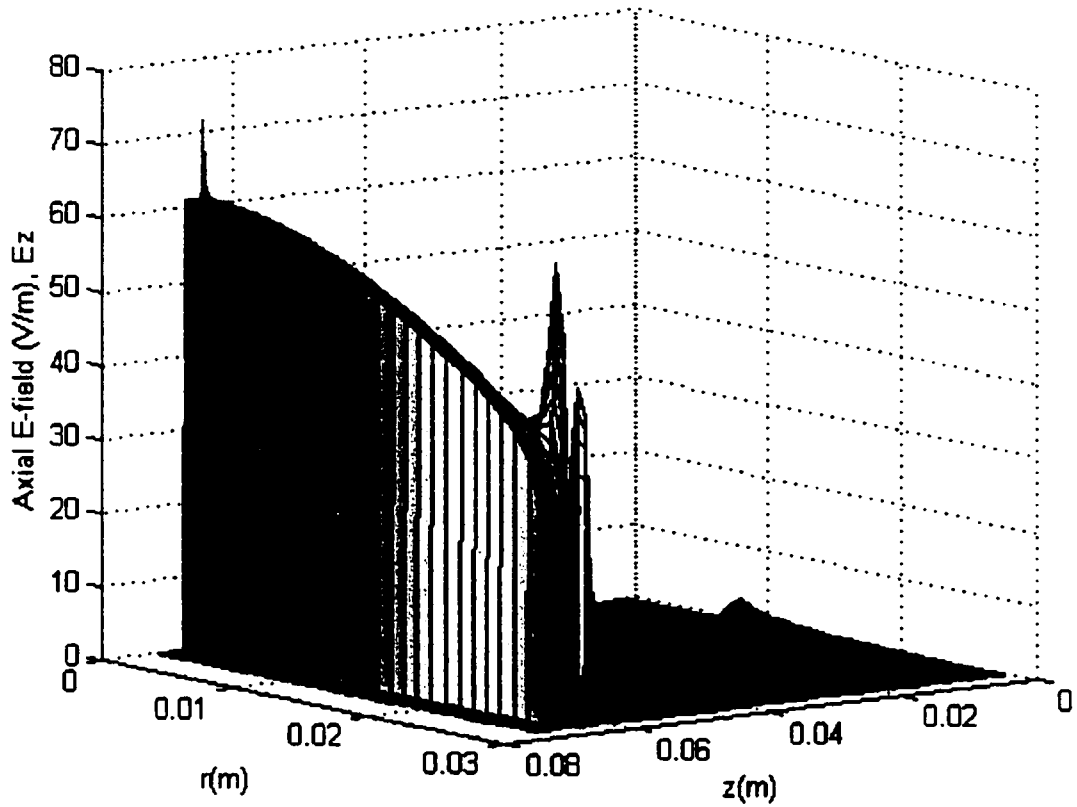


Figure 5.5 A two dimensional (r, z) plot of the magnitude of the axial electric field distribution, E_z , within the loaded cavity operating in the contact mode, containing a material with a relative dielectric constant of $\epsilon_r' = 10$, displayed alongside a half cavity cross-section.

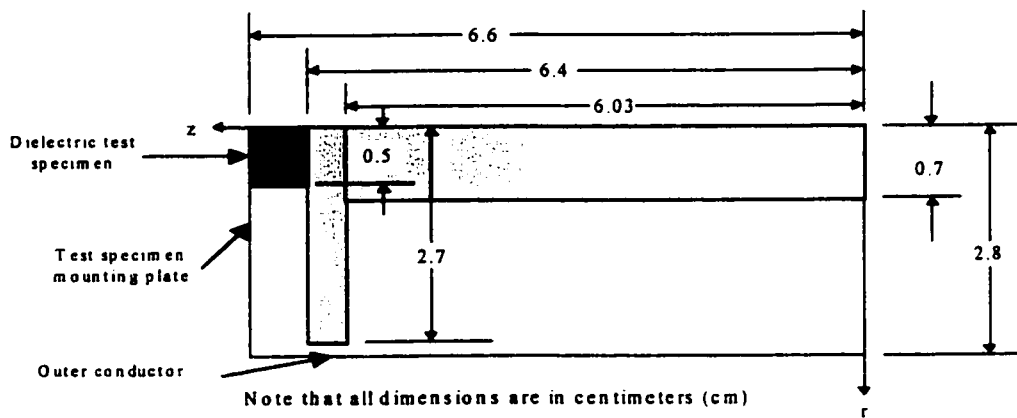
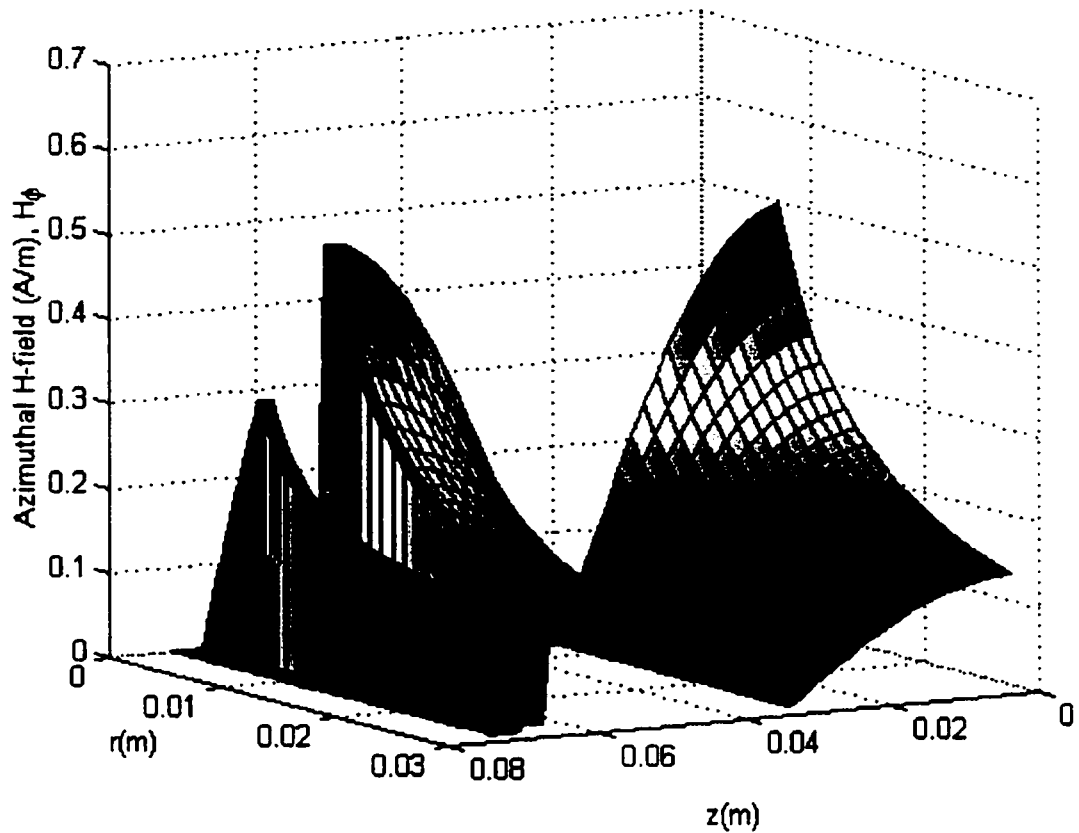


Figure 5.6 A two dimensional (r, z) plot of magnitude of the azimuthal magnetic field distribution, H_ϕ , within the loaded cavity operating in the contact mode containing a material with a relative dielectric constant of $\epsilon_r' = 10$, displayed alongside a half cavity cross-section.

5.3 Empty Cavity Q-factor and Resonant Frequency

From the perturbation arguments derived in Chapter 4, both the empty and loaded cavity Q-factors are required for determining the loss factor of a test specimen. The FDFD program, HERZ, is used to calculate the power dissipation and unloaded Q-factor of the cavity, the results of which are given in Table 5.1. For these calculations, the conductivity of the brass walls is assumed to be $\sigma = 1.1 \times 10^7 (\Omega m)^{-1}$ and the wall currents have a peak value of $I = 22.0$ mA which corresponds to a peak magnetic field of 0.5 A/m at a phase of 0° as described in Section 4.6 of the previous chapter. The HERZ simulation program does not have the capability of accurately modeling the effects of the spring finger contacts or the deleterious effects of the higher order TM_{0n} modes within and surrounding the low impedance coaxial transmission line. Both of these shortcomings of the simulation program cause the calculated power dissipation in the cavity walls to differ from the actual cavity power dissipation value. Conductivity of the cavity walls was not measured and the value in the simulation program corresponds to the manufacturer's specification for the brass used in constructing this cavity. However this conductivity value could vary by up to $\pm 20\%$ (i.e. $0.9 \times 10^7 (\Omega m)^{-1} < \sigma < 1.3 \times 10^7 (\Omega m)^{-1}$). If an uncertainty window of $\pm 20\%$ in calculated unloaded cavity power dissipation and Q-factor is permitted, experimental and numerical results for unloaded cavity Q-factor compare favorably.

Table 5.1 Numerically calculated power dissipation and unloaded Q-factor values for both the unloaded contact and partial contact cavity configurations.

	Unloaded Q-factor (Measured)	Unloaded Q-factor (Theoretical)
Contact mode	≈2800	3247
Partial contact mode	≈2935	3294

As stated in Chapter 4, resonant frequency is determined by finding the frequency at which mean electric stored energy equals mean magnetic stored energy. Thus to determine a cavity's resonant frequency, HERZ computes mean electric and magnetic stored energies at individual frequencies over a predetermined frequency range. At the simulated resonant frequency, the absolute difference between mean electric stored energy and mean magnetic stored energy will be a minimum. To verify the validity of these numerical results, a comparison of numerical and measured resonant frequencies is made in Table 5.2, given below. From these results it is shown that HERZ predicts resonant frequency accurately.

Table 5.2 Numerically calculated and measured resonant frequencies for both the unloaded contact and partial contact cavity configurations.

	Resonant frequency predicted by HERZ, f_0 (GHz)	Measured resonant frequency, f_0 (GHz)	Percent difference (%)
Contact mode	2.436	2.427	0.35
Partial contact mode	2.479	2.479	0.016

5.4 Equations for Dielectric Determination

When a test specimen is inserted into a resonant cavity, its relative dielectric constant, ϵ_r' , and loss tangent, $\tan\delta$, are determined from the loaded cavity's measured resonant frequency shift, Δf_0 , and Q-factor, Q_L respectively. Numerical frequency and Q-factor data for the loaded resonator are generated by the FDFD program, HERZ, for a range of ϵ_r' and $\tan\delta$ values. From these data, least squares polynomial equations are constructed which relate ϵ_r' to Δf_0 and $\tan\delta$ to Q_L , Q_C , F_1 and ϵ_r' for both the contact and partial contact test modes. These equations are:

$$\epsilon_r'(\Delta f_0) = 1 + a_1|\Delta f_0| + a_2|\Delta f_0|^2 + a_3|\Delta f_0|^3 + K \quad (5.5)$$

$$\frac{1}{F_1} = b_0 + b_1\epsilon_r' + b_2(\epsilon_r')^2 + b_3(\epsilon_r')^3 + K \quad (5.6)$$

$$Q_C(\epsilon_r') = Q_0 + c_1\epsilon_r' + c_2(\epsilon_r')^2 + c_3(\epsilon_r')^3 + K \quad (5.7)$$

$$\tan\delta = \left(\frac{1}{F_1}\right)\Delta\left(\frac{1}{Q_0}\right) = \left(\frac{1}{F_1}\right)\Delta\left(\frac{1}{Q_L} - \frac{1}{Q_C}\right) \quad (5.8)$$

where filling factor, F_1 , is defined as the ratio of mean stored electrical energy in the dielectric specimen to that in the test cavity and K represents the higher order terms of the infinite series in Eq. (5.5) through Eq.(5.7).

The coefficients of Eq.(5.5) through Eq.(5.7) are tabulated in Tables 5.3 and 5.4 for both test modes. These numerically generated data are plotted in Figures 5.7 - 5.12 along with the cavity parameters used to determine them.

Utilizing Eqs.(5.5) - (5.8) and the loaded cavity's measured resonant frequency shift, Δf_0 , and Q-factor, Q_L , relative dielectric constant, ϵ_r' , and loss tangent, $\tan\delta$, of a test specimen situated within the cavity can be found. First, to determine a specimen's relative dielectric constant, ϵ_r' , the resonant frequency shift, Δf_0 , of the resonant cavity is measured. Then, this measured value would be used in the appropriate form of Eq.(5.5), depending on test mode utilization, to calculate the specimen's relative dielectric constant. Once the relative dielectric constant is determined, values for Eqs.(5.6) and (5.7) can then be ascertained using the appropriate forms of Eq.(5.6) and Eq.(5.7). In conjunction with the measured cavity Q-factor, Q_L , values found from Eq.(5.6) and Eq.(5.7) are utilized to determine a specimen's loss tangent, via Eq.(5.8).

These calibration equations are incorporated into HPBASIC computer programs (see Chapter 7) that control the measurement and test equipment which serve to measure changes in the test cavity's resonant frequency and Q-factor. From this measured data, the complex dielectric constant of a test specimen is determined.

Table 5.3 Coefficients of the calibration equations for the contact mode.

Equation	Coefficient values						
5.5	a_0 1.0	a_1 7.71E-1	a_2 -2.1E-2	a_3 4.55E-4	a_4 -6.06E-6	a_5 3.53E-8	a_6 0.0
5.6	b_0 1185	b_1 -595.3	b_2 142.82	b_3 -18.96	b_4 1.41	b_5 -5.53E-2	b_6 8.83E-4
5.7	c_0 2800	c_1 -11.35	c_2 -1.5801	c_3 1.3E-2	c_4 -7.9E-3	c_5 -2.38E-4	c_6 1.88E-5

Table 5.4 Coefficients of the calibration equations for the partial contact mode.

Equation	Coefficient values						
5.5	a_0 1.0	a_1 -1.77	a_2 10.61	a_3 -13.91	a_4 9.24	a_5 -3.12	a_6 5.03E-1
5.6	b_0 1363	b_1 -265.7	b_2 59.95	b_3 -5.78	b_4 2.97E-1	b_5 -7.66E-3	b_6 7.77E-5
5.7	c_0 2930	c_1 -5.53	c_2 2.37E-1	c_3 2.39E-2	c_4 -3.33E-3	c_5 1.37E-4	c_6 -1.90E-6

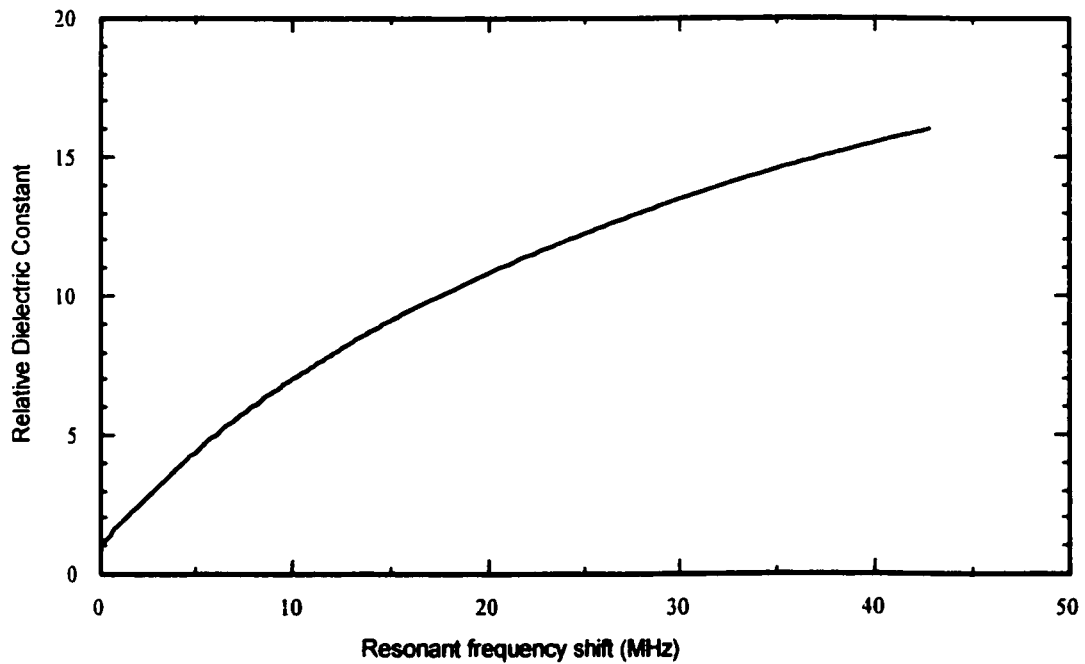


Figure 5.7 Calibration curve for determining relative dielectric constant of a test specimen while the cavity is operated in the contact mode ($f_0 \approx 2.42$ GHz, coaxial center conductor length, $L = 60.2$ mm, test specimen dimensions: $r_4 = 5.0$ mm, $d_1 = 2.0$ mm, see Figure 3.2).

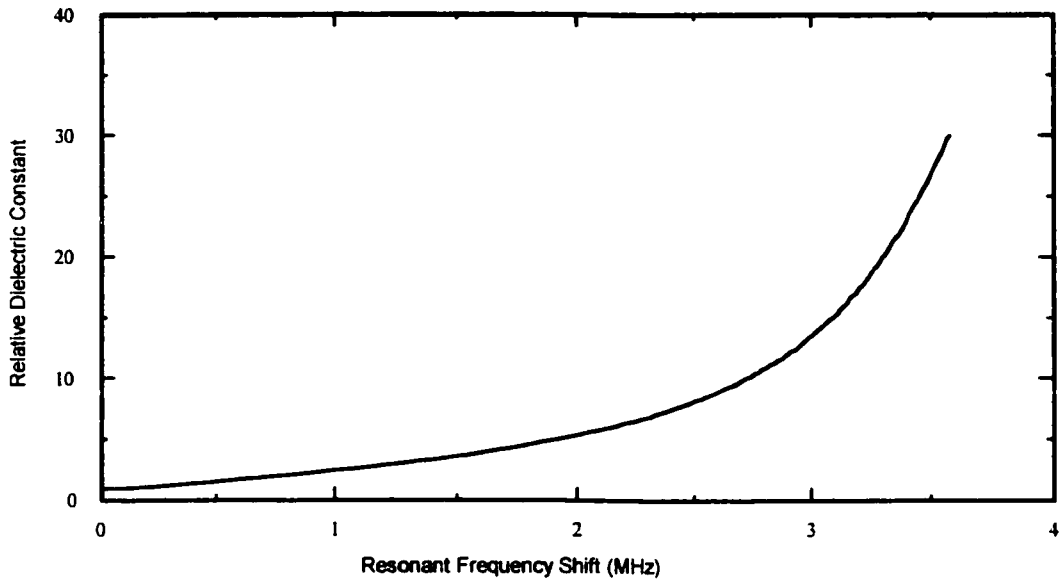


Figure 5.8 Calibration curve for determining relative dielectric constant of a test specimen while the cavity is operated in the partial contact mode ($f_0 \approx 2.48$ GHz, coaxial center conductor length, $L = 59.2$ mm, test specimen dimensions: $r_4 = 5.0$ mm, $d_1 = 2.0$ mm, see Figure 3.2).

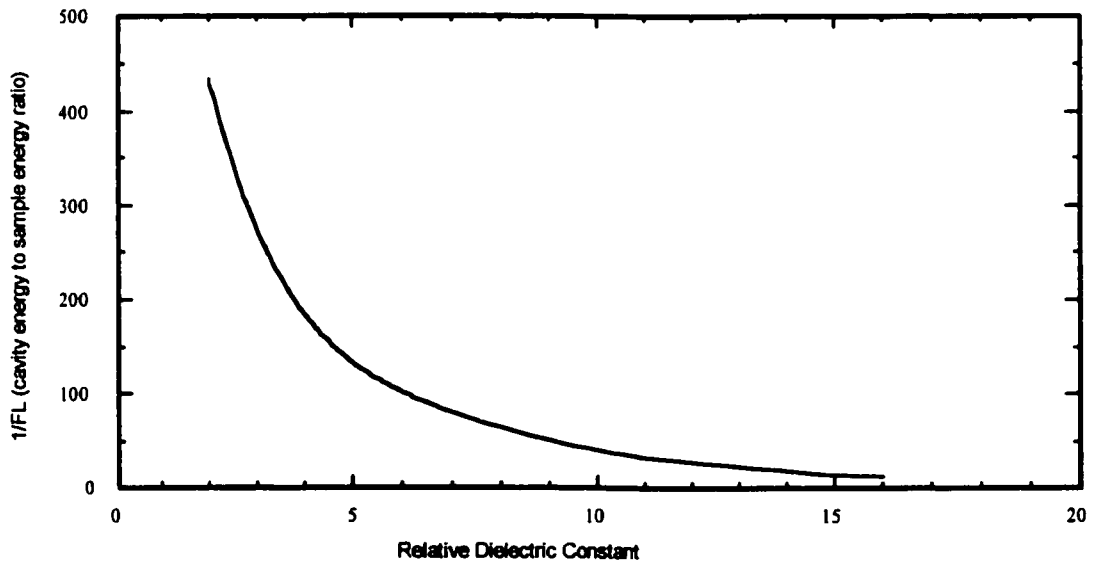


Figure 5.9 Calibration curve for determining the inverse cavity filling factor (F_1)⁻¹ while the cavity is operated in the contact mode ($f_0 \approx 2.42$ GHz, coaxial center conductor length, $L = 60.2$ mm, test specimen dimensions: $r_4 = 5.0$ mm, $d_1 = 2.0$ mm, see Figure 3.2).

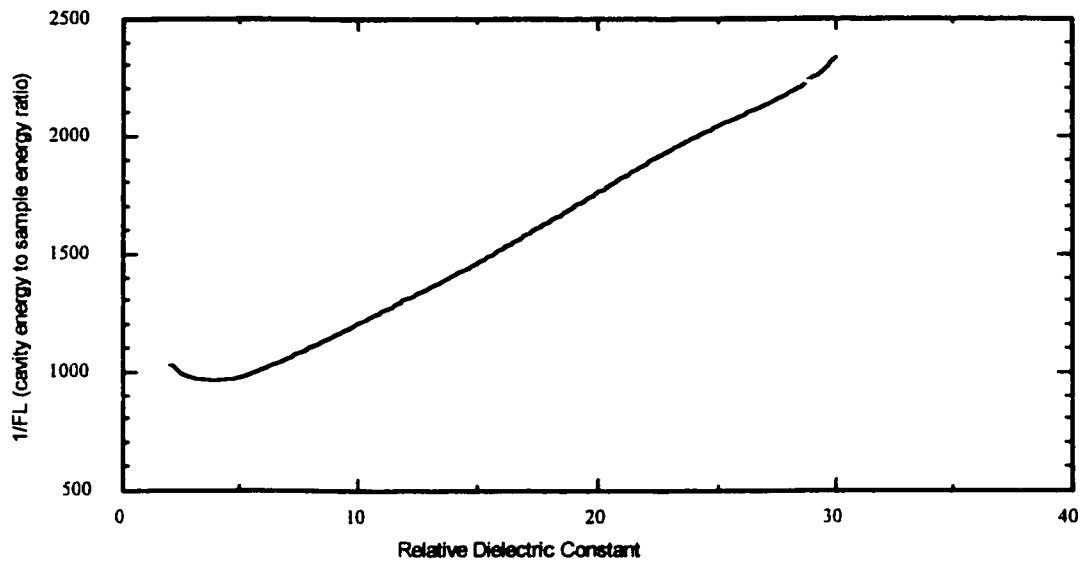


Figure 5.10 Calibration curve for determining the inverse cavity filling factor $(F_i)^{-1}$ while the cavity is operated in the partial contact mode ($f_0 \approx 2.48$ GHz, coaxial center conductor length, $L = 59.2$ mm, test specimen dimensions: $r_4 = 5.0$ mm, $d_1 = 2.0$ mm, see Figure 3.2).

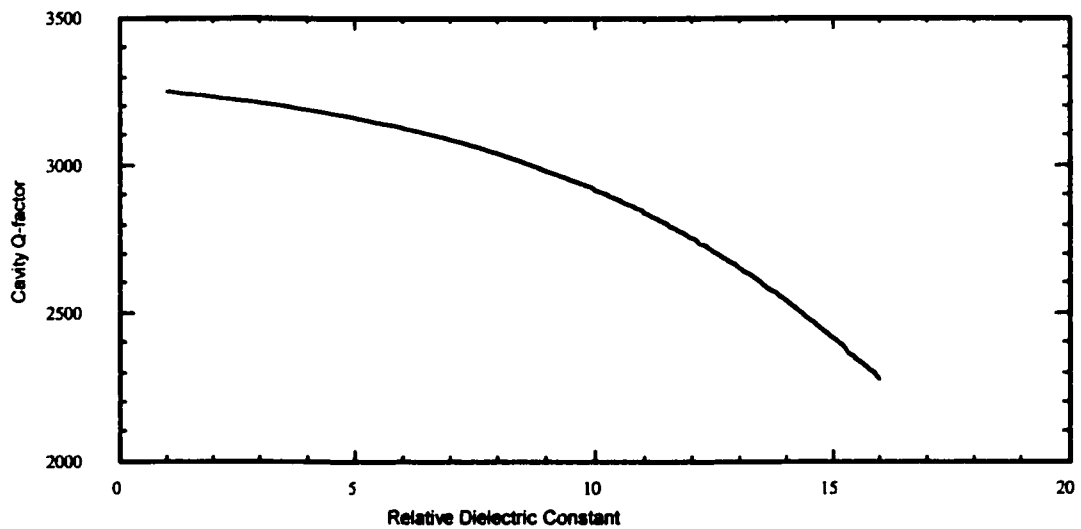


Figure 5.11 Calibration curve for determining cavity Q-factor while testing is performed in the contact mode ($f_0 \approx 2.42$ GHz, coaxial center conductor length, $L = 60.2$ mm, test specimen dimensions: $r_4 = 5.0$ mm, $d_1 = 2.0$ mm, see Figure 3.2). Conductivity of the cavity walls is assumed to be $1.1 \times 10^7 (\Omega\text{m})^{-1}$.

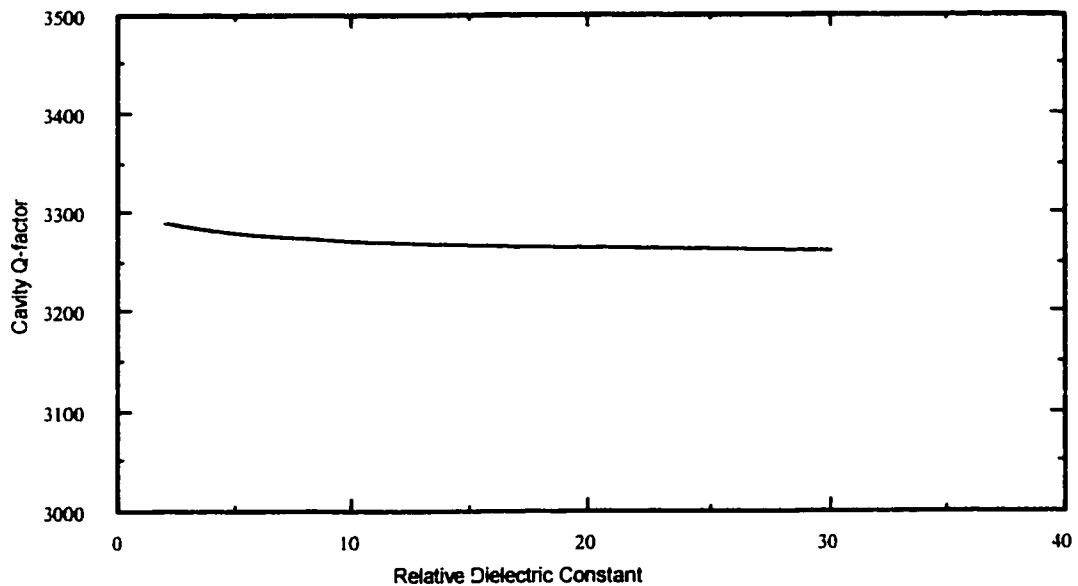


Figure 5.12 Calibration curve for determining cavity Q-factor for testing performed in the partial contact mode ($f_0 \approx 2.48$ GHz, coaxial center conductor length, $L \approx 59.2$ mm, test specimen dimensions: $r_4 \approx 5.0$ mm, $d_1 \approx 2.0$ mm, see Figure 3.2). Conductivity of the cavity walls is assumed to be $1.1 \times 10^7 (\Omega\text{m})^{-1}$.

5.5 Conclusion

Numerically calculated resonant frequencies and empty cavity Q-factors were found and compared to experimental data. Field solutions found from the FDFD program, HERZ compared favorably to analytical solutions found for similar structures. These results give confidence in the HERZ simulation program. Finally, polynomials that relate measured cavity performance to a test specimen's complex dielectric constant have been established.

Now that the resonant field patterns of this cavity have been computed and resonant frequencies and Q-factors of the empty and loaded cavities can be

predicted, measurement limits based on cavity perturbation conditions are determined for this device in the next chapter.

CHAPTER 6

DYNAMIC MEASUREMENT RANGE OF THE DIELECTROMETER

6.1 Introduction

A large dynamic measurement range is achieved through variable geometry of the cavity. In essence two cavity structures are utilized and measurement limits for each loaded cavity geometry are evaluated. The evaluation of the dynamic measurement range of this device is quite involved since all of the following must be considered: mean stored electrical energy in a test specimen, increase in cavity losses caused by the dielectric specimen, frequency sensitivity of the sweep oscillator and effects of the reflectometer's directional couplers. An evaluation that takes into account all of these factors is performed using both numerical and measured results.

6.2 Relative Dielectric Constant Measurement Range

Loaded cavity geometry along with the perturbation condition, $\left| \frac{\Delta f_0}{f_0} \right| < 1\%$, sets the upper limit of measurable dielectric constant for the contact mode. Recall from the perturbation formula Eq.(4.5) that the relative shift in the loaded cavity's resonant frequency is related to the ratio of mean energy stored in the test specimen to that in the test cavity. This energy ratio is calculated within the

FDFD program HERZ and numerical results indicate that to avoid violating this perturbation condition, the maximum measurable relative dielectric constant of a test specimen is $\epsilon_r'_{\max} = 16$.

The upper limit of measurable dielectric constant for the partial contact mode is set solely by the loaded cavity geometry. Introducing an air gap above the test specimen will cause the perturbation of the test cavity to saturate. In other words, there is a limit on the amount of electromagnetic energy a test specimen can store when using the partial contact mode. The perturbation of the test cavity is defined as saturated when this energy storage limit is virtually achieved. Utilizing the simulation program, HERZ, a number of different air gap heights were simulated. For a plate separation of $d_1 = 3.0$ mm (see Figure 3.2) saturation of the cavity perturbation would occur when the relative dielectric constant of a test specimen exceeded $\epsilon_r' \geq 30.0$. Thus, the upper limit of measurable relative dielectric constant for the partial contact mode was set at $\epsilon_r' = 30.0$.

In order to evaluate the minimum measurable relative dielectric constant, $\epsilon_r'_{\min}$, the frequency sensitivity of the sweep oscillator that provides the microwave signal to the test cavity is required. Frequency sensitivity of the sweep oscillator was found to be $\Delta|\Delta f_0| = 0.01$ MHz. The derivative of the polynomial that relates ϵ_r' and Δf_0 must now be evaluated for a test cavity resonant frequency shift of $\Delta f_0 = 0.0$, corresponding to a test specimen of relative

dielectric constant $\epsilon_r' \approx 1.0$, and for the aforementioned frequency sensitivity value, $\Delta|\Delta f_0| = 0.01$ MHz. For these conditions, the uncertainty in measured relative dielectric constant for the contact mode is $\Delta\epsilon_r' = 0.03$ and $\Delta\epsilon_r' = 0.05$ for the partial contact mode. Thus, the minimum relative dielectric constant measurable in the contact mode is $\epsilon_r'_{\min} = 1.03$ and $\epsilon_r'_{\min} = 1.05$ for the partial contact mode.

6.3 Loss Factor or Loss Tangent Measurement Range

6.3.1 Minimum Measurable Loss Tangent

A loaded test cavity's minimum measurable loss tangent is set by the specimen's filling factor, F_1 (a ratio of the mean electrical energy stored in the test specimen to that stored in the test cavity), on the test cavity, Q measurement uncertainty, $\frac{\partial Q}{Q}$, and as will be shown, the empty cavity Q -factor, Q_0 . Analysis of the loaded cavity's lower loss limit, $\tan\delta_{\min}$, will begin by determining when the Q change caused by the test specimen's dielectric loss, namely,

$$\Delta\left(\frac{1}{Q}\right) \approx \left(\frac{1}{Q_L} - \frac{1}{Q_0}\right) \approx \frac{1}{Q_0} \quad (6.1)$$

is approximately equivalent to the Q -measurement uncertainty

$$\Delta\left(\frac{1}{Q}\right) \approx \frac{1}{Q_0 - \partial Q} - \frac{1}{Q_0} \approx \frac{1}{Q_0} \left(\frac{\partial Q}{Q}\right) \quad (6.2)$$

where $\frac{\partial Q}{Q}$ is the relative error in the Q measurement.

Equating Eq.(6.1) and Eq.(6.2) gives

$$\frac{Q_0}{Q_D} = \frac{\delta Q}{Q} \quad (6.3).$$

From perturbation theory, the Q-factor of a dielectric specimen in a resonant cavity [8] is given by

$$\frac{1}{Q_D} = F_1 \tan \delta \quad (6.4)$$

Placing the results of Eq.(6.4) into Eq.(6.3) results in

$$Q_0 F_1 \tan \delta = \frac{\delta Q}{Q} \quad (6.5)$$

Therefore, a minimum loss tangent can be defined as

$$\tan \delta_{(\min)} = \frac{1}{Q_0 F_1} \left(\frac{\delta Q}{Q} \right)_{\min} \quad (6.6)$$

In order to evaluate Eq.(6.6), values for empty cavity Q-factor, Q_0 , cavity filling factor, F_1 , and Q-measurement uncertainty, $\frac{\delta Q}{Q}$, are required. The empty cavity Q-factor is measured from the cavity's frequency response. Typical Q-factor values are 2900 and 2800 for the partial contact mode and contact mode, respectively. The cavity filling factor, F_1 , is a function of the test specimen's relative dielectric constant, i.e. $F_1(\epsilon_r')$. Filling factor values for both test modes are calculated with the FDFD program HERZ. Typical values are provided in Table 6.1, note the larger values for the contact mode as compared to the partial contact mode. Q-measurement uncertainty, $\frac{\delta Q}{Q}$, is dependent upon both the directivities

of the directional couplers used in the reflectometer and the magnitude of the measured reflection coefficient of the cavity's input port at its resonant frequency [8, 60]. For given coupler directivities, $D = 30$ dB and $D = 40$ dB, an analysis of Q-measurement uncertainty, $\frac{\partial Q}{Q}$, as a function of the magnitude of the cavity's input port reflection coefficient at f_0 was performed by Xi [8] and these results, see Figure 6.1, were used to calculate values for Eq.(6.6). When testing a low loss specimen, the loaded cavity's reflection coefficient at f_0 was approximately $|\Gamma| \approx 0.2$. This value was selected since cavity loading on the feed-line remained virtually unchanged from the empty cavity condition when low loss specimens were tested. Utilizing Figure 6.1, Table 6.1, Eq.(6.6) and the unloaded Q-factors previously given, minimum loss tangent values for various relative dielectric constants were calculated and are listed in Table 6.2.

Table 6.1 Filling factor as a function of relative dielectric constant for both the contact and partial contact modes.

	F_1 (Contact mode)	F_1 (Partial contact mode)
$\epsilon_r' = 2$	2.3×10^{-3}	9.68×10^{-4}
$\epsilon_r' = 8$	15.74×10^{-3}	9.09×10^{-4}
$\epsilon_r' = 16$	77.99×10^{-3}	6.55×10^{-4}
$\epsilon_r' = 30$	N/A	4.29×10^{-4}

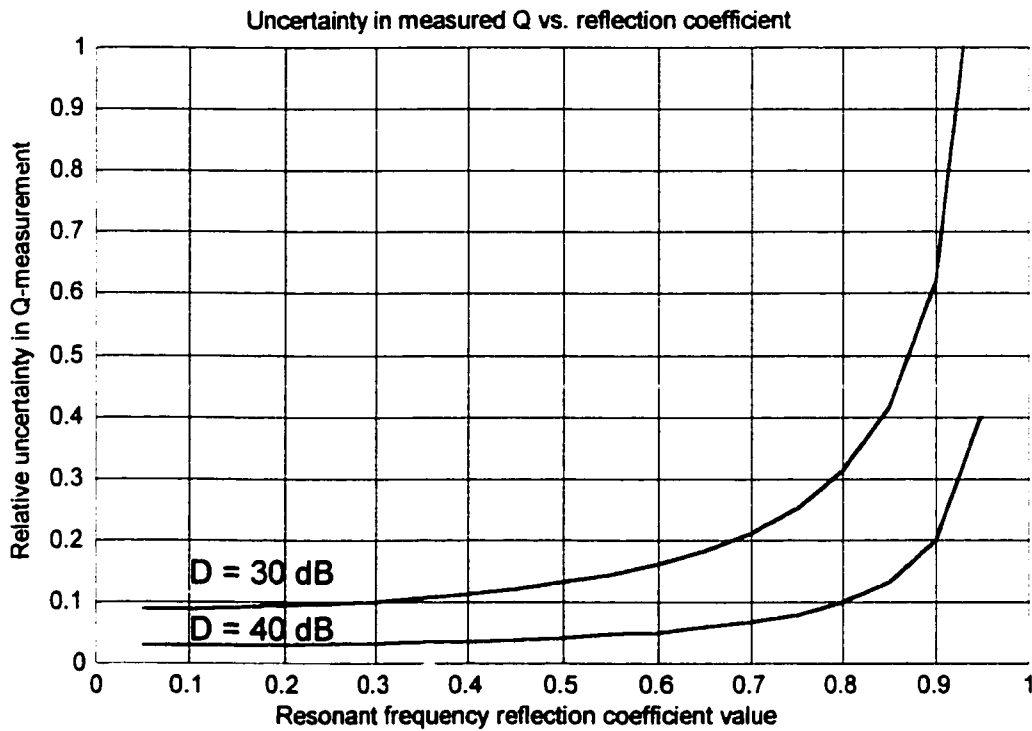


Figure 6.1 Relative error in measured Q-factor versus the reflection coefficient, $|\Gamma_0|$, at the resonant frequency for a reflectometer directivity of D = 30 and 40 dB.

6.3.2 Maximum Measurable Loss Tangent

In order to determine the maximum measurable loss tangent, $\tan\delta_{max}$, it is first necessary to relate the loaded cavity Q-factor, Q_0 , to the unloaded cavity Q-factor, Q_w , via the test cavity's coupling coefficient or normalized input impedance, \bar{R} . Following an analysis similar to Xi [8], these quantities are related in the following manner.

Assume a resonant cavity with an input impedance of $Z(f_0) = Z_0$ is connected to a transmission line of characteristic impedance $Z = Z_0$. The loaded

circuit Q-factor, Q_{LC} , the transmission line Q-factor, Q_{EXT} , and the cavity Q-factor, Q_0 , are related by

$$\frac{1}{Q_{LC}} = \frac{1}{Q_{EXT}} + \frac{1}{Q_0} \quad (6.7).$$

Since the input impedance of the cavity at its resonant frequency is equivalent to the characteristic impedance of the transmission line, we have a matched condition and the transmission line Q-factor, Q_{EXT} , is equivalent to the cavity Q-factor, Q_0 , i.e.,

$$Q_0 = Q_{EXT} \quad (6.8)$$

and Eq.(6.7) can be re-written in the following form

$$\frac{1}{Q_{LC}} = \frac{2}{Q_0} \quad (6.9)$$

or alternatively

$$Q_0 = 2Q_{LC} \quad (6.10).$$

Now suppose a lossy dielectric specimen is inserted into the resonant cavity. The cavity Q-factor, Q_0 , now takes the form

$$\frac{1}{Q_0} = \frac{1}{Q_w} + \frac{1}{Q_D} \quad (6.11)$$

where Q_w is the Q-factor resulting from wall losses within the cavity and Q_D is the Q-factor considering dielectric losses. With the insertion of the lossy dielectric, the cavity's input impedance is no longer equivalent to the transmission line's characteristic impedance. To find the cavity's input

impedance at resonance, an equivalent circuit analog is used. Eq.(6.11) is re-written in the following form

$$\frac{1}{Q_0} = \frac{Z_0}{\omega_0 L} + \frac{R_D}{\omega_0 L} \quad (6.12)$$

where a series resonance is assumed, ω_0 is the resonant frequency in radians, L is the equivalent inductance, Z_0 is the resistance of the unloaded resonant circuit and R_D is the resistance of the dielectric load. Re-writing Eq.(6.12) by normalizing R_D by Z_0 results in

$$\frac{1}{Q_0} = \frac{Z_0}{\omega_0 L} (1 + \bar{R}_D) \quad (6.13)$$

where $\bar{R}_D = \frac{R_D}{Z_0}$.

Now redefine the wall loss Q-factor value, Q_w , and one can obtain the following relationship

$$\frac{1}{Q_w} = \frac{Z_0}{\omega_0 L} \quad (6.14).$$

Placing the result from Eq.(6.14) into Eq.(6.13), it follows that

$$\frac{1}{Q_0} = \frac{1}{Q_w} (1 + \bar{R}_D) \quad (6.15).$$

Eq.(6.15) can be rewritten in the following form

$$\frac{1}{Q_0} = \frac{\bar{R}}{Q_w} \quad (6.16)$$

where \bar{R} is the normalized input impedance of the loaded resonant cavity given by

$$\bar{R} = \bar{R}_D + 1 \quad (6.17).$$

A resonant cavity with $\bar{R} > 1.0$ is defined as being over-coupled to its feed line, as is the case described in Eq.(6.17). An analogous result to Eq.(6.16) for parallel resonance is given by

$$\frac{1}{Q_0} = \frac{1}{RQ_w} \quad (6.18)$$

where \bar{R} is described by

$$\bar{R} = \frac{\bar{R}_D}{\bar{R}_D + 1} \quad (6.19).$$

A resonant cavity with $\bar{R} < 1.0$ is defined as being under-coupled to its feed line, as is the case described in Eq.(6.19).

Eq.(6.16) and Eq.(6.18) can be used for relating the empty cavity Q-factor, Q_w , to the loaded cavity Q-factor, Q_0 , for the cases when the loaded cavity is either under-coupled or over-coupled to its feed line. For the over-coupled case, empty cavity Q-factor is related to the loaded cavity Q-factor [8] by

$$Q_w = \bar{R}Q_0 \quad (6.20).$$

Conversely for the under-coupled case, empty and loaded cavity Q-factors are related [8] by

$$Q_w = \frac{Q_0}{\bar{R}} \quad (6.21).$$

As a result of the cavity geometry utilized for our dielectrometer, the loaded test cavity is under-coupled to its feed line. Thus utilizing Eq.(6.11) in

Eq.(6.21) values for the maximum measurable loss tangent, $\tan\delta_{\max}$, of a test specimen can be found as follows

$$\bar{R} = \frac{Q_o}{Q_w} = \frac{1}{Q_w \left(\frac{1}{Q_w} + \frac{1}{Q_D} \right)} = \frac{1}{1 + \frac{Q_w}{Q_D}} \quad (6.22).$$

The cavity's input port reflection coefficient, $|\Gamma_o|$, at its resonant frequency can then be expressed in terms of $\frac{Q_w}{Q_D}$ as

$$|\Gamma_o| = \frac{1 - \bar{R}}{1 + \bar{R}} = \frac{\frac{Q_w}{Q_D}}{\frac{Q_w}{Q_D} + 2} \quad (6.23).$$

Utilizing Eq.(6.4) the Q-factor ratio, $\frac{Q_w}{Q_D}$, can be written in the following form

$$\frac{Q_w}{Q_D} = Q_w F_1 \tan\delta \quad (6.24).$$

For a given maximum Q-factor ratio, $\left(\frac{Q_w}{Q_D} \right)_{\max}$, Eq. (6.24) can be re-written as

$$\tan\delta_{\max} = \frac{\left(\frac{Q_w}{Q_D} \right)_{\max}}{Q_w F_1} \quad (6.25).$$

At this point, it is necessary to select the maximum value of the Q-factor ratio, $\left(\frac{Q_w}{Q_D} \right)_{\max}$. To maintain reasonable accuracy in loss tangent measurements,

say, $\frac{\Delta \tan\delta}{\tan\delta} < 10\%$ when $D = 40$ dB, a maximum reflection coefficient value of

$|\Gamma_0|_{\max} = 0.5$ is selected. This value corresponds to a maximum Q-factor ratio,

$$\left(\frac{Q_w}{Q_D}\right)_{\max}, \text{ of } \left(\frac{Q_w}{Q_D}\right)_{\max} \leq 2.0.$$

Utilizing Table 6.1, Eq.(6.25) and the unloaded cavity Q-factors previously given, maximum loss tangent values for various relative dielectric constants were calculated and are listed in Table 6.2.

Table 6.2 Loss tangent limits as a function of relative dielectric constant.

	CONTACT MODE		PARTIAL CONTACT MODE	
	$\tan\delta_{\min}$	$\tan\delta_{\max}$	$\tan\delta_{\min}$	$\tan\delta_{\max}$
$\epsilon_r' = 2$	0.004	0.386	0.0089	0.72
$\epsilon_r' = 8$	0.0006	0.060	0.0088	0.77
$\epsilon_r' = 16$	0.0001	0.093	0.0132	1.05
$\epsilon_r' = 30$	N/A	N/A	0.0202	1.63

6.3.3 Discussion

From values calculated utilizing Eq.(6.6) and Eq.(6.25) there is a range of loss tangent values, $0.0088 < \tan\delta < 0.386$, over which either test mode can be used. In order to determine which test mode to employ, a test specimen whose loss tangent falls into this range must be tested using both the contact and partial contact modes. Resonant frequency reflection coefficient values for both loaded cavity configurations are then compared. To obtain accurate measurement results, the test mode that has the smaller reflection coefficient value at the

loaded cavity's resonant frequency must be utilized. Application of this rule has the advantage of maintaining accurate measurement results for a large range of loss values because relatively large Q-factors are maintained while the magnitude of the normalized input impedance of the resonant cavity remains close to unity.

6.4 Conclusion

For our dielectrometer the relative dielectric constant and loss tangent measurement limits have been evaluated. The relative dielectric constant measurement range is $1.03 < \epsilon'_r < 30.0$ and the loss tangent measurement range is $0.0001 < \epsilon''_r < 1.63$. The design goal of attaining four orders of magnitude in loss tangent measurement range has been achieved with the constraint of using an adjustable cavity geometry.

CHAPTER 7

MEASUREMENT PROCEDURES AND RESULTS

7.1 Introduction

In this chapter a description of the algorithms used in the data acquisition computer program are given. The test specimen and dielectrometer calibrations are described. To verify the dielectric measurement method proposed, the measured dielectric properties of four commercial materials are presented. Then elevated temperature permittivity measurement procedures are outlined. Finally, new dielectric data for five rubber materials is presented and discussed.

7.2 Measuring Cavity Frequency Response

In order to measure the cavity's resonant frequency and Q-factor and hence calculate the complex dielectric constant of a test specimen, an HPBASIC computer program was used to control the reflectometer. The HPBASIC program set the frequency band and the sweep time of an HP87352A synthesized sweeper. It also controlled many internal settings of an HP8757D scalar network analyzer. A description of how to determine the cavity's resonant frequency and Q-factor accurately is given below.

7.2.1 Resonant Frequency and Q-factor Determination

To find a value of the loaded cavity's resonant frequency, 15 consecutive resonant frequency measurements were averaged. This procedure reduces frequency uncertainty caused by short-term drift of the frequency synthesizer.

In order to improve Q-factor measurement repeatability and accuracy, the multiple bandwidth measurement method was utilized. Cavity Q-factors were measured utilizing five different bandwidths. This procedure reduces Q-factor measurement uncertainty resulting from an asymmetric resonance curve (dispersion), the frequency uncertainty caused by short-term drift of the synthesizer and return loss measurement uncertainty caused by the reflectometer.

In order to determine the empty or loaded cavity Q-factor utilizing multiple bandwidths, the following methodology was used. The general loaded cavity Q-factor, Q_L , [61] is given by

$$Q_L = \alpha \frac{f_0}{\Delta f} (1 + \bar{R}) \quad (7.1)$$

where \bar{R} is the normalized input impedance of the cavity at resonance. It is determined from the measured reflection coefficient value at the cavity's resonant frequency in the following manner

$$\bar{R} = \frac{1 - |\Gamma_0|}{1 + |\Gamma_0|} \quad (7.2)$$

Δf is the bandwidth between power reflection points and α is termed the bandwidth parameter [61], and is given by

$$\alpha = \sqrt{\frac{|\Gamma_{pp}|^2 - |\Gamma_o|^2}{1 - |\Gamma_{pp}|^2}} \quad (7.3)$$

where $|\Gamma_{pp}|$ is the magnitude of the cavity's complex reflection coefficient at the power points of interest and is described by

$$|\Gamma_{pp}|^2 = x(1 + |\Gamma_o|^2) \quad (7.4)$$

where x is the power reflection ratio. Values of x are selected based upon both a given $|\Gamma_o|$, and the analysis of Q-factor uncertainty as a function of $|\Gamma_{pp}|$ (see Appendix 2). Based on this uncertainty analysis, values of x are chosen so that uncertainty in averaged Q-factor, $(Q_L)_{ave}$, is minimized. In Table 7.1, x values are listed for a range of resonant frequency return loss values.

Table 7.1 Power reflection ratios utilized in calculating cavity Q-factor.

Return Loss Value at the Cavity's Resonant Frequency (dB)	Power reflection ratio (x)				
	1	2	3	4	5
>15 ($ \Gamma_o < 0.178$)	0.1	0.25	0.5	0.75	0.9
15 > RL > 10 ($0.178 > \Gamma_o > 0.316$)	0.25	0.4	0.5	0.6	0.75
10 > RL > 3 ($0.316 > \Gamma_o > 0.707$)	0.4	0.45	0.5	0.55	0.6

Q-factors were measured three times for each of the five bandwidths and a weighted average of the measured data was then calculated. The weighted Q-factor value was determined by

$$(Q_L)_{ave} = \frac{\sum_{i=1}^{15} n_i (Q_L)_i}{\sum_{i=1}^{15} n_i} \quad (7.5)$$

where $(Q_L)_i$ is one of the fifteen individual Q-factor measurements and n_i is the weighting factor.

The weighting factor, n_i , is used to improve Q-factor measurement accuracy, when using the multiple bandwidth method. Analyzing Q_L uncertainty as a function of $|\Gamma_{pp}|$ the following observations are made (see Appendix 2). In practice, high accuracy Q-factor measurements are made using the half-power bandwidth. Conversely, when the reflection coefficient value used for determining bandwidth, $|\Gamma_{pp}|$, approaches either the resonant frequency reflection coefficient value, $|\Gamma_0|$, or unity, Eq.(7.1) tends to critical values and uncertainty in Q-factor, Q_L , tends to infinity. Thus the weighting factor, n_i , is selected to be maximum at the half power points and decreases to zero as the reflection coefficient value used for determining bandwidth, $|\Gamma_{pp}|$, approaches either the resonant frequency reflection coefficient value, $|\Gamma_0|$, or unity. Thus a simple weighting function that meets these criteria is given by

$$n_i(|\Gamma_{pp}|) = 1 - |\Gamma_0|^2 - 2 \left| \frac{(1 + |\Gamma_0|^2)}{2} - |\Gamma_{pp}|^2 \right| \quad (7.6)$$

The major advantage of this approach is that high accuracy Q-factors are weighted heavily while low accuracy Q-factors are weighted lightly thus yielding more accurate averaged Q-factors.

7.3 Test Specimen and Dielectrometer Calibration

7.3.1 Test Specimen Size

Nominal test specimen dimensions were $r = 5.0\text{mm}$ and $t = 2.0\text{mm}$. The maximum allowable variation in the volume of the test specimen was 5%. Test specimen thickness should be within $\pm 0.5\%$ of the nominal thickness, while its radius should be within $\pm 2.0\%$ of the nominal radius.

7.3.2 HPBASIC Calibration Programs

In the next section, three HPBASIC programs, CAL, CAL1 and CAL2, are used for calibration of the dielectrometer. The HPBASIC program, CAL, is used only for measuring the resonant frequency and Q-factor of the unloaded cavity. CAL1 is used only for measuring the changes in the cavity's resonant frequency and Q-factor between the unloaded and loaded cavity conditions. The HPBASIC program, CAL2, calculates a test specimen's complex relative dielectric constant,

for only the constant temperature condition. Common operational characteristics of each of the three HPBASIC programs include:

1. Each program prompts the user to choose the number of resonant frequency and Q-factor measurement combinations that are made while the program runs. One measurement combination is one resonant frequency and Q-factor measurement.
2. Between consecutive measurement combinations, the program pauses and awaits user permission to continue running.
3. After the last resonant frequency and Q-factor measurement combination, the program terminates.

7.3.3 Dielectrometer Calibration

After having set up the measurement and heating system as described by the block diagram of Figure 3.1, the following steps should be taken before dielectric measurements over a temperature range are performed on a test specimen.

1. Warm-up test equipment for at least an hour and a half to stabilize the R.F. oscillator.
2. Calibrate reflectometer with a short circuit.
3. Run HPBASIC calibration program, CAL, keeping the half wavelength coaxial resonator fixed to the specimen mounting plate until the calibration program terminates running.

- a. Verify from measurement results that resonant frequency stability is within $\pm 0.005\text{MHz}$ and that the Q factor stability is within 1%.
 - b. The number of averaged resonant frequency and Q-factor combinations determined during one program run should be between five and ten.
4. If the resonant frequency and Q-factor stability requirements have not been achieved, allow test equipment to warm up for an additional 15 minutes and then repeat Step 2.
5. Repeat steps 2 and 3 for the following case. Before running calibration program, CAL, remove the half wavelength coaxial resonator from the base of the test specimen mounting plate (see Figure 3.2), then replace the coaxial resonator on the mounting plate. Begin running calibration program, CAL, to determine averaged resonant frequency and Q-factor. After the first measurement combination is made, remove the coaxial resonator from the mounting plate and then replace the resonator on the mounting plate. Allow the calibration program to continue running to determine the second measurement combination. Repeat this process until the calibration program terminates running.
6. Run the HPBASIC program, CAL1, for measuring resonant frequency and Q-factor of a cavity loaded with a commercial dielectric. The

number of measurement combinations should be equivalent to the number of calibration dielectric test specimens available.

a. For calibration specimens with similar dielectric constants, resonant frequency stability should be within $\pm 0.15\text{MHz}$, and Q-factor stability should be within 1.0%. A larger resonant frequency shift uncertainty is permitted since the calibration specimens utilized vary in volume by $\pm 5\%$.

7. Run the HPBASIC program, CAL2, for measuring the dielectric properties of calibration dielectric test specimens. The number of measurement combinations should be equivalent to the number of calibration dielectric test specimens available.

a. Resulting dielectric data should be within 3.0% of their values specified by the manufacturer and measured loss tangent should be less than the specified limit of $\tan \delta < 0.002$ (contact mode) or $\tan \delta < 0.02$ (partial contact mode).

b. If these conditions are not met return to Step 2 and begin dielectrometer calibration again.

8. Once the system is calibrated, place insulation around the cavity. Once this is done, elevated temperature dielectric testing can be performed.

7.4 Verification of Dielectric Measurement Technique

To verify the dielectric measurement method presented in this thesis, dielectric properties of commercial materials were measured at room temperature. Results are listed in Tables 7.2 and 7.3, along with data specified by the manufacturer for comparison.

Table 7.2 Dielectric data for Eccosorb HiK500 materials measured using the contact mode and dielectric data specified by the manufacturer.

Material name	Eccosorb HiK500 K4	Eccosorb HiK500 K8	Eccosorb HiK500 K12
$(\epsilon_r')_{\text{measured}}$	4.00 ± 0.03	8.00 ± 0.15	12.1 ± 0.2
$(\epsilon_r')_{\text{specified}}$	$4.00 \pm 3\%$	$8.00 \pm 3\%$	$12.00 \pm 3\%$
$(\tan \delta)_{\text{measured}}$	<0.001	<0.0006	<0.00013
$(\tan \delta)_{\text{specified}}$	<0.002	<0.002	<0.002

Table 7.3 Dielectric data for Eccosorb HiK500 materials measured using the partial contact mode and dielectric data specified by the manufacturer.

Material name	Eccosorb HiK500 K4	Eccosorb HiK500 K8	Eccosorb HiK500 K12	Eccosorb HiK500 K20
$(\epsilon_r')_{\text{measured}}$	4.1 ± 0.5	7.9 ± 0.2	12.1 ± 0.2	20.5 ± 1.5
$(\epsilon_r')_{\text{specified}}$	$4.00 \pm 3\%$	$8.00 \pm 3\%$	$12.00 \pm 3\%$	$20.0 \pm 10\%$
$(\tan \delta)_{\text{measured}}$	<0.009	<0.009	<0.01	<0.015
$(\tan \delta)_{\text{specified}}$	<0.002	<0.002	<0.002	<0.002

The commercial Eccosorb materials are a solid ceramic and they have the following dielectric properties, $\epsilon_r' = 4, 8, 12, 20$ and $\tan \delta < 0.002$. The discrepancy in measured relative dielectric constant between this work and data supplied by the manufacturer, was less than 3% for materials with dielectric constants of $\epsilon_r' = 4, 8$ and 12 and less than 10% for the material with a relative dielectric constant of $\epsilon_r' = 20$.

It was not possible to measure the Eccosorb materials' specific loss tangent values since the dielectrometer did not have the necessary Q-factor measurement sensitivity. However when tested in the contact mode, maximum loss tangent values found for Eccosorb materials' K4, K8 and K12 were less than the maximum values specified by the manufacturer. Thus, the loss tangent measurement approach used for the contact mode is validated. For the partial contact mode, minimum measurable loss tangents exceeded the maximum values specified for each of the Eccosorb materials. Thus, a systematic validation of the loss tangent measurement approach for the partial contact mode was not possible using these materials.

7.5 Elevated Temperature Permittivity Measurement Procedure

Two HP BASIC programs, RUBDIELA (partial contact mode) and RUBDIELB (contact mode) running on an HP200 computer controlled the swept frequency reflectometer. The basic procedure for measuring a test specimen's complex dielectric constant over temperature must follow the steps outlined below;

- (1) calibrate the reflectometer by replacing the cavity with a coaxial short circuit;
- (2) measure the empty cavity's resonant frequency and Q-factor, and insure that the measurement of each of these parameters is repeatable;

- (3) heat the cavity containing the test specimen and measure the resonant frequency shift and loaded cavity Q-factor at each temperature set point assigned;
- (4) calculate the dielectric properties of the test specimen from the measured changes in resonant frequency and Q-factor between the empty and loaded cavity conditions.

7.6 Elevated Temperature Dielectric Measurements

In this section, measured dielectric properties of the five Royalene rubber materials over the temperature range of 20°C to 120°C are given. Before these results are presented, however, changes in resonant frequency and Q-factor caused by cavity heating are given in a graphical format for both the contact and partial contact modes.

7.6.1. Cavity Heating and Changes in Empty Cavity Frequency Response

Two power resistors attached to the underside of the test specimen mounting plate (see Figure 3.2) heat the cavity. Heating of the cavity causes it to expand and change shape, thereby lowering its resonant frequency. Spring finger contact is also affected when the cavity is heated, having the deleterious effect of lowering the cavity's Q-factor.

There are two ways to predict changes in the empty cavity's resonant frequency and Q-factor resulting from cavity heating. One way is to use a numerical simulation. The other is to directly measure resonant frequency and Q of the empty cavity at selected temperatures.

Within the numerical simulation, cavity dimensions are changed so as to reflect changes in cavity temperature. The coefficient of linear expansion for brass is used to predict the increase in the cavity's radial and axial dimensions at specific temperatures. However, because of the heating scheme employed, the temperature profile of the cavity is not uniform throughout its length, and hence simulated results based on uniform expansion are inaccurate.

An experimental approach is the only reliable method to find the empty cavity's resonant frequency and Q as a function of temperature for this particular dielectrometer configuration. Using a reflectometer, the empty cavity's resonant frequency and Q are measured at selected temperatures. Empty cavity elevated temperature characteristics were measured a number of times to assure repeatability. After measurement repeatability is verified, equations that relate resonant frequencies and Q-factors to the cavity's elevated temperature are established.

Figures 7.1 and 7.2 show the absolute decrease in the empty cavity's resonant frequency as the cavity was heated from room temperature to 120°C for both the contact and partial contact modes. The temperature dependent empty cavity Q-factors, for both the contact and partial contact modes, are shown in

Figures 7.3 and 7.4. Linear approximations to these curves were used in calculating the final data.

The HPBASIC programs RUBDIELA (partial contact mode) and RUBDIELB (contact mode) contain functions that calculate the temperature dependent unloaded cavity resonant frequencies and Q-factors. During dielectric testing, the interface to the HPBASIC program prompted the user to input the measured set point temperature of the test specimen. Once the temperature is entered, the HPBASIC program calculated the unloaded cavity's adjusted resonant frequency and Q-factor. Next, resonant frequency and Q-factor shifts of the resonant cavity were determined and the test specimen's dielectric properties were calculated. Following a dielectric measurement at temperature, T , the test specimen was heated to the next set point temperature and the above process would be repeated once temperature stability was achieved. This continued until the maximum set point temperature was attained.

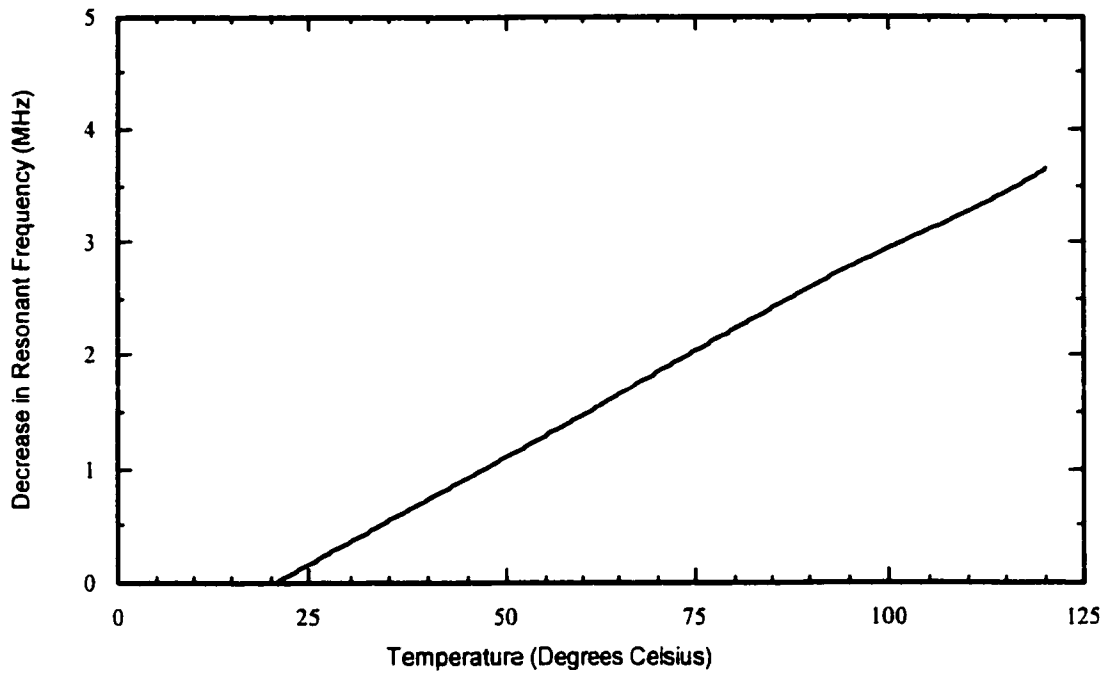


Figure 7.1 Decrease in empty cavity resonant frequency when heating the test cavity from 20°C to 125°C (contact mode).

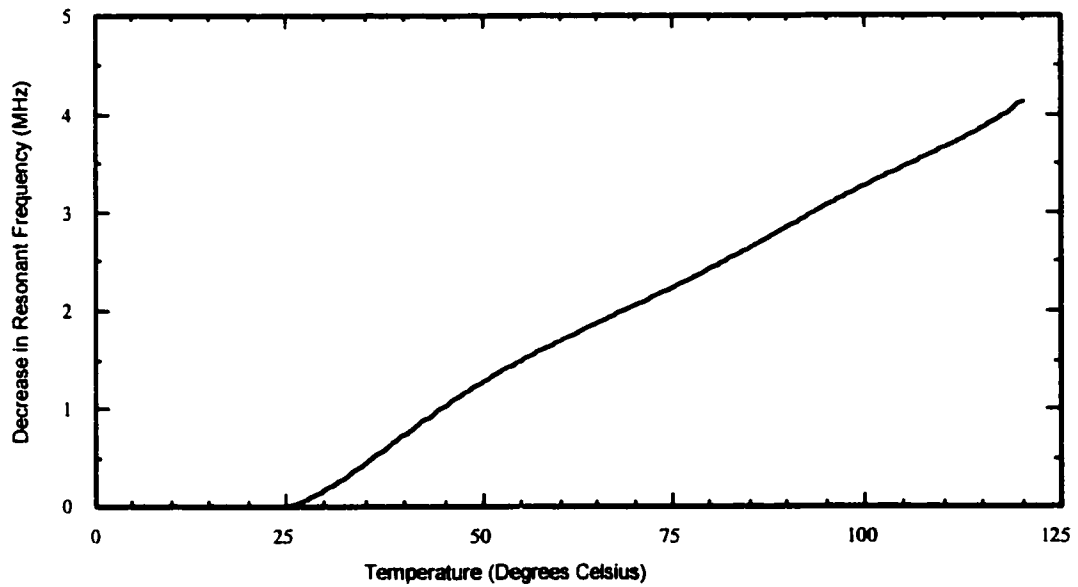


Figure 7.2 Decrease in empty cavity resonant frequency when heating the test cavity from 20°C to 125°C (partial contact mode).

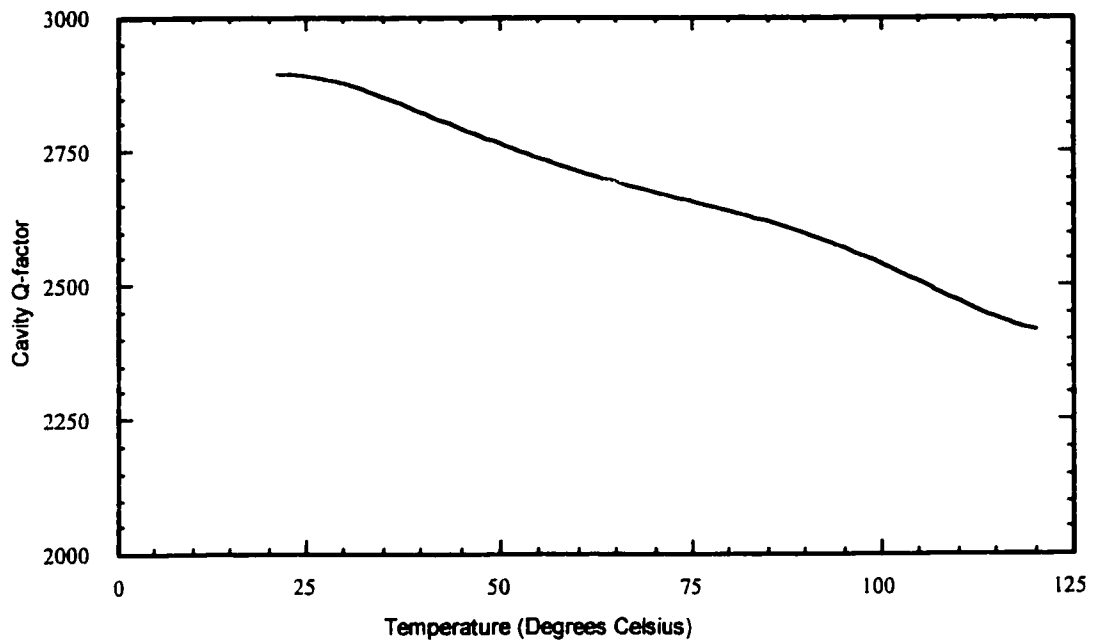


Figure 7.3 Decrease in empty cavity Q-factor when heating the test cavity from 20°C to 125°C (contact mode).

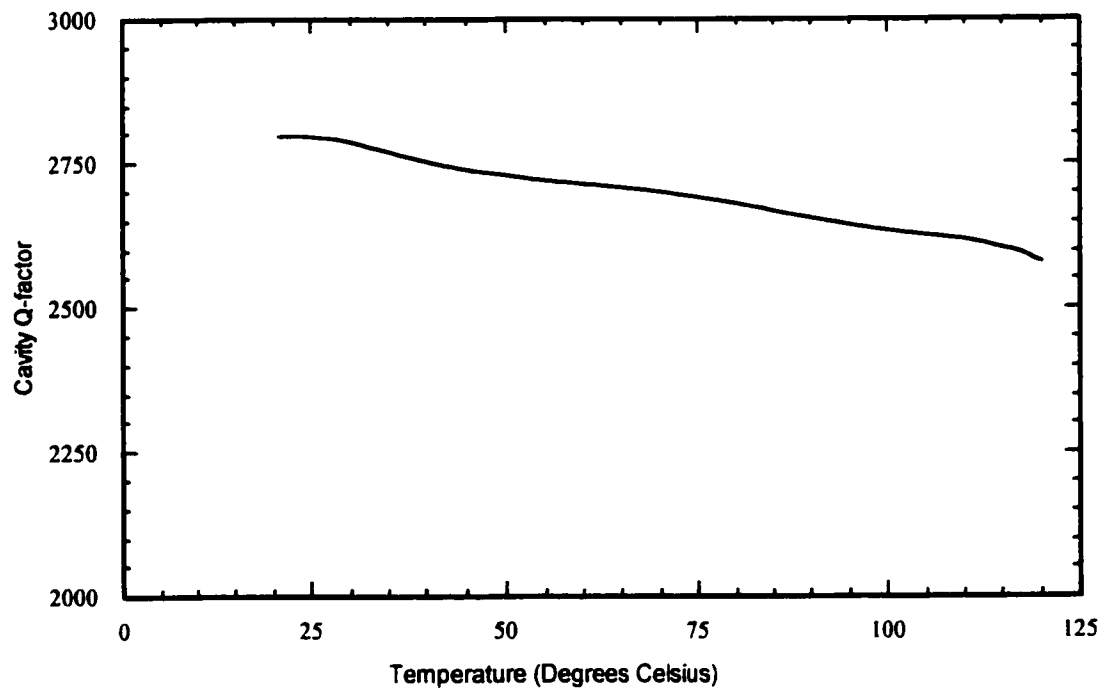


Figure 7.4 Decrease in empty cavity Q-factor when heating the test cavity from 20°C to 125°C (partial contact mode).

7.6.2 Experimental Results and Discussion

Dielectric properties of the five Royalene rubber materials were measured and the results are presented in Table 7.4. Relative dielectric constants and loss tangents are plotted as a function of temperature in Figures 7.5 and 7.6. In Table 7.5, the chemical constituent levels of each of the five Royalene rubber materials are listed.

Table 7.4 Measured room temperature dielectric properties of five Royalene rubber materials. Materials' A, B, C and E were tested using the partial contact mode, while the contact mode was used for testing material D.

Royalene Rubber Material	ϵ_r'	$\tan \delta$
Royalene A	18.4 ± 0.2	0.355 ± 0.005
Royalene B	9.0 ± 0.2	0.101 ± 0.001
Royalene C	12.2 ± 0.3	0.240 ± 0.006
Royalene D	4.13 ± 0.01	0.0059 ± 0.0002
Royalene E	10.9 ± 0.2	0.1594 ± 0.005

All five Royalene rubber materials were heated to 120°C. However, the dielectric properties of Royalene A, Royalene B and Royalene E did not change above 80°C. The dielectric properties of Royalene C and Royalene D did not change above temperatures of 70°C.

Royalene A had the highest relative dielectric constant and loss factor of the five Royalene rubber materials. It also exhibited the largest change in its dielectric properties with temperature. Its relative dielectric constant at 80°C

increased by over 50% from its room temperature value while its relative loss factor increased by over 400%.

Table 7.5 Chemical constituent levels of each of the five Royalene rubber materials tested.

Royalene rubber material	Royalene A	Royalene B	Royalene C	Royalene D	Royalene E
ROYALENE 3356	100.0	100.0	100.0	100.0	100.0
N 660 GPF BLACK	100.0	72.0	58.0	42.0	28.0
N550 FEF BLACK	50.0	36.0	29.0	21.0	14.0
YORK WHITING	45.0	45.0	45.0	45.0	45.0
ZINC OXIDE	10.0	10.	10.0	10.0	10.0
ZINC STEARATE	1.5	1.5	1.5	1.5	1.5
RHENOSOR B C/GW	10.0	10.0	10.0	10.0	10.0
SUNPAR 2280	110.0	90.0	80.0	70.0	60.0
MISTRON VAPOR	--	62.0	93.0	127.0	158.0
MBT	1.5	1.5	1.5	1.5	1.5
RUTAZATE	1.5	1.5	1.5	1.5	1.5
SULFADS	1.2	1.2	1.2	1.2	1.2
TUEX	1.0	1.0	1.0	1.0	1.0
SULFUR	1.5	1.5	1.5	1.5	1.5
TOTAL	433.2	433.2	433.2	433.2	433.2
% CARBON BLACK	35	25	20	15	10

Royalene D had the smallest relative dielectric constant of the five Royalene rubber materials. Its relative dielectric constant changed only slightly

over the temperature testing range while its relative loss factor doubled. Also, its loss tangent was more than an order of magnitude lower than that of the other Royalene rubber materials.

Royalene B, Royalene C and Royalene E exhibited similar temperature behavior over the temperature range of 20°C to 120°C. Their relative dielectric constants varied between 9.0 and 15.0 and their relative loss factors varied between 0.90 and 5.25.

These Royalene rubber materials each contain different levels of chemical constituents. No correlation between the dielectric data obtained and the chemical constituent levels of the Royalene rubber materials was attempted.

7.7 Conclusions

Algorithms for determining accurate cavity resonant frequencies and Q-factors over temperature are given. Room temperature dielectric measurements performed on the Eccosorb materials fully validated the contact mode measurement method and in part validated the partial contact mode measurement method. Measured dielectric properties of the five Royalene rubber materials, Royalene A, B, C, D and E, over the temperature range of 20°C to 120°C are presented. To determine the uncertainty in the measured dielectric data, a prediction of the accuracy of the measurement system is required. In the next chapter, an uncertainty analysis of the reflectometer is performed so as to predict the dielectric measurement accuracy.

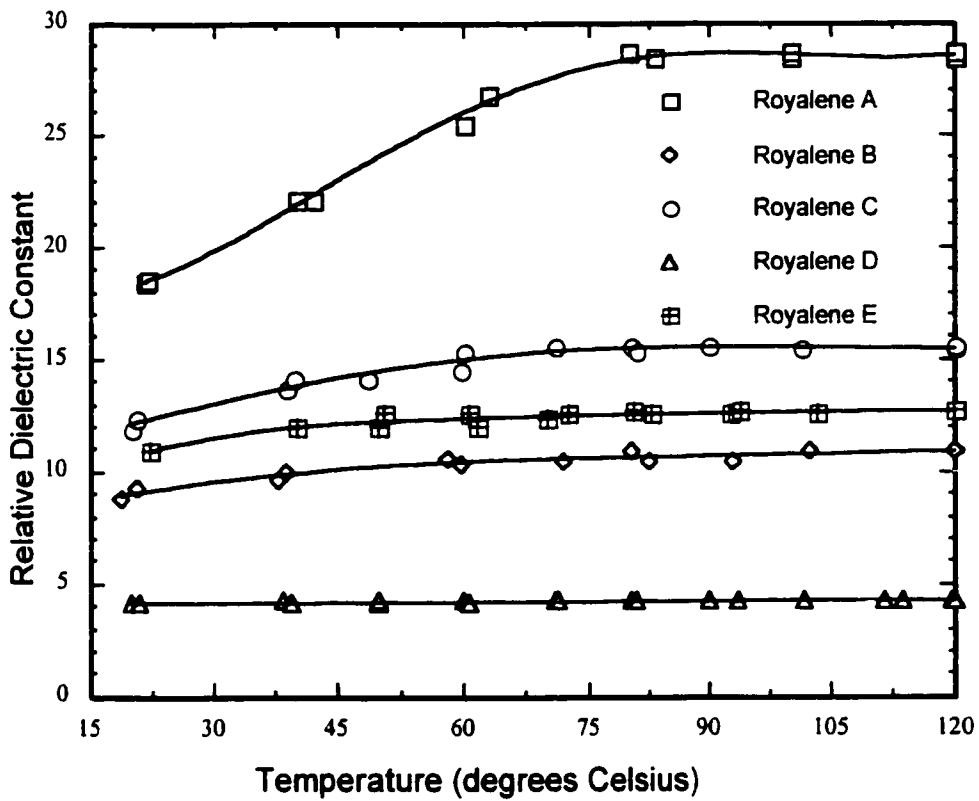


Figure 7.5 Measured relative dielectric constants of the Royalene rubber materials, A - E, at 2.45GHz, as functions of temperature.

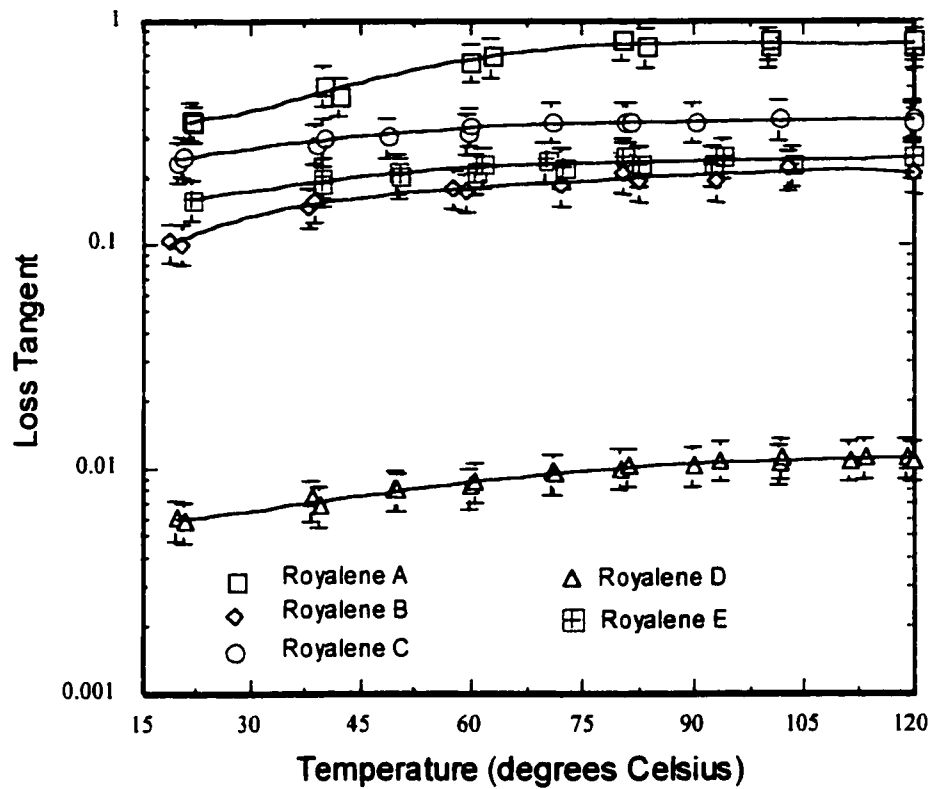


Figure 7.6 Measured loss tangents of the Royalene rubber materials, A - E, at 2.45, GHz, as functions of temperature, presented in a semi-log format.

CHAPTER 8

UNCERTAINTY ANALYSIS OF THE REFLECTOMETER AND EFFECTS ON DIELECTRIC MEASUREMENT ACCURACY

8.1 Introduction

In this chapter the measurement accuracy of the reflectometer is analyzed in order to predict uncertainty in the dielectric measurements. Dielectric measurement uncertainty is determined for both measured dielectric constant and loss tangent. In Appendix 2, detailed derivations of the equations used in this chapter are given.

8.2 Analysis of Reflectometer Uncertainty upon the Dielectric Measurement Accuracy

8.2.1 Relative Dielectric Constant Measurement Uncertainty Analysis

Assuming room temperature conditions and a 2 mm thick test specimen with a 5 mm radius, uncertainty in the specimen's measured dielectric properties attributable to reflectometer uncertainties are given below.

Uncertainty in the measured dielectric constant is dependent upon the frequency stability ($\Delta f = \pm 0.005 \text{ MHz}$) of the synthesized sweep oscillator. When determining the uncertainty in the resonant frequency shift of the cavity, the frequency uncertainty doubles since one adds the uncertainty of the measured empty cavity resonant frequency to the uncertainty of the shifted resonant

frequency of the loaded cavity. Thus, the uncertainty in the measured resonant frequency shift of the test cavity is $\Delta(\Delta f_0) = \pm 0.01$ MHz.

To estimate uncertainty in measured dielectric constant, the partial derivative of the relative dielectric constant, $\Delta\epsilon_r'$, versus resonant frequency shift, $|\Delta f_0|$, behavior needs to be examined, i.e.

$$|\Delta\epsilon_r'| = \frac{\partial\epsilon_r'}{\partial(|\Delta f_0|)} \Delta|\Delta f_0| \quad (8.1)$$

where $\frac{\partial\epsilon_r'}{\partial(|\Delta f_0|)}$ is the slope of the dielectric constant versus resonant frequency shift function and $\Delta|\Delta f_0|$ is the uncertainty in the measured resonant frequency shift. An analytical expression for the uncertainty of the measured relative dielectric constant, $|\Delta\epsilon_r'|$, of a test specimen is given by

$$|\Delta\epsilon_r'| = \left(a_1 + 2a_2|\Delta f_0| + 3a_3|\Delta f_0|^2 + 4a_4|\Delta f_0|^3 + K \right) \left(\Delta|\Delta f_0| \right) \quad (8.2)$$

where $\Delta|\Delta f_0| = 0.01$ MHz, a_i are the polynomial coefficients of Eq.(5.5) and K represents all additional corresponding higher order terms. Using the coefficient values from Tables 5.3 and 5.4 uncertainty in measured relative dielectric constant for both the contact and partial contact modes are given in Tables 8.1 and 8.2.

Table 8.1 Uncertainty in measured relative dielectric constant for the contact mode.

ϵ_r'	2.00	4.00	8.00	12.00	14.00	16.00
$ \Delta\epsilon_r' $	0.0085	0.0073	0.0052	0.0036	0.0030	0.0024
$\frac{ \Delta\epsilon_r' }{\epsilon_r'}\%$	0.43	0.18	0.065	0.030	0.021	0.015

Table 8.2 Uncertainty in measured relative dielectric constant for the partial contact mode.

ϵ_r'	2.00	4.00	8.00	10.00	15.00	20.00	30.00
$ \Delta\epsilon_r' $	0.024	0.031	0.070	0.097	0.19	0.32	0.48
$\frac{ \Delta\epsilon_r' }{\epsilon_r'}\%$	1.2	0.78	0.88	0.97	1.3	1.6	1.6

8.2.2 Loss Tangent Measurement Uncertainty Analysis

Uncertainty in measured loss tangent is a function of both uncertainty in the measured Q of the loaded cavity and the uncertainty in the test specimen's relative dielectric constant. Uncertainty in measured Q-factor, for a resonant cavity is dependent upon both the directivity of the reflectometer's directional couplers and the cavity's return loss value at its resonant frequency. For a given directional coupler directivity value, D, uncertainty in measured Q-factor is determined as a function of the cavity's measured input impedance [8, 59]. In order to evaluate the relative uncertainty in a test specimen's measured loss tangent resulting from uncertainty in the measured input impedance of the cavity, one uses the following equation (see Appendix 2)

$$\left[\frac{\Delta \tan \delta}{\tan \delta} \right]_Q = -2 \frac{\Delta \bar{Q}}{\bar{Q}} \quad (8.3)$$

where $\left[\frac{\Delta \tan \delta}{\tan \delta} \right]_Q$ is the relative uncertainty in a test specimen's measured loss tangent resulting from the measurement in the cavity's Q and $\frac{\Delta \bar{Q}}{\bar{Q}}$ can be treated as an average relative error in Q measurements. To obtain high accuracy Q-factors, coupler directivity should be large ($D \geq 40$ dB) while the magnitude of the normalized input impedance should be unity. Measured loss tangent uncertainty can remain low, $\frac{\Delta \tan \delta}{\tan \delta} < 5\%$ when $D \geq 40$ dB and the cavity's measured reflection coefficient is $|\Gamma| < 0.2$ [8]. Tables 8.3 and 8.4 present uncertainty data in the measured loss tangent of a test specimen attributable to uncertainty in measured Q-factor for the contact and partial contact modes.

Table 8.3 Uncertainty in measured loss tangent for the contact mode as a function of directivity, D and relative dielectric constant, ϵ_r' .

ϵ_r'	2.00	4.00	8.00	12.00	14.00	16.00
$\left[\frac{\Delta \tan \delta}{\tan \delta} \right]_{D=30\text{dB}}$ %	18.9	18.8	19.0	19.3	19.5	19.5
$\left[\frac{\Delta \tan \delta}{\tan \delta} \right]_{D=40\text{dB}}$ %	5.9	5.8	6.0	6.3	6.5	6.5

Table 8.4 Uncertainty in measured loss tangent for the partial contact mode as a function of directivity, D and relative dielectric constant, ϵ_r' .

ϵ_r'	2.00	4.00	8.00	10.00	15.00	20.00	30.00
$\left[\frac{\Delta \tan \delta}{\tan \delta} \right]_{D=30\text{dB}}$ %	18.5	18.3	18.6	18.7	19.0	19.5	20.3
$\left[\frac{\Delta \tan \delta}{\tan \delta} \right]_{D=40\text{dB}}$ %	5.5	5.3	5.6	5.7	6.0	6.5	7.3

Uncertainty in a test specimen's measured relative dielectric constant also causes uncertainty in its measured loss tangent as shown below

$$\left| \frac{\Delta \tan \delta}{\tan \delta} \right|_{\varepsilon_r'} = \left| \frac{1}{\Delta \left(\frac{1}{Q_0} \right)} \left(\frac{c_1 + 2c_2 \varepsilon_r' + 3c_3 (\varepsilon_r')^2 + K}{Q_C^2(\varepsilon_r')} \right) \Delta \varepsilon_r' \right| + \left| \zeta \Delta \varepsilon_r' \right| \quad (8.4)$$

where $\Delta \left(\frac{1}{Q_0} \right)$ is the measured change in the cavity's inverse Q-factor, $Q_C(\varepsilon_r')$ is the cavity Q-factor when loaded with a lossless dielectric, ζ is the error transfer function, K represents all additional corresponding higher order terms and $\Delta \varepsilon_r'$ is the uncertainty in the test specimen's measured relative dielectric constant (details of the derivation of Eq.(8.4) are given in Appendix 2). In Tables 8.5 and 8.6, uncertainties in measured loss tangent attributable to uncertainty in measured dielectric constant are listed as functions of directivity and relative dielectric constant, ε_r' , for both test modes. It is apparent from the results in both tables that uncertainty in loss tangent as a function of dielectric constant is essentially independent of the coupler directivity. As well, the loss tangent measurement uncertainty values listed in the Tables 8.5 and 8.6 are significantly smaller in magnitude than those listed in Tables 8.3 and 8.4. Thus the major contributor to overall loss tangent measurement uncertainty is return loss measurement and coupler directivity.

Table 8.5 Uncertainty in measured loss tangent attributable to uncertainty in measured dielectric constant for the contact mode as a function of directivity, D and relative dielectric constant, ϵ_r' .

ϵ_r'	2.00	4.00	8.00	12.00	14.00	16.00
$\frac{ \Delta \tan \delta }{\tan \delta} \bigg _{D=30\text{dB}}$ %	0.5	0.3	0.3	0.4	0.3	0.3
$\frac{ \Delta \tan \delta }{\tan \delta} \bigg _{D=40\text{dB}}$ %	0.6	0.6	0.4	0.8	0.8	0.8

Table 8.6 Uncertainty in measured loss tangent attributable to measured dielectric constant for the partial contact mode as a function of directivity, D and relative dielectric constant, ϵ_r' .

ϵ_r'	2.00	4.00	8.00	10.00	15.00	20.00	30.00
$\frac{ \Delta \tan \delta }{\tan \delta} \bigg _{D=30\text{dB}}$ %	0.2	0.05	0.4	0.5	0.8	1.2	3.5
$\frac{ \Delta \tan \delta }{\tan \delta} \bigg _{D=40\text{dB}}$ %	0.3	0.2	0.6	0.6	1.0	1.2	6.8

8.3 Overall Effect of Reflectometer Uncertainty on Dielectric Measurement Accuracy

The overall dielectric measurement uncertainty is the summation of all the uncertainty contributions. In Tables 8.7 and 8.8, the overall uncertainty in measured dielectric constant and loss tangent as a function of directivity and dielectric constant is given. It is apparent from the results listed that the uncertainty in measured dielectric constant is quite acceptable. Loss tangent measurement accuracy improves when couplers with high directivity are utilized. In addition, measurement accuracy between the test modes is comparable. Measured data for this work used a reflectometer with a directivity of $D \geq 30$ dB.

Table 8.7 Overall reflectometer uncertainty in the measurement of dielectric constant and loss tangent (contact mode).

ϵ_r'	2.00	4.00	8.00	12.00	14.00	16.00
$ \Delta\epsilon_r' $	0.0085	0.0073	0.0052	0.0036	0.0030	0.0024
$\frac{ \Delta\epsilon_r' }{\epsilon_r'}\%$	0.43	0.18	0.065	0.030	0.021	0.015
$\frac{ \Delta \tan \delta }{\tan \delta} \%$ D = 30dB	19.4	19.1	19.3	19.7	19.7	19.8
$\frac{ \Delta \tan \delta }{\tan \delta} \%$ D = 40dB	6.5	6.3	6.7	7.6	7.3	7.3

Table 8.8 Overall reflectometer uncertainty in the measurement of dielectric constant and loss tangent (partial contact mode).

ϵ_r'	2.00	4.00	8.00	10.00	15.00	20.00	30.00
$ \Delta\epsilon_r' $	0.024	0.031	0.070	0.097	0.19	0.32	0.48
$\frac{ \Delta\epsilon_r' }{\epsilon_r'}\%$	1.2	0.78	0.88	0.97	1.3	1.6	1.6
$\frac{ \Delta \tan \delta }{\tan \delta} \%$ D = 30dB	18.7	18.4	19.0	19.2	19.8	20.7	23.8
$\frac{ \Delta \tan \delta }{\tan \delta} \%$ D = 40dB	5.8	5.5	6.2	6.3	7.0	7.7	13.9

8.4 Conclusions

An uncertainty analysis of the reflectometer was performed. The results found indicate that the measurement accuracy is comparable to that listed in the literature for measurement of both dielectric constant and loss tangent. In Appendix 2, derivations of the equations used in this chapter are presented.

CHAPTER 9

CONCLUSION

A microwave dielectrometer has been presented which is capable of measuring a material's complex dielectric constant for temperatures up to 120°C, at 2.45 GHz over a range of $1.03 < \epsilon_r' < 30.0$ and $0.0001 < \tan\delta < 1.63$. The following features characterize this system.

A hybrid coaxial cavity that has a complex internal geometry was used for microwave testing. A cylindrical parallel plate waveguide section contained a dielectric test specimen. The length of the coaxial section mainly determined resonant frequency of the cavity. Magnetic energy was coupled to the cylindrical parallel plate waveguide from the half wavelength coaxial section via a low impedance coaxial transmission line. By virtue of a strongly focused E-field in the center of the cylindrical parallel plate waveguide, a high measurement sensitivity has been achieved.

By using two different modes of operation, this dielectrometer was used to measure a large range of loss tangents or loss factors (4 orders of magnitude). The partial contact mode allowed loss tangent measurements to be made on materials whose loss tangent ranged between $1.0 > \tan\delta > 0.01$. Dielectric measurements on low loss materials ($0.01 > \tan\delta > 0.0001$) were made in the contact mode.

Dielectric data was determined from measured changes in resonator parameters and numerically calculated calibration curves. Calibration curves were obtained by numerically simulating specific test specimen and test cavity characteristics.

Field patterns within the test cavity could be approximated by analytical solutions for a half wavelength coaxial resonator and a radial transmission line. Within the coaxial section, electric and magnetic field characteristics mirror field solutions for an ideal $\frac{\lambda}{2}$ resonant coaxial cavity. Electric and magnetic field characteristics for the cylindrical parallel plate waveguide were found to be nearly identical to field patterns for the radial transmission line.

Resonance characteristics of the hybrid coaxial cavity were calculated using a finite difference frequency domain technique. Electric and magnetic mean stored energies were calculated and these quantities were used for determining a cylindrical cavity's resonant frequency. Power losses in the cavity walls and in a test specimen were calculated and these quantities were used for determining loaded cavity Q-factor.

The dynamic measurement range was limited by the measurement sensitivity of the reflectometer. The limiting factor for low loss measurement limits was uncertainty in return loss measurements, while the limiting factor for extending the dielectric constant measurement range was test specimen loading

on the test cavity. For the partial contact mode, there was not enough frequency sensitivity to measure relative dielectric constants that exceeded $\epsilon_r' > 30$.

Uncertainties in determined dielectric data attributable to the reflectometer were examined in detail. Analysis showed that measurement of dielectric constant is highly accurate, while measurement of loss tangent has a maximum uncertainty of less than 25% when testing very high loss materials. This measurement accuracy is comparable to other dielectrometers described in the literature.

Problems with this dielectrometer include its lack of portability, difficulty in changing inner conductor length as well as the necessity to remove the half wavelength coaxial resonator from atop the specimen mounting plate in order to place a test specimen within the testing apparatus.

To improve measurement repeatability and accuracy, an alternative cavity configuration must be utilized. One possibility, a single piece resonant cavity, would require a different test specimen insertion technique. One possible insertion technique is to use a modified re-entrant cavity technique. Also, inner conductor length will have to be adjusted externally. A technique for doing this is described by Tian [48].

The result of this project is a microwave dielectrometer that can measure a wide range of loss tangents over a desired temperature range. As well, dielectric data obtained as functions of temperature will be useful for developing a microwave curing process for the five Royalene rubber materials tested. With

dielectric data obtained as a function of temperature, the resulting curing process can be optimized so as to minimize energy usage and curing duration. Chemical and mechanical properties of microwave cured rubbers will not be differentiable from those of conventionally cured rubbers.

This thesis work has laid the basis for an understanding of the characteristics of the hybrid coaxial cavity dielectrometer. As well, this work will promote further development of this device. An improved test specimen insertion scheme should be developed for this device. Finally, a contribution has been made to the study of the microwave dielectric properties of rubber as a function of temperature.

REFERENCES

- [1] Schwarz, H.F., Bosisio, R.G., Wertheimer, M.R., and Couderc, D., "Microwave Curing of Synthetic Rubbers," *J. of Microwave Power*, Vol. 8 pp. 302-322, 1973.
- [2] Gohlisch, H.J., "Salt Bath and UHF Methods," *Rubber Age*, Vol. 103, No.4, p.49, April, 1971.
- [3] Evans, C.W., "Continuous Vulcanization in Europe: Present and Future," *Rubber Age*, Vol. 103, No.5, p. 53, May, 1971.
- [4] Tinga, W.R., "Microwave Material Interactions and Process Design Modeling," *Ceramic Transactions*, Vol. 36, 1993.
- [5] Ma, L., Paul, D.L., Pathecary, N., Raiton, C., Bows, J., Barratt, L., Mullin, J., and Simons, J., "Experimental Validation of a Combined Electromagnetics and Thermal FDTD Model of a Microwave Heating Process," *MTT 43(11)*, pp. 2565-2572, 1995.
- [6] Altschuler, H.M., "Dielectric Constant," in Sucher, M., and Fox, J., *Handbook of Microwave Measurements*, vol. II. Brookline, N.Y.: Polytechnic Press, 1963, Ch. 9.
- [7] Osepchuk, J.M., "Microwave Technology," in Kirk-Othmer, *Encyclopedia of Chemical Technology*, Kirk and Othmer, Eds. New York: Wiley, 1981, pp. 492 - 522.

- [8] Xi, W., **High Temperature Microwave Dielectrometer Using a Re-entrant Cavity**, Ph. D. Thesis, University of Alberta, 1992.
- [9] Pozar, D.M., **"Microwave Engineering," Ch.2**, Addison Wesley, 1993.
- [10] Roberts, S., and Von Hippel, A., **"A New Method for Measuring Dielectric Constants and Loss in the Range of Centimeter Waves,"** J. Appl. Phys., vol. 17, pp.610 - 616, 1946.
- [11] Ganchev, S.I., Bhattacharyya, J., Bakhtiari, S., Qaddoumi, N., Brandenburg, D., Zoughi, R., **"Microwave Diagnosis of Rubber Compounds,"** MTT, 42(1) pp. 18-24, 1994.
- [12] Ganchev, S.I., Bakhtiari, S., and Zoughi, R., **"A Novel Numerical Technique for Dielectric Measurements of Lossy Dielectrics,"** IEEE Trans. Instr. Meas., vol. 41, pp. 361-365, 1992.
- [13] Tantot, O., Chatard-Moulinm M., and Guillon, P., **"Dielectric Measurement of Multi-Layered Medium Using an Open - Ended Waveguide."**
- [14] Rueggeberg, W., **"Determination of Complex Permittivity of Arbitrarily Dimensioned Dielectric Modules at Microwave Frequencies,"** MTT, 19(6), pp. 517 - 521, 1971.
- [15] Xi, W., Tinga, W.R., Voss, W.A.G., and Tian, B.Q., **"New Results for Coaxial Re-entrant Cavity with Partially Dielectric Filled Gap,"** MTT 40(4), pp. 747-753, 1992.

- [16] Terselius, B., and Ranby, B., "Cavity Perturbation Measurements of the Dielectric Properties of Vulcanizing Rubber and Polyethylene Compounds," *J. of Microwave Power*, 13(4) pp. 327-355 (1978).
- [17] Xi, W., Tinga, W.R., "Microwave Heating and Characterization of Machinable Ceramics," *Microwave Processing of Materials III*, San Francisco, 12 pages, 1992.
- [18] Couderc, D., Giroux, M. and Bosisio, R.G., "Dynamic High Temperature Microwave Complex Permittivity Measurements on Samples Heated via Microwave Absorption," *J. Microwave Power*, vol.8 pp.69-82, 1973.
- [19] Ippen,J., "Formulation for Continuous Vulcanization in Microwave Heating Systems," *Rubber Chem. Techn.*, vol. 44, pp.294-308, 1971.
- [20] Jow, J., Hawley, M.C., Finzel,J., Asmussen, J., Jr., Lin, H.H., et al., "Microwave Processing and Diagnosis of Chemically Reacting Materials in a Single Mode Cavity Applicator," *IEEE Trans. Microwave Theory Tech.*, vol. MTT-35, pp.1435-1443, 1987.
- [21] Kaczkowski, A., and Milewski, A., "High - Accuracy Wide Range Measurement Method for Determination of Complex Permittivity in Re-entrant Cavity Part B-Experimental Analysis of Measuring Errors," *IEEE Trans. MTT*, vol. 28(3), pp228-231, 1980.
- [22] Tinga, W.R., Tian, B.Q., and Voss, W.A.G., "New High Temperature Multipurpose Applicator," *Mat. Res. Soc. Proc.*, vol. 189, pp. 111-116, 1991.

- [23] Xi, W., and Tinga, W.R., "A High Temperature Dielectrometer," *Ceramics Trans. Microwaves: Theory and Applications in Material Processing*, vol.21, American Ceramics Society, Cincinnati:1991, pp. 215-221 , vol. 21.
- [24] Tian, B.Q., and Tinga, W.R., "Single Frequency Relative Q Measurements," *IEEE Trans. Microwave Theory Tech.*, vol. MTT-41, pp. 1922-1927, 1993.
- [25] Baysar, A. and Kuester, J.L., "Dielectric Property Measurements of Materials Using the Cavity Perturbation Technique," *IEEE Trans. Microwave Theory Tech.*, MTT-42, pp.2108-2111, 1992.
- [26] Meng, B., Booske, J. and Cooper, R., "Extended Cavity Perturbation Technique to Determine the Complex Permittivity of Dielectric Materials," *IEEE Trans. Microwave Theory Tech.*, MTT-43, pp.2633-2636, 1995.
- [27] Meng, B., Booske, J. and Cooper, R., "A System to Measure Complex Permittivity of Low Loss Ceramics at Microwave Frequencies and Over Large Temperature Ranges," *Rev. Sci. Instrum.* 66(2), pp. 1068-1071, 1995.
- [28] Xi, W., and Tinga, W.R., "Error Analysis and Permittivity Measurements with Re-Entrant High Temperature Dielectrometer," *J. Microwave Power*, 28(2) pp. 104-122, 1993.
- [29] Tian, B.Q., Tinga, W.R., and Xi, W., "Single Frequency Dielectric Heating and Measuring," *Mat. Res. Soc. Symp. Proc.* vol. 269, pp. 83 - 89, 1992.

- [30] Pohl, V., Fricke, D., and Muhlbauer, A., "Correction Procedures for the Measurement of Permittivities with the Cavity Perturbation Method," *J. Microwave Power*, 30(1) pp. 10 - 26, 1995.
- [31] Tian, B.Q., and Tinga, W.R., "New Self-Oscillating, Self-Heating Microwave Active Dielectrometer," *Ceramic Transactions*, vol. 36 pp. 517 - 527, 1993.
- [32] Asfar, M.N., Li, X., and Chi, H., "An Automated 60 GHz Open Resonator System for Precision Dielectric Measurement," *IEEE Trans. Microwave Theory Tech.*, MTT-38, pp.1845-1853, 1990.
- [33] Komiyaman B., Kiyokawa, M., and Matsui, T., "Open Resonator for Precision Dielectric Measurements in the 100 GHz Band," *IEEE Trans. Microwave Theory Tech.*, MTT-39, pp.1792-1796, 1991.
- [34] Wei, Y.Z., and Sridhar, S., "Radiation-Corrected Open - Ended Coax-Line Technique for Dielectric Measurements of Liquids up to 20 GHz," *IEEE Trans. Microwave Theory Tech.*, MTT-39, pp.526-531, 1991.
- [35] Stafebell, K.F. and Misra, D., "An Experimental Technique for *In Vivo* Permittivity Measurement of Materials at Microwave Frequencies," *IEEE Trans. Microwave Theory Tech.*, MTT-38, pp.337-339, 1990.
- [36] Nyshadham, A., Sibbald, C.L., and Stuchly, S.S., "Permittivity Measurements Using Open - Ended Sensors and Reference Liquid Calibration-An Uncertainty Analysis," *IEEE Trans. Microwave Theory Tech.*, MTT-40, pp.305-314, 1991.

- [37] Colpitts, B.G., "Temperature Sensitivity of Coaxial Probe Complex Permittivity Measurements: Experimental Approach," IEEE Trans. Microwave Theory Tech., MTT-41, pp.229-233, 1993.
- [38] Anderson, J.M., Sibbald, C.L. and Stuchly, S.S., "Dielectric Measurements Using a Rational Function Model," IEEE Trans. Microwave Theory Tech., MTT-42, pp.199-204, 1994.
- [39] Chen, G., Li, K. and Ji, Z., "Bilayered Dielectric Measurement With an Open - Ended Coaxial Probe," IEEE Trans. Microwave Theory Tech., MTT-42, pp.966-971, 1994.
- [40] Okoniewski, M., Anderson, J., Caputa, K. and Stuchly, S.S., "Further Analysis of Open - Ended Dielectric Sensors," IEEE Trans. Microwave Theory Tech., MTT-42, pp.1986-1989, 1995.
- [41] Berube, D., Ghannouchi, F.M., and Savard, P., "A Comparative Study of Four Open - Ended Coaxial Probe Models for Permittivity Measurements of Lossy Dielectric/Biological Materials at Microwave Frequencies," IEEE Trans. Microwave Theory Tech., MTT-44, pp.1928-1934, 1996.
- [42] Bringhurst, S., and Iskander, M.F., "Open - Ended Metallized Ceramic Coaxial Probe for High - Temperature Dielectric Properties Measurements," IEEE Trans. Microwave Theory Tech., MTT-44, pp.926-935, 1996.
- [43] Tinga, W.R., "Rapid High Temperature Measurement of Microwave Dielectric Properties," Mat. Res. Soc. Symp. vol. 269, pp. 505 - 516, 1992.

- [44] Pozar, D.M., "Microwave Engineering," Ch.7, Addison Wesley, 1993.
- [45] Pozar, D.M., "Microwave Engineering," Ch.4, Addison Wesley, 1993.
- [46] Marcuvitz, N., "Waveguide Handbook," Ch.2, McGraw - Hill, 1951.
- [47] Pozar, D.M., "Microwave Engineering," Ch.3, Addison Wesley, 1993.
- [48] Tian, B.Q., Single Frequency High Temperature Microwave Dielectrometers, Ph.D. Thesis, University of Alberta, 1993.
- [49] Sedra, A.S., Smith, K.C., "Microelectronic Circuits," Ch.4, New York: Saunders College Publishing, 1991.
- [50] Horowitz, P., Hill, W., "The Art of Electronics," Ch. 4. Cambridge University Press, 1989.
- [51] Sedra, A.S., Smith, K.C., "Microelectronic Circuits," Ch.2, New York: Saunders College Publishing, 1991.
- [52] Omega Engineering Temperature Measurement Handbook and Encyclopedia, H3-H5.
- [53] Jackson, J.P., "Classical Electrodynamics," New York: John Wiley & Son, Inc. 1975.
- [54] Paul, C.R. and Nasar, S.A., "Introduction to Electromagnetic Fields," New York: McGraw Hill Book Company, 1987.
- [55] Ghandi, O.P., "Microwave Engineering and Applications," Ch. 8, New York: Peragamon Press, 1981.

- [56] Thompson, R.B., Chute, F.S. and Vermeulen, F.E., "Use of a Stealth Boundary with Finite Difference Frequency Domain Simulations of Simple Antenna Problems," *ACES Journal*, Vol. 9(1) pp. 78-87, 1994.
- [57] Albani, M. and Bernardi, P., "A Numerical Method Based on the Discretization of Maxwell's Equations in Integral Form," *IEEE Trans. MTT*, MTT - 22, p.446,1974.
- [58] Ramo, S., Whinnery, J.R. and Van Duzer, T., "Fields and Waves in Communication Electronics," John Wiley & Sons, N.Y., 1965.
- [59] Pozar, D.M., "Microwave Engineering," Ch.5, Addison Wesley, 1993.
- [60] Hewlett Packard, "Directivity Measurements," Application Note 183, December 1978.
- [61] Sucher, M., "Measurement of Q," in Sucher, M., and Fox, J., *Handbook of Microwave Measurements*, vol. II. Brookline, N.Y.: Polytechnic Press, 1963, Ch. 8.

APPENDIX 1

THE HERZ SIMULATION PROGRAM

This appendix gives the entire FORTRAN77 code for the finite difference frequency domain program called HERZ. Documentation of the code is contained within the following listing provided. The code was originally written by F. Vermeulen and subsequently modified by T. Reeves to include subroutines for calculation of mean stored energy, losses, Q-factor, and resonant frequency.

A1.1 HERZ Program

```
PROGRAM HERZCOMPLEXMU
C THIS PROGRAM CALCULATES THE 2-DIMENSIONAL TIME
C HARMONIC MAGNETIC AND ELECTRIC FIELD DISTRIBUTIONS FOR
C CERTAIN PROBLEMS THAT EXHIBIT CYLINDRICAL SYMMETRY.
C THE RADIAL DIRECTION IS R, AND THE AXIAL DIRECTION IS Z.
C THE FIELDS THAT ARE CALCULATED ARE THE
C CIRCUMFERENTIALLY DIRECTED MAGNETIC FIELD AND THE
C RADIALLY AND AXIALLY DIRECTED ELECTRIC FIELDS. THE
C PROBLEM DOMAIN IS SUBDIVIDED INTO GRID BLOCKS HAVING
C VARIABLE RADIAL AND AXIAL DIMENSIONS. THE ELECTRICAL
C CONDUCTIVITY, RELATIVE DIELECTRIC CONSTANT, AND
C COMPLEX RELATIVE MAGNETIC PERMEABILITY OF EACH GRID
C BLOCK ARE SPECIFIED. THE GRID BLOCKS MAY HAVE ARBITRARY
C ELECTRICAL PROPERTIES.
C
C PROBLEM EXCITATION IS ACHIEVED BY SPECIFYING THE
C MAGNITUDES AND PHASES OF THE TANGENTIAL ELECTRIC
C EXCITATION FIELDS EVERYWHERE ON THE BOUNDARY, AND THE
C MAGNITUDES AND PHASES OF THE CIRCUMFERENTIAL
C MAGNETIC EXCITATION FIELDS AT THE CENTER OF EVERY GRID
C BLOCK.
C
C A SINGLE LAYER OF "PHANTOM" GRID BLOCKS BORDERS ON
C EACH OF THE FOUR SIDES OF THE PROBLEM DOMAIN. THE
```

C "PHANTOM" GRID BLOCKS ADJACENT TO THE AXIS OF SYMMETRY
C ARE GIVEN ZERO ELECTRICAL CONDUCTIVITY, AND THOSE
C ADJACENT TO THE REMAINING THREE SIDES INFINITE
C ELECTRICAL CONDUCTIVITY. THIS ARTIFICE MAKES IT POSSIBLE
C TO USE THE SAME ALGORITHM REPEATEDLY TO GENERATE AS
C MANY EQUATIONS FOR THE MAGNETIC FIELD H AS THERE ARE
C GRID BLOCKS IN THE PROBLEM DOMAIN. THESE EQUATIONS
C HAVE THE FORM $KK * RH = F$, WHERE KK IS THE SYMMETRIC
C COEFFICIENT MATRIX, F IS THE EXCITATION VECTOR, AND R IS
C RADIAL DISTANCE. THE COEFFICIENTS KK OF THESE EQUATIONS
C ARE STORED IN A COMPRESSED COEFFICIENT MATRIX K WHICH
C IS THEN USED TO SOLVE THE EQUATIONS BY GAUSSIAN
C ELIMINATION TO YIELD RH . THE MAGNETIC FIELD DISTRIBUTION
C H IS THEN USED TO SOLVE FOR THE ELECTRIC FIEL.D
C DISTRIBUTION E .

C=====

C ADDENDUM -- JULY 11,1996

C
C IF THE HERZ PROGRAM IS USED TO MODEL A RESONANT CAVITY,
C THE QUALITY FACTOR AND RESONANT FREQUENCY CAN BE
C DETERMINED FOR THE CAVITY. THE RESONANT FREQUENCY IS
C FOUND BY FINDING THE FREQUENCY AT WHICH THE ELECTRIC
C STORED ENERGY EQUALS MAGNETIC STORED ENERGY WITHIN
C THE CAVITY. THE QUALITY FACTOR IS CALCULATED BY FINDING
C THE TOTAL POWER DISSIPATED IN THE CAVITY, AND FINDING
C THE TOTAL ELECTRIC AND MAGNETIC ENERGY STORED IN THE
C CAVITY. IF ONE IS NOT USING THE PROGRAM FOR THE PURPOSES
C OF ANALYSING A RESONANT CAVITY BLOCK OUT THE CALL FOR
C THE SUBROUTINES ENERGY AND POWER1, AS WELL, BLOCK OUT
C THE INCREMENTING OF THE FREQUENCY AND QUALITY FACTOR
C CALCULATION.

C=====

C
C
C----- INPUT VARIABLES

C
C=====

C ADDENDUM -- JULY 11, 1996

C ND - THE NUMBER OF FREQUENCY INCREMENTS THAT WILL BE
C USED

C=====

C NR - NUMBER OF RADIAL GRID BLOCKS IN THE PROBLEM
C DOMAIN

C NZ - NUMBER OF AXIAL GRID BLOCKS IN THE PROBLEM DOMAIN

C DELTAR(NR) - VECTOR CONTAINING THE BLOCK DIMENSIONS IN
 C THE RADIAL DIRECTION, STARTING WITH THE BLOCK
 C NEAREST THE AXIS (M)
 C DELTAZ(NZ) - VECTOR CONTAINING THE BLOCK DIMENSIONS IN
 C THE AXIAL DIRECTION, STARTING WITH THE BLOCK
 C NEAREST THE ORIGIN (M)
 C NREG - THE NUMBER OF REGIONS OF DIFFERENT ELECTRICAL
 C PROPERTIES THAT ARE OVERLAID TO DEFINE THE
 C ELECTRICAL PROPERTIES OF THE PROBLEM DOMAIN
 C DOMIND(4,NREG) - ARRAY THAT DEFINES THE GRID INDICES OF
 C THE BOUNDARIES OF ALL REGIONS. ITS N'TH COLUMN
 C CONSISTS OF MINI, MAXI, MINJ, MAXJ OF THE N'TH REGION,
 C WHERE
 C MINI - THE INTEGER INDEX THAT DEFINES FOR
 C ANY REGION THE LINE OF GRID BLOCKS PARALLEL
 C TO AND NEAREST THE AXIS
 C MAXI - THE INTEGER INDEX THAT DEFINES FOR ANY
 C REGION THE LINE OF GRID BLOCKS PARALLEL TO
 C AND FURTHEST FROM THE AXIS
 C MINJ - THE INTEGER INDEX THAT DEFINES FOR ANY
 C REGION THE LINE OF GRID BLOCKS PERPENDICULAR
 C TO THE AXIS AND NEAREST THE ORIGIN
 C MAXJ - THE INTEGER INDEX THAT DEFINES FOR ANY
 C REGION THE LINE OF GRID BLOCKS PERPENDICULAR
 C TO THE AXIS AND FURTHEST FROM ORIGIN
 C DOMPRP(4,NREG) - ARRAY WHOSE N'TH COLUMN CONSISTS OF
 C SIGMA (ELECTRICAL CONDUCTIVITY S/M), EPSREL
 C (RELATIVE DIELECTRIC CONSTANT), MUREL (RELATIVE REAL
 C MAGNETIC PERMEABILITY), AND MURELI (RELATIVE IMAGINARY
 C MAGNETIC PERMEABILITY) OF THE N'TH REGION
 C
 C FREQ - FREQUENCY OF OPERATION (HZ)
 C EXCMAG(2*(NR+NZ)) - VECTOR CONTAINING THE MAGNITUDES
 C OF THE TANGENTIAL ELECTRIC EXCITATION FIELDS EVERY-
 C WHERE ON THE BOUNDARY. A DATA VALUE HAS TO BE ENTERED
 C FOR EVERY GRID BLOCK ADJACENT TO THE BOUNDARY,
 C INCLUDING THOSE ADJACENT TO THE AXIS OF SYMMETRY. THE
 C FIRST DATA VALUE REPRESENTS THE RADIALY OUTWARD
 C DIRECTED EXCITATION FIELD AT THE GRID BLOCK NEAREST THE
 C ORIGIN. THE DATA VALUES THAT FOLLOW REPRESENT
 C RADIALY OUTWARD DIRECTED EXCITATION FIELDS IN THE
 C SAME PLANE AS THE FIRST DATA VALUE, BUT AT SUCCESSIVELY
 C LARGER RADII. PROCEEDING IN A COUNTERCLOCKWISE
 C DIRECTION ALONG THE BOUNDARY, AFTER NR DATA VALUES

C HAVE BEEN ENTERED FOR RADIAL EXCITATION FIELDS, NZ DATA
 C VALUES ARE ENTERED FOR THE Z-DIRECTED EXCITATION FIELDS
 C AT THE OUTER BOUNDARY. CONTINUING IN A
 C COUNTERCLOCKWISE DIRECTION, A FURTHER NR DATA VALUES
 C ARE ENTERED FOR THE RADIALLY OUTWARD DIRECTED
 C EXCITATION FIELD, STARTING WITH THE FIELD FURTHEST FROM
 C THE AXIS. LASTLY, MOVING ALONG THE AXIS IN THE NEGATIVE
 C Z-DIRECTION, THE LAST NZ Z-DIRECTED EXCITATION FIELDS ARE
 C ENTERED AS DATA. THE LAST ELEMENT IN THE VECTOR IS THE Z-
 C DIRECTED ELECTRIC EXCITATION FIELD ON THE AXIS AND
 C NEAREST THE ORIGIN (V/M).
 C EXCANG(2*(NR+NZ)) - VECTOR CONTAINING THE PHASES
 C CORRESPONDING TO EXCMAG(2*(NR+NZ)) (DEGREES)
 C HCOLMG(NRNZ) - VECTOR CONTAINING THE MAGNITUDES OF
 C THE CIRCUMFERENTIAL MAGNETIC EXCITATION FIELD AT
 C THE CENTER OF EVERY DOMAIN GRID BLOCK SPECIFIED IN
 C COLUMN ORDER (A/M)
 C HCOLAN(NRNZ) - VECTOR CONTAINING THE PHASES
 C CORRESPONDING TO HCOLMG(NRNZ) (DEGREES)
 C HROWMG(NRNZ) - VECTOR CONTAINING THE MAGNITUDES OF
 C THE CIRCUMFERENTIAL MAGNETIC EXCITATION FIELD AT
 C THE CENTER OF EVERY DOMAIN GRID BLOCK SPECIFIED IN
 C ROW ORDER(A/M). THOSE VALUES OF THE
 C CIRCUMFERENTIAL MAGNETIC EXCITATION FIELD THAT
 C HAVE ALREADY BEEN SPECIFIED AS HCOLMG(NRNZ) ARE
 C SPECIFIED HERE AS 0.0.
 C HROWAN(NRNZ) - VECTOR CONTAINING THE PHASES
 C CORRESPONDING TO HROWMG(NRNZ) (DEGREES). THOSE
 C VALUES OF THE CIRCUMFERENTIAL MAGNETIC
 C EXCITATION FIELD THAT HAVE ALREADY BEEN SPECIFIED
 C AS HCOLAN(NRNZ) ARE SPECIFIED HERE AS 0.0.

=====

C ADDENDUM — JULY 11, 1996

C RS(NR,NZ) - ARRAY CONTAINING THE RESISTANCE OF EACH
 C DOMAIN GRID BLOCK USED FOR CALCULATING THE
 C CONDUCTING SURFACE'S RESISTANCE

=====

C

C----- OUTPUT VARIABLES

C HMAG(NR,NZ) - ARRAY CONTAINING THE MAGNITUDES OF
 C MAGNETIC FIELD INTENSITIES AT THE CENTERS OF ALL
 C GRID BLOCKS (A/M)

C HANG(NR,NZ) - ARRAY CONTAINING THE ANGLES OF MAGNETIC
 C FIELD INTENSITIES AT THE CENTERS OF ALL GRID BLOCKS

C (DEGREES)
 C ERMAG(NR,NZ) - ARRAY CONTAINING THE MAGNITUDES OF
 C RADIAL ELECTRIC FIELD INTENSITY COMPONENTS AT THE
 C CENTERS OF CALL GRID BLOCKS (V/M)
 C ERANG(NR,NZ) - ARRAY CONTAINING THE ANGLES OF RADIAL
 C ELECTRIC FIELD INTENSITY COMPONENTS AT THE
 C CENTERS OF ALL GRID BLOCKS (DEGREES)
 C EZMAG(NR,NZ) - ARRAY CONTAINING THE MAGNITUDES OF
 C AXIAL ELECTRIC FIELD INTENSITY COMPONENTS AT THE
 C CENTERS OF ALL GRID BLOCKS (V/M)
 C EZANG(NR,NZ) - ARRAY CONTAINING THE ANGLES OF AXIAL
 C ELECTRIC FIELD INTENSITY COMPONENTS AT THE
 C CENTERS OF ALL GRID BLOCKS (DEGREES)
 C HTRATE(NR,NZ) - TIME AVERAGE HEATING RATE AT THE
 C CENTERS OF ALL GRID BLOCKS (W/M**3)

=====

C ADDENDUM --- JULY 11, 1996

C
 C JOUL(NR,NZ) - ARRAY CONTAINING THE ELECTRICAL STORED
 C ENERGY IN EACH DOMAIN GRID BLOCK
 C JOUL1(NR,NZ) - ARRAY CONTAINING THE MAGNETIC STORED
 C ENERGY IN EACH DOMAIN GRID BLOCK
 C POW - THE TOTAL POWER DISSIPATED IN THE CAVITY
 C POWER(NR,NZ) - ARRAY CONTAINING THE POWER DISSIPATED IN
 C EACH DOMAIN GRID BLOCK
 C QUAL(ND) - VECTOR CONTAINING THE QUALITY FACTOR OF THE
 C CAVITY
 C TOTEN - THE TOTAL ELECTRICAL ENERGY STORED IN THE
 C CAVITY
 C TOTEN1 - THE TOTAL MAGNETIC ENERGY STORED IN THE CAVITY

=====

C
 C ZIN - INPUT IMPEDANCE AT THE PLANE PERPENDICULAR TO THE
 C AXIS AND THROUGH THE ORIGIN (OHMS)

C
 C----- VARIABLES USED WITHIN PROGRAM

=====

C ADDENDUM --- JULY 11, 1996
 C DELTA - THE SIZE OF THE FREQUENCY INCREMENT
 C DELTAF(ND) - THE SIZE OF THE FREQUENCY DROP OR GAIN

=====

C
 C NR1 - NR+1

C NZ1 - NZ+1
 C NPERI - 2*(NR+NZ)
 C NRNZ - NR*NZ
 C SIGJWE(0:NR1,0:NZ1) - ARRAY CONTAINING SIGMA+JW*EPSILON
 C OF EVERY DOMAIN AND PHANTOM GRID BLOCK
 C WMU(NR,NZ) - ARRAY CONTAINING W*MU OF EVERY DOMAIN
 C GRID BLOCK, WHERE MU IS THE ABSOLUTE COMPLEX
 C PERMEABILITY
 C R(0:NR1) - VECTOR THAT CONTAINS ALL THE RADIAL DISTANCES
 C FROM THE AXIS TO THE CENTER OF EVERY GRID BLOCK.
 C ARBITRARY VALUES FOR THE RADIAL DISTANCES TO THE
 C CENTERS OF THE INNERMOST AND OUTERMOST PHANTOM
 C GRID BLOCKS ARE LOCATED IN R(0) AND R(NR1).
 C DELR(0:NR1) - VECTOR THAT CONTAINS ALL RADIAL GRID BLOCK
 C DIMENSIONS. ARBITRARY RADIAL GRID BLOCK
 C DIMENSIONS FOR THE INNERMOST AND OUTERMOST
 C PHANTOM GRID BLOCKS ARE LOCATED IN DELR(0) AND
 C DELR(NR1).
 C Z(NZ) - VECTOR THAT CONTAINS ALL THE AXIAL DISTANCES
 C FROM THE ORIGIN TO THE CENTER OF EVERY DOMAIN
 C GRID BLOCK
 C DELZ(0:NZ1) - VECTOR THAT CONTAINS ALL AXIAL GRID BLOCK
 C DIMENSIONS. ARBITRARY AXIAL GRID BLOCK DIMENSIONS
 C FOR THE PHANTOM GRID BLOCKS NEAREST AND
 C FURTHEST FROM THE ORIGIN ARE LOCATED IN DELZ(0)
 C AND DELZ(NZ1).
 C KK(NRNZ,NRNZ) - SYMMETRIC ARRAY OF THE COMPLEX
 C COEFFICIENTS KK OF THE EQUATIONS $KK \cdot H = F$. THE
 C COEFFICIENT MATRIX KK IS COMPUTED AND STORED ONLY
 C FOR INITIAL TESTING OF THIS PROGRAM.
 C K(NRNZ,NR1) - ARRAY OF THE COMPLEX COEFFICIENTS OF THE
 C COMPRESSED MATRIX K. NOTE THAT NR1 IS THE HALF
 C BANDWIDTH OF THE MATRIX KK (INCLUDING THE
 C DIAGONAL).
 C KCOPY(NRNZ,NR1) - A COPY OF K(NRNZ,NR1). KCOPY IS USED BY
 C SUBROUTINE GAUSEL AND RETURNED TO THE MAIN
 C PROGRAM IN ALTERED FORM.
 C HEXC(NRNZ) - COMPLEX VECTOR CONTAINING THE
 C CONSOLIDATED COLUMN PRIORITY AND ROW PRIORITY
 C COMPLEX MAGNETIC EXCITATION FIELDS, IN COLUMN
 C ORDER
 C F(NRNZ) - COMPLEX VECTOR WHOSE ELEMENTS RECEIVE
 C CONTRIBUTIONS FROM THE REAL AND IMAGINARY PARTS
 C OF THE COMPLEX EXCITATION VOLTAGES CONSTRUCTED


```

C      FROM EXCMAG(NPERI), EXCANG(NPERI), DELR(0:NR1) AND
C      DELZ(0:NZ1). CONTRIBUTIONS TO F ARE ALSO MADE BY
C      THE MAGNETIC EXCITATION FIELDS HCOLMG(NRNZ),
C      HCOLAN(NRNZ), HROWMG(NRNZ), AND HROWAN(NRNZ).
C      FCOPY(NRNZ) - A COPY OF F(NRNZ). FCOPY IS USED BY
C      SUBROUTINE GAUSEL AND RETURNED TO THE MAIN
C      PROGRAM IN ALTERED FORM.
C      RH(NRNZ) - COMPLEX VECTOR RH WHOSE ELEMENTS ARE THE
C      SOLUTION TO  $KK \cdot RH = F$ . RH IS THE PRODUCT
C      (RADIALDISTANCE)*(MAGNETIC FIELD INTENSITY).
C

```

```

C=====
C      ADDENDUM --- JULY 11, 1996
C      WED(NR,NZ) - ARRAY CONTAINING  $W \cdot \text{IMAG}(\epsilon)$  OF EVERY
C      DOMAIN GRID BLOCK WHERE  $\text{IMAG}(\epsilon)$  IS THE
C      IMAGINARY PART OF THE COMPLEX PERMITTIVITY
C=====
C

```

```

C----- DIMENSIONING AND DECLARATION OF INPUT AND OUTPUT
C          VARIABLES

```

```

      INTEGER NR, NZ, NREG, ND

```

```

C#####

```

```

C----- INPUT OF FIRST DATA SET

```

```

C      IF ONLY ELECTRIC EXCITATION IS PRESENT CHOOSE NR,NZ.GE.1!
C      IF ONLY MAGNETIC EXCITATION, OR ELECTRIC AND MAGNETIC
C      EXCITATION IS PRESENT, CHOOSE NR,NZ.GE.3!
C      ND SHOULD ALWAYS BE SET TO AN ODD NUMBER
C

```

```

      PARAMETER (NR=70, NZ=85, NREG=6, ND=1)

```

```

C#####

```

```

      INTEGER DOMIND(4,NREG), NPERI, NRNZ, L1,COUNT

```

```

      REAL DELTAR(NR), DELTAZ(NZ), DOMPRP(4,NREG)

```

```

      PARAMETER (NPERI=2*(NR+NZ))

```

```

      REAL FREQ, EXCMAG(NPERI), EXCANG(NPERI)

```

```

      REAL FREQ1(ND)

```

```

      PARAMETER (NRNZ=NR*NZ)

```

```

      REAL HCOLMG(NRNZ), HCOLAN(NRNZ), HROWMG(NRNZ)

```

```

      REAL HROWAN(NRNZ)

```

```

C

```

```

      REAL HMAG(NR,NZ), HANG(NR,NZ), ERMAG(NR,NZ)

```

```

      REAL ERANG(NR,NZ), FREQO, QO, DEL

```

```

      REAL EZMAG(NR,NZ), EZANG(NR,NZ)

```

```

      REAL QUAL(ND), JOUL(NR,NZ), POWER(NR,NZ), TOTEN

```

REAL POW, JOUL1(NR,NZ), TOTEN1, POW1(NR,NZ)
REAL RA,ZA,EZO(NRNZ),EZ,ANG
CHARACTER*1 TAB

C

*2345678901234567890123456789012345678901234567890123456789012345

C----- DIMENSIONING AND DECLARATION OF VARIABLES USED

C WITHIN PROGRAM

INTEGER NR1,NZ1
PARAMETER (NR1=NR+1, NZ1=NZ+1)
COMPLEX SIGJWE(0:NR1,0:NZ1), WMU(NR,NZ), TAND, FL
REAL R(0:NR1), DELR(0:NR1), Z(NZ), DELZ(0:NZ1), DTOTEN
REAL PO1(NR,NZ), PO2(NR,NZ), PO3(NR,NZ), PO4(NR,NZ)
REAL RS(0:NR1,0:NZ1),FREQ2
REAL WEPSD1, WED(NR,NZ), EPSREL1(NR,NZ)
REAL DELTAF(ND), DELTA, QUAL1, JOULD(NR,NZ), TOTEND
COMPLEX K(NRNZ,NR1), KCOPY(NRNZ,NR1), HEXC(NRNZ)
COMPLEX F(NRNZ)
COMPLEX FCOPY(NRNZ), RH(NRNZ)
TAB=CHAR(9)

C#####

C----- INPUT OF REMAINING DATA SET

DATA DELTAR /5*.0001,14*.0003,2*.0001,6*.000025,1*.00005,3*.0001,
C 4*.0004,20*.001,2*.0003,2*.0001,
C 1*.00005,1*.00003,9*.0000133333333333/
DATA DELTAZ /36*.0016772222222222,4*.00035,1*.000175,2*.000075,
C 1*.00002,1*.000004,2*.000001,1*.000004,1*.000015,
C 1*.00006,1*.0002,3*.0006,2*.0004475,1*.000125,
C 1*.00004,3*.00001,4*.00002,15*.0001266666666666,
C 3*.0004166666,2*.001875/

C NEXT LINE: MINI,MAXI,MINJ,MAXJ

DATA DOMIND /1, 70, 1, 85,
C 5, 35, 1, 46,
C 5, 55, 47, 59,
C 1, 71, 81, 83,
C 1, 52, 84, 85,
C 1, 2, 1, 45/

C NEXT LINE: SIGMA, EPSREL, MUREL, MURELI

DATA DOMPRP /0.0, 1.0, 1.0, 0.0,
C 1.0e30, 1.0, 1.0, 0.0,
C 1.0e30, 1.0, 1.0, 0.0,
C 1.0e30, 1.0, 1.0, 0.0,
C 1.0e30, 1.0, 1.0, 0.0,

C 1.0e30, 1.0, 1.0, 0.0/

DATA FREQ /2.435525e9/
DATA FREQO /2.435525e9/

DATA EXCMAG /310*0.0/
DATA EXCANG /310*0.0/

DATA HCOLMG /35*0.0,0.5,5914*0.0/
DATA HCOLAN /5950*0.0/
DATA HROWMG /5950*0.0/
DATA HROWAN /5950*0.0/

C INVOKE OR DELETE: 1.DECLARATION COMPLEX KK(NRNZ,NRNZ)

C 2.CALL TO SUBROUTINE TESTKK

C#####
*2345678901234567890123456789012345678901234567890123456789012345

C=====

C

OPEN (UNIT=4, FILE='HCOMR2',STATUS='NEW')
OPEN (UNIT=7, FILE='ERCOMR2',STATUS='NEW')
OPEN (UNIT=8, FILE='EZCOMR2',STATUS='NEW')
C OPEN (UNIT=14, FILE='HCOMZ',STATUS='NEW')
C OPEN (UNIT=17, FILE='ERCOMZ',STATUS='NEW')
C OPEN (UNIT=18, FILE='EZCOMZ',STATUS='NEW')
C OPEN (UNIT=40, FILE='QUAL',STATUS='NEW')
C OPEN (UNIT=50, FILE='QUAL2',STATUS='NEW')
OPEN (UNIT=60, FILE='PROG1D',STATUS='NEW')

C

C CALCULATION OF THE RESONANT FREQUENCY

C

COUNT=0
SUM=0.0
DELTA=1.0E3
DO 99 L1=1,ND
FREQ=2.435525e9
SUM=(L1-ND)
DELTA F(L1)=DELTA*SUM
FREQ1(L1)=FREQ+DELTA F(L1)
FREQ=FREQ1(L1)
DEL=FREQO-FREQ

```

C=====
C
C----- ASSIGNMENT OF ELECTRICAL PROPERTIES TO ALL DOMAIN
C   AND PHANTOM GRID BLOCKS
C
C   CALL ASSIGN
C   (NR,NZ,NR1,NZ1,NPERI,NREG,DOMIND,DOMPRP,FREQ,EXCMAG,
C   SIGJWE,WED,WEPD1,R,PROG1,L1,EPSREL1,FREQO,WMU)

C
C----- CALCULATION OF THE RADIAL DISTANCES TO THE CENTERS
C   OF ALL DOMAIN GRID BLOCKS
C   SUM=0.0
C   DO 10 I=1,NR
C       R(I)=SUM+DELTAR(I)/2.0
C       SUM=SUM+DELTAR(I)
10  CONTINUE
C----- ASSIGNMENT OF ARBITRARY RADIAL DISTANCES TO THE
C   CENTERS OF PHANTOM GRID BLOCKS THAT ARE ADJACENT TO
C   THE AXIS AND FURTHEST FROM THE AXIS
C   R(0)=1.0
C   R(NR1)=1.0

C
C----- CONSTRUCTION OF THE VECTOR DELR(0:NR1) THAT
C   CONTAINS THE RADIAL DIMENSIONS OF THE PROBLEM DOMAIN
C   GRIDBLOCKS, AS WELL AS ARBITRARY RADIAL DIMENSIONS FOR
C   THE PHANTOM GRID BLOCKS THAT ARE ADJACENT TO THE AXIS
C   AND FURTHEST FROM THE AXIS.
C   DO 12 I=1,NR
C       DELR(I)=DELTAR(I)
12  CONTINUE
C   DELR(0)=1.0
C   DELR(NR1)=1.0

C
C----- CALCULATION OF THE AXIAL DISTANCES TO THE CENTERS OF
C   ALL DOMAIN GRID BLOCKS
C   SUM=0.0
C   DO 14 J=1,NZ
C       Z(J)=SUM+DELTAZ(J)/2.0
C       SUM=SUM+DELTAZ(J)
14  CONTINUE
C

```

```

C----- CONSTRUCTION OF THE VECTOR DELZ(0:NZ1) THAT
C   CONTAINS THE AXIAL DIMENSIONS OF THE PROBLEM DOMAIN
C   GRIDBLOCKS, AS WELL AS ARBITRARY AXIAL DIMENSIONS FOR
C   THE PHANTOM GRID BLOCKS THAT ARE NEAREST TO AND
C   FURTHEST FROM THE ORIGIN
      DO 16 J=1,NZ
          DELZ(J)=DELTAZ(J)
16   CONTINUE

      DELZ(0)=1.0
      DELZ(NZ1)=1.0
C----- COMPUTATION OF THE COMPRESSED COEFFICIENT ARRAY K
      CALL
      COEFFK(NR,NZ,NR1,NZ1,R,DELR,DELZ,SIGJWE,WMU,NRNZ,K,
C   PROG1)
C
C----- COMPUTATION OF THE CONTRIBUTION TO THE COMPLEX
C   EXCITATION VOLTAGES F BY THE ELECTRIC EXCITATION ON
C   THE BOUNDARIES OF THE PROBLEM DOMAIN. THIS
C   COMPUTATION DOES NOT CHANGE THE COMPRESSED
C   COEFFICIENT ARRAY K.

      CALL VOLTF
C   (EXCMAG,EXCANG,NR,NR1,NZ,NZ1,NRNZ,NPERI,DELR,DELZ,
C   F,PROG1)
C
C----- COMPUTATION OF THE CONTRIBUTION TO THE COMPLEX
C   EXCITATION VOLTAGES F BY THE MAGNETIC EXCITATION
C   WITHIN THE PROBLEM DOMAIN. THIS COMPUTATION CHANGES
C   THE COMPRESSED COEFFICIENT ARRAY K IF MAGNETIC
C   EXCITATION IS PRESENT.
      CALL MGNETF
C   (HCOLMG, HCOLAN, HROWMG, HROWAN, NR, NR1, NZ, NRNZ,
C   R,K,F,HEXC)

      DO 20 J=1,NR1
          DO 22 I=1,NRNZ
              KCOPY(I,J)=K(I,J)
22         CONTINUE
20   CONTINUE
C
C----- A COPY OF THE EXCITATION VOLTAGE VECTOR F IS PLACED
C   INTO FCOPY
      DO 24 I=1,NRNZ

```

```

                FCOPY(I)=F(I)
24    CONTINUE
C
C----- COMPUTATION OF THE VECTOR RH BY GAUSSIAN
C    ELIMINATION
        CALL GAUSEL (NRNZ,NR1,KCOPY,FCOPY,RH)
C
C----- COMPUTATION OF THE RADIAL ELECTRIC FIELD ARRAY AND
C    THE AXIAL ELECTRIC FIELD ARRAY

        CALL GAUSEL (NRNZ,NR1,KCOPY,FCOPY,RH,PROG1)

        CALL EFIELD (NR,NZ,NR1,NZ1,NRNZ,NPERI,DELR,DELZ,R,SIGJWE,
C    EXCMAG,EXCANG,RH,HEXC,ERMAG,ERANG,EZMAG,EZANG,
C    PROG1)

C
C----- COMPUTATION OF TIME AVERAGE ELECTRICAL HEATING
C    RATES
        CALL HOT (NR,NZ,NR1,NZ1,SIGJWE,ERMAG,EZMAG,HTRATE)

C----- COMPUTATION OF HMAG(NR,NZ) AND HANG(NR,NZ) FROM
C    RH
C
        PI=3.141592654
        DO 30 J=1,NZ
            DO 40 I=1,NR
                M=I+(J-1)*NR
                HMAG(I,J)=CABS(RH(M))/R(I)
                IF(HMAG(I,J).EQ.0.0) THEN
                    HANG(I,J)=0.0
                ELSE
                    HANG(I,J)=(180.0/PI)*ATAN2(AIMAG(RH(M)),REAL(RH(M)))
                END IF
            40    CONTINUE
        30    CONTINUE
C----- COMPUTATION OF TOAL ELECTRICAL AND MAGNETIC ENERGY
C    IN THE CAVITY
        CALL ENERGY
C    (NR,NZ,NR1,NZ1,ERMAG,EZMAG,DELZ,R,DELR,TOTEN,SIGJWE,
C    JOUL, JOUL1,HMAG,TOTEN1,EPSREL1,DTOTEN,TOTEND,JOULD)
        WRITE(60,*) TOTEN,TOTEN1,DTOTEN,FREQ,DEL

```

C----- COMPUTATION OF POWER DISSIPATED IN THE CAVITY

CALL POWER1

C (NR,NZ,NR1,NZ1,ERMAG,EZMAG,HMAG,DELZ,R,DELR,SIGJWE,
C WED,WMU, POWER,POW,FREQ, PO1, PO2,PO3,PO4,RS,POW1,
C PROG1)

FL=2*TOTEND/(TOTEN+TOTEN1)

QUAL=PI*FREQ*(TOTEN+TOTEN1)/POW

WRITE(60,10) QUAL

10 FORMAT (1X,'QUALITY FACTOR IS 'F5.8)

WRITE (60,20) FREQ

20 FORMAT (1X,'THE FREQUENCY IS 'E15.8)

WRITE (60,37) FL

37 FORMAT (1X,'THE FILLING FACTOR IS ',E15.8)

99 CONTINUE

C RESULTS OF CALCULATIONS ARE WRITTEN TO NEW FILES

C 'OUTHZR', 'HCOMR', 'HCOMZ', 'ERCOMR', 'ERCOMZ', 'EZCOMR',

C 'EZCOMZ', 'HEATR', 'HEATZ', 'PROG1'QUAL', 'QUAL1'

CALL OUTPUT

C (NR,NZ,NRNZ,NR1,RH,R,Z,HMAG,HANG,ERMAG,ERANG,EZMAG,
EZANG)

STOP

END

*2345678901234567890123456789012345678901234567890123456789012345

C=====

C

SUBROUTINE ASSIGN

C (NR,NZ,NR1,NZ1,NPERI,NREG,DOMIND,DOMPRP,FREQ,EXCMAG,
SIGJWE,WED,WEPD1,R,PROG1,L1,EPSREL1,FREQO,WMU)

C THIS SUBROUTINE ASSIGNS ELECTRICAL PROPERTIES TO EVERY

C DOMAIN AND PHANTOM GRID BLOCK

C

C----- INPUT VARIABLES

C NR - NUMBER OF RADIAL GRID BLOCKS IN THE PROBLEM DOMAIN

C NZ - NUMBER OF AXIAL GRID BLOCKS IN THE PROBLEM DOMAIN

C NR1 - NR+1

C NZ1 - NZ+1

C NPERI - 2*(NR+NZ)

C NREG -THE NUMBER OF REGIONS OF DIFFERENT ELECTRICAL

```

C   PROPERTIES THAT ARE OVERLAID TO DEFINE THE ELECTRICAL
C   PROPERTIES OF THE PROBLEM DOMAIN
C   DOMIND(4,NREG) - ARRAY THAT DEFINES THE GRID INDICES OF
C   THE BOUNDARIES OF ALL REGIONS. ITS N'TH COLUMN CONSISTS
C   OF MINI, MAXI, MINJ, MAXJ OF THE N'TH REGION
C   DOMPRP(4,NREG) - ARRAY WHOSE N'TH COLUMN CONSISTS OF
C   SIGMA (ELECTRICAL CONDUCTIVITY), EPSREL (RELATIVE
C   DIELECTRIC CONSTANT), MUREL (RELATIVE MAGNETIC
C   PERMEABILITY), AND MURELI (RELATIVE IMAGINARY MAGNETIC
C   PERMEABILITY) OF THE
C   N'TH REGION
C   FREQ - FREQUENCY OF OPERATION
C   EXCMAG(NPERI) - MAGNITUDES OF THE R AND Z-DIRECTED
C   TANGENTIAL ELECTRIC EXCITATION FIELDS AT THE BOUNDARY
C
C----- OUTPUT VARIABLES
C   SIGJWE(0:NR1,0:NZ1) - ARRAY CONTAINING SIGMA +JW*EPSILON OF
C   EVERY DOMAIN AND PHANTOM GRID BLOCK
C   WMU(NR,NZ) - ARRAY CONTAINING W*MU OF EVERY DOMAIN GRID
C   BLOCK, WHERE MU IS THE ABSOLUTE COMPLEX PERMEABILITY
C   WED(NR,NZ) - ARRAY CONTAINING W*IMAG(EPS) OF EVERY DOMAIN
C   GRID BLOCK WHERE IMAG(EPS) IS THE IMAGINARY PART OF THE
C   COMPLEX PERMITTIVITY
C

```

```

INTEGER NR,NZ
INTEGER NREG,DOMIND(4,NREG)
REAL DOMPRP(4,NREG), FREQ, EXCMAG(NPERI), MUNOT
REAL WEPSD1,EPSREL1(NR,NZ)
REAL WED(NR,NZ),EPS
COMPLEX SIGJWE(0:NR1,0:NZ1), WMU(NR,NZ)

```

```

PI=3.141592654
EPSNOT=1.0E-9/(36.0*PI)
MUNOT=4.0*PI*1.0E-7
W=2.0*PI*FREQ

```

```

C
C----- ASSIGN SIGMA+JW*EPSILON AND W*MU TO EVERY DOMAIN
C   GRID BLOCK
C   DO 10 N=1,NREG
C       MINI=DOMIND(1,N)
C       MAXI=DOMIND(2,N)
C       MINJ=DOMIND(3,N)

```



```

MAXJ=DOMIND(4,N)
SIG=DOMPRP(1,N)
IF ((SIG.GT.0.00).AND.(SIG.LT.1.0e30)) THEN
SIG=SIG*FREQ/FREQO
ELSE
END IF
EPS=DOMPRP(2,N)
WEPS=W*DOMPRP(2,N)*EPSNOT
OMEGMU=W*DOMPRP(3,N)*MUNOT
OMEGMI=W*DOMPRP(4,N)*MUNOT
IF (SIG.EQ.0.0) THEN
WEPSD1=0.0
ELSE
WEPSD1=SIG/W
END IF

DO 20 I=MINI,MAXI
      DO 30 J=MINJ,MAXJ
        EPSREL1(I,J)=EPS
        SIGJWE(I,J)=CMPLX(SIG,WEPS)
        WMU(I,J)=CMPLX(OMEGMU,-OMEGMI)
        WED(I,J)=WEPSD1
30      CONTINUE
20    CONTINUE
10  CONTINUE
C
C----- ASSIGN ZERO ELECTRICAL CONDUCTIVITY TO THOSE
C PHANTOM GRID BLOCKS ADJACENT TO AXIS AT WHOSE
C LOCATION A ZERO TANGENTIAL ELECTRIC EXCITATION FIELD IS
C SPECIFIED, AND INFINITE ELECTRICAL CONDUCTIVITY TO ALL
C OTHER PHANTOM GRID BLOCKS
DO 40 I=1,NR
      SIGJWE(I,0)=CMPLX(1.0E30,0.0)
      SIGJWE(I,NZ1)=CMPLX(1.0E30,0.0)
40  CONTINUE

DO 50 J=1,NZ
      IF (EXCMAG(NPERI+1-J).EQ.0.0) THEN
        SIGJWE(0,J)=CMPLX(0.0,0.0)
      ELSE
        SIGJWE(0,J)=CMPLX(1.0E30,0.0)
      END IF
      SIGJWE(NR1,J)=CMPLX(1.0E30,0.0)

```

50 CONTINUE
RETURN
END

C-----
C

C SUBROUTINE COEFFK(NR,NZ,NR1,NZ1,R,DELR,DELZ,SIGJWE,WMU,
C NRNZ,K,PROG1)

C
C THIS SUBROUTINE COMPUTES THE COEFFICIENTS K OF THE
C COMPRESSED COEFFICIENT ARRAY K

C
C----- INPUT VARIABLES

C NR - NUMBER OF RADIAL GRID BLOCKS IN THE PROBLEM DOMAIN
C NZ - NUMBER OF AXIAL GRID BLOCKS IN THE PROBLEM DOMAIN
C NR1 - NR + 1
C NZ1 - NZ + 1
C R(0:NR1) - VECTOR THAT CONTAINS THE RADIAL DISTANCES FROM
C THE AXIS TO THE CENTER OF EVERY DOMAIN AND
C PHANTOM GRID BLOCK
C DELR(0:NR1) - VECTOR THAT CONTAINS THE RADIAL GRID BLOCK
C DIMENSIONS OF EVERY DOMAIN AND PHANTOM GRID
C BLOCK
C DELZ(0:NZ1) - VECTOR THAT CONTAINS THE AXIAL GRID BLOCK
C DIMENSIONS OF EVERY DOMAIN AND PHANTOM GRID
C BLOCK
C SIGJWE(0:NR1,0:NZ1) - ARRAY CONTAINING SIGMA +JW*EPSILON OF
C EVERY DOMAIN AND PHANTOM GRID BLOCK.
C WMU(NR,NZ) - ARRAY CONTAINING W*MU OF EVERY DOMAIN GRID
C BLOCK, WHERE MU IS THE ABSOLUTE COMPLEX
C PERMEABILITY
C NRNZ - NR*NZ

C
C----- OUTPUT VARIABLES
C K(NRNZ,NR1) - COMPRESSED COEFFICIENT ARRAY
C

INTEGER NR,NZ,NR1,NZ1,NRNZ
REAL R(0:NR1), DELR(0:NR1), DELZ(0:NZ1)
COMPLEX SIGJWE(0:NR1,0:NZ1), WMU(NR,NZ)
COMPLEX K(NRNZ,NR1)

```

COMPLEX B,C,D,K1,K2,K3,K4,K5
C
C----- INITIALIZE THE ENTIRE ARRAY K(NRNZ,NR1) TO ZERO
DO 10 J=1,NR1
    DO 20 I=1,NRNZ
        K(I,J)=(0.0,0.0)
20    CONTINUE
10    CONTINUE
C
C----- CALCULATE THE COEFFICIENTS OF K(NRNZ,NR1)

DO 30 J=1,NZ
    DO 40 I=1,NR
        A=-2.0*DELZ(J)
        B=SIGJWE(I-1,J)*(R(I-1)+DELR(I-1)/4.0)*DELR(I-1)
        C=SIGJWE(I,J)*(R(I)-DELR(I)/4.0)*DELR(I)
        K2=A/(B+C)

        A=-2.0*DELR(I)/R(I)
        B=SIGJWE(I,J)*DELZ(J)
        C=SIGJWE(I,J+1)*DELZ(J+1)
        K3=A/(B+C)

        A=-2.0*DELZ(J)
        B=SIGJWE(I,J)*(R(I)+DELR(I)/4.0)*DELR(I)
        C=SIGJWE(I+1,J)*(R(I+1)-DELR(I+1)/4.0)*DELR(I+1)
        K4=A/(B+C)

        A=-2.0*DELR(I)/R(I)
        B=SIGJWE(I,J-1)*DELZ(J-1)
        C=SIGJWE(I,J)*DELZ(J)
        K5=A/(B+C)

        D=(0.0,1.0)*WMU(I,J)*DELR(I)*DELZ(J)/R(I)

        K1=D-K2-K3-K4-K5
        M=I+NR*(J-1)
        K(M,1)=K1
C----- COEFFICIENTS KK ARE CALCULATED ONLY FOR THOSE H
C    THAT LIE IN GRID BLOCKS WITHIN THE PROBLEM DOMAIN
        IF(J.LT.NZ) K(M,1+NR)=K3

        IF(I.LT.NR) K(M,2)=K4

```

40 CONTINUE
30 CONTINUE
RETURN
END

C-----
C
C SUBROUTINE VOLTF
C (EXCMAG,EXCANG,NR,NR1,NZ,NZ1,NRNZ,NPERI,DEL,
C DELZ,F,PROG1)
C
C THIS SUBROUTINE CALCULATES THE CONTRIBUTIONS BY THE
C ELECTRIC EXCITATION FIELDS ON ALL FOUR DOMAIN
C BOUNDARIES TO THE COMPLEX EXCITATION VOLTAGES F IN THE
C EQUATION $KK \cdot RH = F$
C
C----- INPUT VARIABLES
C EXCMAG(NPERI) - MAGNITUDES OF THE R AND Z-DIRECTED
C TANGENTIAL ELECTRIC EXCITATION FIELDS AT THE
C BOUNDARY
C EXCANG(NPERI) - VECTOR CONTAINING THE PHASES
C CORRESPONDING TO EXCMAG(NPERI) (DEGREES)
C NR - NUMBER OF DOMAIN GRID BLOCKS IN THE RADIAL
C DIRECTION
C NR1 - NR + 1
C NZ - NUMBER OF DOMAIN GRID BLOCKS IN THE AXIAL
C DIRECTION
C NZ1 - NZ + 1
C NRNZ - NR*NZ
C NPERI - 2*(NR+NZ)
C DELR(0:NR1) - VECTOR THAT CONTAINS ALL RADIAL GRID BLOCK
C DIMENSIONS
C DELZ(0:NZ1) - VECTOR THAT CONTAINS ALL AXIAL GRID BLOCK
C DIMENSIONS
C----- OUTPUT VARIABLE
C F(NRNZ) - COMPLEX EXCITATION VOLTAGES F IN THE EQUATION
C $KK \cdot H = F$
C

INTEGER NR,NR1,NZ,NZ1,NRNZ,NPERI
REAL EXCMAG(NPERI),EXCANG(NPERI), DELR(0:NR1)
REAL DELZ(0:NZ1)

```

      COMPLEX F(NRNZ)
C
C----- INITIALIZE F(NRNZ) TO ZERO
      DO 5 NF=1,NRNZ
          F(NF)=CMPLX(0.0,0.0)
5      CONTINUE
C
C----- CALCULATE THE CONTRIBUTIONS TO F(NRNZ)
      FACTOR=3.141592654/180.0
      DO 10 I=1,NR
          EXCANR=EXCANG(I)*FACTOR
          FREAL=EXCMAG(I)*COS(EXCANR)*DELR(I)
          FIMAG=EXCMAG(I)*SIN(EXCANR)*DELR(I)
          F(I)=CMPLX(FREAL,FIMAG)

10     CONTINUE

      DO 20 I=1,NR
          NEXC=NZ+2*NR+1-I
          EXCANR=EXCANG(NEXC)*FACTOR
          FREAL=EXCMAG(NEXC)*COS(EXCANR)*DELR(I)
          FIMAG=EXCMAG(NEXC)*SIN(EXCANR)*DELR(I)
          F((NZ-1)*NR+I)=F((NZ-1)*NR+I)-CMPLX(FREAL,FIMAG)

20     CONTINUE

      DO 30 J=1,NZ
          NEXC=NR+J
          EXCANR=EXCANG(NEXC)*FACTOR
          FREAL=EXCMAG(NEXC)*COS(EXCANR)*DELZ(J)
          FIMAG=EXCMAG(NEXC)*SIN(EXCANR)*DELZ(J)
          F(NR*J)=F(NR*J)+CMPLX(FREAL,FIMAG)

30     CONTINUE

      DO 40 J=1,NZ
          NEXC=NPERI+1-J
          EXCANR=EXCANG(NEXC)*FACTOR
          FREAL=EXCMAG(NEXC)*COS(EXCANR)*DELZ(J)
          FIMAG=EXCMAG(NEXC)*SIN(EXCANR)*DELZ(J)
          F((J-1)*NR+1)=F((J-1)*NR+1)-CMPLX(FREAL,FIMAG)

40     CONTINUE
      RETURN

```

```

      END
C234567890123456789012345678901234567890123456789012345678901234
C=====
C
      SUBROUTINE MGNETF
      C (HCOLMG,HCOLAN,HROWMG,HROWAN,NR,NR1,NZ,
      C NRNZ,R,K,F,HEXC, PROG1)
C
C THIS SUBROUTINE CALCULATES THE CONTRIBUTION TO THE
C COMPLEX EXCITATION VOLTAGES F BY THE MAGNETIC
C EXCITATION WITHIN THE PROBLEM DOMAIN. THIS SUBROUTINE
C CHANGES THE COMPRESSED COEFFICIENT ARRAY K IF
C MAGNETIC EXCITATION IS PRESENT.
C
C----- INPUT VARIABLES
C HCOLMG(NRNZ) - VECTOR CONTAINING THE MAGNITUDES OF THE
C CIRCUMFERENTIAL MAGNETIC EXCITATION FIELD SPECIFIED IN
C COLUMN ORDER (A/M)
C HCOLAN(NRNZ) - VECTOR CONTAINING THE PHASES
C CORRESPONDING TO HCOLMG(NRNZ) (DEGREES)
C HROWMG(NRNZ) - VECTOR CONTAINING THE MAGNITUDES OF THE
C CIRCUMFERENTIAL MAGNETIC EXCITATION FIELD SPECIFIED IN
C ROW ORDER (A/M). THOSE VALUES OF THE CIRCUMFERENTIAL
C MAGNETIC EXCITATION FIELD THAT HAVE ALREADY BEEN
C SPECIFIED AS HCOLMG(NRNZ) ARE SPECIFIED HERE AS 0.0.
C HROWAN(NRNZ) - VECTOR CONTAINING THE PHASES
C CORRESPONDING TO HROWMG(NRNZ) (DEGREES). THOSE
C VALUES OF THE CIRCUMFERENTIAL MAGNETIC EXCITATION
C FIELD THAT HAVE ALREADY BEEN SPECIFIED AS HCOLAN(NRNZ)
C ARE SPECIFIED HERE AS 0.0.
C NR - NUMBER OF RADIAL GRID BLOCKS IN THE PROBLEM DOMAIN
C NR1 - NR+1
C NZ - NUMBER OF AXIAL GRID BLOCKS IN THE PROBLEM DOMAIN
C NRNZ - NR*NZ
C R(0:NR1) - VECTOR THAT CONTAINS ALL THE RADIAL DISTANCES
C FROM THE AXIS TO THE CENTER OF EVERY GRID BLOCK.
C ARBITRARY VALUES FOR THE RADIAL DISTANCES TO THE
C CENTERS OF THE INNERMOST AND OUTERMOST PHANTOM GRID
C BLOCKS ARE LOCATED IN R(0) AND R(NR1).
C K(NRNZ,NR1) - ARRAY OF THE COMPLEX COEFFICIENTS OF THE
C COMPRESSED MATRIX K. NOTE THAT NR1 IS THE HALF
C BANDWIDTH OF THE MATRIX KK (INCLUDING THE
C DIAGONAL).THIS SUBROUTINE CHANGES THE COMPRESSED
C MATRIX K IF MAGNETIC EXCITATION IS PRESENT.

```

C F(NRNZ) - COMPLEX VECTOR F WHOSE ELEMENTS RECEIVE
 C CONTRIBUTIONS FROM THE REAL AND IMAGINARY PARTS OF
 C THE COMPLEX EXCITATION VOLTAGES. IN THIS SUBROUTINE
 C FURTHER CONTRIBUTIONS TO F ARE MADE BY THE MAGNETIC
 C EXCITATION FIELDS HCOLMG(NRNZ), HCOLAN(NRNZ),
 C HROWMG(NRNZ), AND HROWAN(NRNZ).
 C

C----- OUTPUT VARIABLES

C K(NRNZ,NR1) - ALTERED COMPRESSED COEFFICIENT MATRIX
 C F(NRNZ) - COMPLEX EXCITATION VECTOR IN THE EQUATION
 C $KK \cdot RH = F$
 C

C----- VARIABLES USED WITHIN SUBROUTINE

C HEXC(NRNZ) - COMPLEX VECTOR CONTAINING THE CONSOLIDATED
 C COLUMN PRIORITY AND ROW PRIORITY COMPLEX MAGNETIC
 C EXCITATION FIELDS, IN COLUMN ORDER
 C

INTEGER NR,NR1,NZ,NRNZ,I,J
 REAL HCOLMG(NRNZ),HCOLAN(NRNZ),HROWMG(NRNZ)
 REAL HROWAN(NRNZ)
 REAL R(0:NR1)
 COMPLEX K(NRNZ,NR1),F(NRNZ),HEXC(NRNZ)

C
 C----- INITIALIZE HEXC(NRNZ) TO ZERO

DO 10 M=1,NRNZ
 HEXC(M)=CMPLX(0.0,0.0)

10 CONTINUE

C
 C----- ASSIGN VALUES TO HEXC(M) USING THE MAGNETIC FIELD
 C EXCITATION ENTERED IN COLUMN ORDER

FACTOR=3.141592654/180.0
 DO 20 M=1,NRNZ
 IF(HCOLMG(M).NE.0.0) THEN
 HXCANR=HCOLAN(M)*FACTOR
 HREAL=HCOLMG(M)*COS(HXCANR)
 HIMAG=HCOLMG(M)*SIN(HXCANR)
 HEXC(M)=CMPLX(HREAL,HIMAG)
 END IF

```

20  CONTINUE
C
C----- ADD TO HEXC(M) THE MAGNETIC FIELD EXCITATION
C  ENTERED IN ROW ORDER
      DO 30 M=1,NRNZ
          J=1+(M-1)/NR
          I=M-(J-1)*NR
          MM=(I-1)*NZ+J
          IF(HROWMG(MM).NE.0.0) THEN
              HXCANR=HROWAN(MM)*FACTOR
              HREAL=HROWMG(MM)*COS(HXCANR)
              HIMAG=HROWMG(MM)*SIN(HXCANR)
              HEXC(M)=HEXC(M)+CMPLX(HREAL,HIMAG)
          END IF
30  CONTINUE
C
C----- BEGIN MODIFICATION OF K AND F

      DO 40 M=1,NRNZ
C  FIRST MODIFICATION OF K AND F. NOTE THAT ANY E FIELD ON
C  BOUNDARY ADJACENT TO GRID BLOCK M WILL NOW BE
C  IGNORED BY BEING OVERWRITTEN.
          IF(CABS(HEXC(M)).NE.0.0) THEN
              J=1+(M-1)/NR
              I=M-(J-1)*NR
              F(M)=HEXC(M)*R(I)
              K(M,1)=CMPLX(1.0,0.0)
C
C----- USING ALL BUT THE FIRST COEFFICIENT OF THE COMPRESSED
C  COEFFICIENT MATRIX K IN ROW M, SUBTRACT SUCCESSIVE
C  VALUES OF COEFFICIENT*RH FROM SUCCESSIVE VALUES OF F
C  BELOW F(M), AND THEN REPLACE EACH OF THE COEFFICIENTS
C  USED BY ZERO IN THE COMPRESSED COEFFICIENT MATRIX K

              DO 50 N=2,NR1
                  IF((M-1+N).LE.NRNZ) THEN
                      F(M-1+N)=F(M-1+N)-K(M,N)*HEXC(M)*R(I)
                  ELSE
                      END IF

                  IF((M-1+N).LE.NRNZ) THEN
                      K(M,N)=CMPLX(0.0,0.0)

                  ELSE

```



```

                END IF
50             CONTINUE
C
C----- USING ALL BUT THE FIRST COEFFICIENT OF THE COMPRESSED
C          COEFFICIENT MATRIX K ON THE UPSLANTING TO RIGHT
C          DIAGONAL THROUGH K(M,1), SUBTRACT SUCCESSIVE VALUES OF
C          COEFFICIENT*RH FROM SUCCESSIVE VALUES OF F ABOVE F(M),
C          AND THEN REPLACE EACH OF THE COEFFICIENTS USED BY ZERO
C          IN THE COMPRESSED COEFFICIENT MATRIX K
                DO 60 N=2,NR1
                IF((M+1-N).GT.0) THEN
                F(M+1-N)=F(M+1-N)-K(M+1-N,N)*HEXC(M)*R(I)
                ELSE
                END IF

                IF((M+1-N).GT.0) THEN
                K(M+1-N,N)=CMPLX(0.0,0.0)

                ELSE
                END IF

60             CONTINUE
                END IF
40          CONTINUE
                RETURN
                END
C
C=====
C
C          SUBROUTINE GAUSEL (NSIZE,MBAND,K,F,H,PROG1)
C
C          THIS ROUTINE SOLVES THE LINEAR ALGEBRAIC SYSTEM OF
C          EQUATIONS  $KK \cdot H = F$  BY GAUSSIAN ELIMINATION WITHOUT
C          PIVOTING. THE MATRIX  $KK$  IS SYMMETRIC AND BANDED. ROWS
C          IN THE UPPER TRIANGLE OF THE MATRIX  $KK$  ARE SHIFTED TO
C          THE LEFT UNTIL THE DIAGONAL TERMS ARE IN THE FIRST
C          COLUMN OF THE COMPRESSED MATRIX  $K$ . THIS SUBROUTINE
C          OPERATES DIRECTLY ON  $K$ . THE SOLUTION IS RETURNED IN THE
C          VECTOR  $H$ .
C
C----- INPUT VARIABLES
C  NSIZE - ORDER OF MATRIX  $KK$ 
C  MBAND - HALF BANDWIDTH OF  $KK$  (INCLUDING DIAGONAL)
C   $K(NSIZE,MBAND)$  - COMPRESSED COEFFICIENT MATRIX

```

```

C   F(NSIZE) - EXCITATION VECTOR
C
C----- OUTPUT VARIABLES
C   H(NSIZE) - MAGNETIC FIELD VECTOR
C
      INTEGER NSIZE,MBAND
      COMPLEX K(NSIZE,MBAND)
      COMPLEX F(NSIZE)
      COMPLEX H(NSIZE)
      COMPLEX C
C
C   THE ABOVE DIMENSION STATEMENTS PERMIT AN R-Z PROBLEM
C   DOMAIN CONSISTING OF A TOTAL OF NSIZE GRID BLOCKS
C-----
      NSIZM1=NSIZE-1
C----- FORWARD REDUCTION OF MATRIX
      DO 30 N=1,NSIZM1
          DO 20 L=2,MBAND
              I=N+L-1
              IF((K(N,L).EQ.(0.0,0.0)).OR.(I.GT.NSIZE)) GO TO 20
              C=K(N,L)/K(N,1)
              J=0
                  DO 10 M=L,MBAND
                      J=J+1
                      K(I,J)=K(I,J)-C*K(N,M)
10              CONTINUE
                  K(N,L)=C
20          CONTINUE
30      CONTINUE
C----- FORWARD REDUCTION OF RIGHT HAND SIDE
      DO 60 N=1,NSIZM1
          DO 50 L=2,MBAND
              I=N+L-1
              IF(I.LE.NSIZE) F(I)=F(I)-K(N,L)*F(N)
50          CONTINUE
          F(N)=F(N)/K(N,1)
60      CONTINUE
          F(NSIZE)=F(NSIZE)/K(NSIZE,1)

```

C----- BACK SUBSTITUTION

H(NSIZE)=F(NSIZE)

DO 90 N=1,NSIZM1

J=NSIZE-N

H(J)=F(J)

DO 80 L=2,MBAND

M=J+L-1

IF(M.LE.NSIZE) H(J)=H(J)-K(J,L)*H(M)

80 CONTINUE

90 CONTINUE

RETURN

END

C

C=====

C

SUBROUTINE EFIELD (NR,NZ,NR1,NZ1,NRNZ,NPERI,DELR,DELZ,

C R,SIGJWE,EXCMAG,EXCANG,RH,HEXC,ERMAG,ERANG,

C EZMAG,EZANG,PROG1)

C

C THIS SUBROUTINE COMPUTES THE MAGNITUDES AND PHASE

C ANGLES OF THE RADIAL AND AXIAL ELECTRIC FIELD

C INTENSITIES AT THE CENTERS OF ALL GRID BLOCKS

C

C----- INPUT VARIABLES

C NR - NUMBER OF DOMAIN GRID BLOCKS IN THE RADIAL

C DIRECTION

C NZ - NUMBER OF DOMAIN GRID BLOCKS IN THE AXIAL DIRECTION

C NR1 - NR+1

C NZ1 - NZ+1

C NRNZ - NR*NZ

C NPERI - 2*(NR+NZ)

C DELR(0:NR1) - VECTOR THAT CONTAINS ALL RADIAL GRID BLOCK

C DIMENSIONS

C DELZ(0:NZ1) - VECTOR THAT CONTAINS ALL AXIAL GRID BLOCK

C DIMENSIONS

C R(0:NR1) - VECTOR THAT CONTAINS THE RADIAL DISTANCES FROM

C THE AXIS TO THE CENTER OF EVERY DOMAIN AND PHANTOM

C GRID BLOCK

C SIGJWE(0:NR1,0:NZ1) - ARRAY CONTAINING SIGMA +JW*EPSILON OF

C EVERY DOMAIN AND PHANTOM GRID BLOCK

C EXCMAG(NPERI) - VECTOR CONTAINING THE MAGNITUDE OF THE

C \TANGENTIAL ELECTRIC FIELD VECTOR EVERYWHERE ON THE

C BOUNDARY

C EXCANG(NPERI) - VECTOR CONTAINING THE ANGLE OF THE
 C TANGENTIAL ELECTRIC FIELD VECTOR EVERYWHERE ON THE
 C BOUNDARY
 C RH(NRNZ) - THE PRODUCT (RADIAL DISTANCE)*(MAGNETIC FIELD
 C INTENSITY)
 C HEXC(NRNZ) - COMPLEX VECTOR CONTAINING THE CONSOLIDATED
 C COLUMN PRIORITY AND ROW PRIORITY COMPLEX MAGNETIC
 C EXCITATION FIELDS, IN COLUMN ORDER
 C

C----- OUTPUT VARIABLES

C ERMAG(NR,NZ) - ARRAY CONTAINING THE MAGNITUDES OF
 C RADIAL ELECTRIC FIELD INTENSITY COMPONENTS AT THE
 C CENTERS OF ALL GRID BLOCKS (V/M)
 C ERANG(NR,NZ) - ARRAY CONTAINING THE ANGLES OF RADIAL
 C ELECTRIC FIELD INTENSITY COMPONENTS AT THE CENTERS OF
 C ALL GRID BLOCKS (DEGREES)
 C EZMAG(NR,NZ) - ARRAY CONTAINING THE MAGNITUDES OF AXIAL
 C ELECTRIC FIELD INTENSITY COMPONENTS AT THE CENTERS OF
 C ALL GRID BLOCKS (V/M)
 C EZANG(NR,NZ) - ARRAY CONTAINING THE ANGLES OF AXIAL
 C ELECTRIC FIELD INTENSITY COMPONENTS AT THE CENTERS OF
 C ALL GRID BLOCKS (DEGREES)
 C

INTEGER NR,NZ,NR1,NZ1,NRNZ,NPERI
 REAL DELR(0:NR1), DELZ(0:NZ1), R(0:NR1)
 COMPLEX SIGJWE(0:NR1,0:NZ1), RH(NRNZ), HEXC(NRNZ)
 REAL EXCMAG(NPERI), EXCANG(NPERI)
 REAL ERMAG(NR,NZ), ERANG(NR,NZ), EZMAG(NR,NZ)
 REAL EZANG(NR,NZ)
 COMPLEX A1,A2,A3,A4,A5,A6,ASAVE
 REAL B

C
 C----- SUBROUTINE VOLTF USES THE ELECTRIC EXCITATION AT THE
 C BOUNDARIES TO GENERATE THE ELEMENTS OF THE COMPLEX
 C EXCITATION VECTOR F. IF MAGNETIC EXCITATION IS SPECIFIED
 C FOR A GRID BLOCK ADJACENT TO A BOUNDARY OF THE
 C DOMAIN, THEN THE SUBROUTINE MGNETF OVERWRITES THE
 C ELEMENT IN VECTOR F CORRESPONDING TO THAT GRID BLOCK.
 C HENCE, THE ELECTRIC EXCITATION AT THE BOUNDARY OF THAT
 C GRID BLOCK IS NOW IGNORED. IN THIS SUBROUTINE WE USE
 C EXTRAPOLATION TO GENERATE THE ELECTRIC FIELD
 C COMPONENT PARALLEL TO THE BOUNDARY AT THE CENTER OF
 C THE GRID BLOCK ADJACENT TO THE BOUNDARY WHENEVER

```

C    MAGNETIC EXCITATION IS PRESENT ADJACENT TO A BOUNDARY.
C
C----- ASSIGNMENT OF MAGNITUDE AND ANGLE OF RADIAL
C    ELECTRIC FIELD INTENSITY AT THE CENTER OF EVERY DOMAIN
C    GRID BLOCK
      FACTOR=180.0/3.141592654
      DO 10 I=1,NR
        ANGLE=EXCANG(I)/FACTOR
        EREAL=EXCMAG(I)*COS(ANGLE)
        EIMAG=EXCMAG(I)*SIN(ANGLE)
        A1=CMPLX(EREAL,EIMAG)

      DO 20 J=1,NZ
        IF (J.EQ.NZ) THEN
          ANGLE=EXCANG(NZ+2*NR+1-I)/FACTOR
          EREAL=EXCMAG(NZ+2*NR+1-I)*COS(ANGLE)
          EIMAG=EXCMAG(NZ+2*NR+1-I)*SIN(ANGLE)
          A5=CMPLX(EREAL,EIMAG)
        ELSE
          A2=RH((J-1)*NR+I)-RH(J*NR+I)
          B=2.0/R(I)
          A4=SIGJWE(I,J)*DELZ(J)+SIGJWE(I,J+1)*DELZ(J+1)
          A5=A2*B/A4
        END IF
        A6=(A1+A5)/2.0
        ERMAG(I,J)=CABS(A6)
        IF(ERMAG(I,J).EQ.0.0) THEN
          ERANG(I,J)=0.0
        ELSE
          ERANG(I,J)=FACTOR*ATAN2(AIMAG(A6),REAL(A6))
        END IF

C
C    IF MAGNETIC EXCITATION IS PRESENT ADJACENT TO BOUNDARY
C    EXTRAPOLATE AND THEN OVERWRITE THE RADIAL ELECTRIC
C    FIELD INTENSITY IN DOMAIN GRID BLOCK ADJACENT TO
C    BOUNDARY
      IF(J.EQ.2.AND.CABS(HEXC(I)).NE.0.0) THEN
        A6=A1+0.5*DELZ(1)*(A1-A5)/DELZ(2)
        ERMAG(I,1)=CABS(A6)
        IF(ERMAG(I,1).EQ.0.0) THEN
          ERANG(I,1)=0.0
        ELSE
          ERANG(I,1)=FACTOR*ATAN2(AIMAG(A6),REAL(A6))

```

```
END IF
END IF
```

```
IF (J.EQ.NZ.AND.CABS(HEXC((NZ-1)*NR+I)).NE.0.0) THEN
A6=A1+0.5*DELZ(NZ)*(A1-ASAVE)/DELZ(NZ-1)
ERMAG(I,NZ)=CABS(A6)
IF(ERMAG(I,NZ).EQ.0.0) THEN
ERANG(I,NZ)=0.0
ELSE
ERANG(I,NZ)=FACTOR*ATAN2(AIMAG(A6),REAL(A6))
END IF
END IF
```

```
ASAVE=A1
A1=A5
```

```
20      CONTINUE
10     CONTINUE
```

```
C
```

```
C----- ASSIGNMENT OF MAGNITUDE AND ANGLE OF AXIAL
C ELECTRIC FIELD INTENSITY AT THE CENTER OF EVERY DOMAIN
C GRID BLOCK. THE AXIAL ELECTRIC FIELD INTENSITY IN THE
C DOMAIN GRID BLOCK ADJACENT TO THE CENTRAL AXIS IS
C CALCULATED BY EXTRAPOLATION WHEN ELECTRIC EXCITATION
C IS PRESENT ON THE CENTRAL AXIS AND ALSO WHEN MAGNETIC
C EXCITATION IS PRESENT ADJACENT TO CENTRAL AXIS.
```

```
DO 40 J=1,NZ
ANGLE=EXCANG(NR+J)/FACTOR
EREAL=EXCMAG(NR+J)*COS(ANGLE)
EIMAG=EXCMAG(NR+J)*SIN(ANGLE)
A1=CMPLX(EREAL,EIMAG)
```

```
IF(NR.EQ.1) THEN
ANGLE=EXCANG(NPERI+1-J)/FACTOR
EREAL=EXCMAG(NPERI+1-J)*COS(ANGLE)
EIMAG=EXCMAG(NPERI+1-J)*SIN(ANGLE)
A5=CMPLX(EREAL,EIMAG)
A6=(A1+A5)/2.0
EZMAG(1,J)=CABS(A6)
IF(EZMAG(1,J).EQ.0.0) THEN
EZANG(1,J)=0.0
ELSE
EZANG(1,J)=FACTOR*ATAN2(AIMAG(A6),REAL(A6))
```

```

END IF
ELSE

DO 50 I=NR,2,-1
A2=2.0*(RH(NR*(J-1)+I)-RH(NR*(J-1)+I-1))
A3=SIGJWE(I-1,J)*(R(I-1)+DELR(I-1)/4.0)*DELR(I-1)
A4=SIGJWE(I,J)*(R(I)-DELR(I)/4.0)*DELR(I)
A5=A2/(A3+A4)
A6=(A1+A5)/2.0
EZMAG(I,J)=CABS(A6)
IF(EZMAG(I,J).EQ.0.0) THEN
EZANG(I,J)=0.0
ELSE
EZANG(I,J)=FACTOR*ATAN2(AIMAG(A6),REAL(A6))
END IF

```

```

IF(I.EQ.2) THEN
A6=A5+(A5-A1)*(0.5*DELR(1))/DELR(2)
EZMAG(1,J)=CABS(A6)
IF(EZMAG(1,J).EQ.0.0) THEN
EZANG(1,J)=0.0
ELSE
EZANG(1,J)=FACTOR*ATAN2(AIMAG(A6),REAL(A6))
END IF
END IF

```

C
C
C
C
C

IF MAGNETIC EXCITATION IS PRESENT ADJACENT TO OUTER
BOUNDARY EXTRAPOLATE AND THEN OVERWRITE THE RADIAL
ELECTRIC FIELD INTENSITY IN DOMAIN GRID BLOCK ADJACENT
TO BOUNDARY

```

IF(I.EQ.NR-1.AND.CABS(HEXC(J*NR)).NE.0.0) THEN
A6=A1+0.5*DELR(NR)*(A1-A5)/DELR(NR-1)
EZMAG(NR,J)=CABS(A6)
IF(EZMAG(NR,J).EQ.0.0) THEN
EZANG(NR,J)=0.0
ELSE
EZANG(NR,J)=FACTOR*ATAN2(AIMAG(A6),REAL(A6))
END IF
END IF

```

50 A1=A5
CONTINUE
END IF

40 CONTINUE
RETURN
END

```
C=====
C
C SUBROUTINE HOT (NR,NZ,NR1,NZ1,SIGJWE,ERMAG,EZMAG,HTRATE)
C
C THIS SUBROUTINE CALCULATES THE TIME AVERAGE HEATING
C RATES AT THE CENTERS OF ALL DOMAIN GRID BLOCKS. IF SIGMA
C OF A GRID BLOCK EQUALS 1.0E30, THEN HTRATE FOR THAT GRID
C BLOCK IS SET TO ZERO!
C
C----- INPUT VARIABLES
C NR - NUMBER OF RADIAL GRID BLOCKS IN THE PROBLEM DOMAIN
C NZ - NUMBER OF AXIAL GRID BLOCKS IN THE PROBLEM DOMAIN
C NR1 - NR+1
C NZ1 - NZ+1
C SIGJWE(0:NR1,0:NZ1) - ARRAY CONTAINING SIGMA +JW*EPSILON OF
C EVERY DOMAIN AND PHANTOM GRID BLOCK
C ERMAG(NR,NZ) - ARRAY CONTAINING THE MAGNITUDES OF
C RADIAL ELECTRIC FIELD INTENSITY COMPONENTS AT THE
C CENTERS OF ALL GRID BLOCKS (V/M)
C EZMAG(NR,NZ) - ARRAY CONTAINING THE MAGNITUDES OF AXIAL
C ELECTRIC FIELD INTENSITY COMPONENTS AT THE CENTERS OF
C ALL GRID BLOCKS (V/M)
C
C----- OUTPUT VARIABLE
C HTRATE(NR,NZ) - TIME AVERAGE HEATING RATE AT THE CENTERS
C OF ALL GRID BLOCKS (W/M**3)
C
C INTEGER NR,NZ,NR1,NZ1
C COMPLEX SIGJWE(0:NR1,0:NZ1)
C REAL ERMAG(NR,NZ),EZMAG(NR,NZ),HTRATE(NR,NZ)
C
C----- CALCULATE HEATING RATE AT THE CENTERS OF ALL GRID
C BLOCKS
C DO 10 J=1,NZ
C DO 20 I=1,NR
C IF (REAL(SIGJWE(I,J)).EQ.1.0E30) THEN
C HTRATE(I,J)=0.0
C ELSE
C HTRATE(I,J)=0.5*REAL(SIGJWE(I,J))*
C (ERMAG(I,J)**2+EZMAG(I,J)**2)
C END IF
```


20 CONTINUE
10 CONTINUE
RETURN
END

C=====

C ADDENDUM --- JULY 11, 1996
C SUBROUTINE ENERGY

C (NR,NZ,NR1,NZ1,ERMAG,EZMAG,DELZ,R,DELR,TOTEN,SIGJWE,
C JOUL,JOUL1,HMAG,TOTEN1,EPSREL1,DTOTEN,TOTEND,JOULD)

C
C THIS SUBROUTINE CALCULATES THE TIME AVERAGE ELECTRICAL
C AND MAGNETIC STORED ENERGY IN ALL OF THE DOMAIN GRID
C BLOCKS. IF SIGMA OF A GRID BLOCK DOES NOT EQUAL ZERO
C THEN JOUL(I,J) AND JOUL1(I,J) IS SET TO ZERO. FINALLY, THE
C TOTAL ENERGY STORED IN THE CAVITY IS CALCULATED BY
C SUMMING EACH GRID BLOCK COMPONENT
C

C----- INPUT VARIABLES

C NR - NUMBER OF RADIAL GRID BLOCKS IN THE PROBLEM DOMAIN

C NZ - NUMBER OF AXIAL GRID BLOCKS IN THE PROBLEM DOMAIN

C NR1 - NR+1

C NZ1 - NZ+1

C SIGJWE(0:NR1,0:NZ1) - ARRAY CONTAINING SIGMA +JW*EPSILON OF
C EVERY DOMAIN AND PHANTOM GRID BLOCK

C ERMAG(NR,NZ) - ARRAY CONTAINING THE MAGNITUDES OF
C RADIAL ELECTRIC FIELD INTENSITY COMPONENTS AT THE
C CENTERS OF ALL GRID BLOCKS (V/M)

C EZMAG(NR,NZ) - ARRAY CONTAINING THE MAGNITUDES OF AXIAL
C ELECTRIC FIELD INTENSITY COMPONENTS AT THE CENTERS OF
C ALL GRID BLOCKS (V/M)

C HMAG(NR,NZ) - ARRAY CONTAINING THE MAGNITUDES OF
C MAGNETIC FIELD INTENSITIES AT THE CENTERS OF ALL GRID
C BLOCKS (A/M)

C R(0:NR1) - VECTOR THAT CONTAINS ALL THE RADIAL DISTANCES
C FROM THE AXIS TO THE CENTER OF EVERY GRID BLOCK.
C ARBITRARY VALUES C FOR THE RADIAL DISTANCES TO THE
C CENTERS OF THE INNERMOST AND OUTERMOST PHANTOM GRID
C BLOCKS ARE LOCATED IN R(0) AND R(NR1).

C DELR(0:NR1) - VECTOR THAT CONTAINS ALL RADIAL GRID BLOCK
C DIMENSIONS. ARBITRARY RADIAL GRID BLOCK DIMENSIONS FOR
C THE INNERMOST AND OUTERMOST PHANTOM GRID BLOCKS ARE
C LOCATED IN DELR(0) AND DELR(NR1).

C DELZ(0:NZ1) - VECTOR THAT CONTAINS ALL AXIAL GRID BLOCK

```
C   DIMENSIONS. ARBITRARY AXIAL GRID BLOCK DIMENSIONS FOR
C   THE PHANTOM GRID BLOCKS NEAREST AND FURTHEST FROM
C   THE ORIGIN ARE LOCATED IN DELZ(0) AND DELZ(NZ1).
```

```
C
C----- OUTPUT VARIABLES
```

```
C   JOUL(NR,NZ) - ARRAY CONTAINING THE ELECTRICAL STORED
C               ENERGY IN EACH DOMAIN GRID BLOCK
C   JOUL1(NR,NZ) - ARRAY CONTAINING THE MAGNETIC STORED
C               ENERGY IN EACH DOMAIN GRID BLOCK
C   TOTEN - THE TOTAL ELECTRICAL ENERGY STORED IN THE
C           CAVITY
C   TOTEN1 - THE TOTAL MAGNETIC ENERGY STORED IN THE CAVITY
C
```

```
INTEGER NR,NZ,NR1,NZ1
REAL ERMAG(NR,NZ),EZMAG(NR,NZ),DELZ(0:NZ1),R(0:NR1)
REAL EPSNOT,PI,JOUL1(NR,NZ),MUNOT,HMAG(NR,NZ),DTOTEN
REAL DELR(0:NR1),JOUL(NR,NZ),TOTEN,TOTEN1,EPSREL1(NR,NZ)
REAL JOULD(NR,NZ),TOTEND
COMPLEX SIGJWE(0:NR1,0:NZ1)
```

```
C
C----- SET THE INITIAL CONDITION OF NO ENERGY IN THE CAVITY
C
```

```
TOTEN=0.0
TOTEN1=0.0
DTOTEN=0.0
```

```
C
C----- CALCULATE THE ELECTRICAL AND MAGNETIC ENERGIES IN
C   THE CAVITY
```

```
DO 50 J=1,NZ
  DO 60 I=1,NR
    R(0)=0.0
    IF(REAL(SIGJWE(I,J)).GT.1.0E+5) THEN
      JOUL(I,J)=0.0
    ELSE
      PI=3.141592654
      EPSNOT=1.0e-9/(36.0*PI)
```

```

MUNOT=PI*4.0e-7
JOUL(I,J)=0.5*EPSNOT*EPSREL1(I,J)*PI*DELZ(J)*
C ((R(I)+DELR(I)/2.0)**2-(R(I)-DELR(I)/2.0)**2)*
C (ERMAG(I,J)**2+EZMAG(I,J)**2)
JOUL1(I,J)=0.5*MUNOT*PI*DELZ(J)*(HMAG(I,J)**2)*
C ((R(I)+DELR(I)/2.0)**2-(R(I)-DELR(I)/2.0)**2)

```

```

TOTEN=TOTEN+JOUL(I,J)
TOTEN1=TOTEN1+JOUL1(I,J)
END IF

```

```

60 CONTINUE
50 CONTINUE

```

```

DTOTEN=TOTEN1-TOTEN
RETURN
END

```

C

C=====

C ADDENDUM --- JULY 11, 1996
C SUBROUTINE POWER1

```

C (NR,NZ,NR1,NZ1,ERMAG,EZMAG,HMAG,DELZ,R,DELR,SIGJWE,
C WED,WMU,POWER,POW,FREQ,PO1,PO2,PO3,PO4,RS,POW1,PROG1)

```

C THIS SUBROUTINE CALCULATES THE TOTAL POWER DISSIPATED
C IN EACH DOMAIN GRID BLOCK AND FOR THE ENTIRE CAVITY. IF
C SIGMA OF A GRID BLOCK IS SET TO ZERO THEN POWER(I,J) IS SET
C TO ZERO. THE TOTAL POWER IS FOUND BY SUMMING EACH GRID
C BLOCK COMPONENT

C

C----- INPUT VARIABLES

```

C NR - NUMBER OF RADIAL GRID BLOCKS IN THE PROBLEM DOMAIN
C NZ - NUMBER OF AXIAL GRID BLOCKS IN THE PROBLEM DOMAIN
C NR1 - NR+1
C NZ1 - NZ+1
C SIGJWE(0:NR1,0:NZ1) - ARRAY CONTAINING SIGMA +JW*EPSILON OF
C EVERY DOMAIN AND PHANTOM GRID BLOCK
C ERMAG(NR,NZ) - ARRAY CONTAINING THE MAGNITUDES OF RADIAL
C ELECTRIC FIELD INTENSITY COMPONENTS AT THE CENTERS OF
C ALL GRID BLOCKS (V/M)
C EZMAG(NR,NZ) - ARRAY CONTAINING THE MAGNITUDES OF AXIAL

```

C ELECTRIC FIELD INTENSITY COMPONENTS AT THE CENTERS OF
 C ALL GRID BLOCKS (V/M)
 C FREQ - FREQUENCY OF OPERATION (HZ)
 C HMAG(NR,NZ) - ARRAY CONTAINING THE MAGNITUDES OF
 C MAGNETIC FIELD INTENSITIES AT THE CENTERS OF ALL GRID
 C BLOCKS (A/M)
 C R(0:NR1) - VECTOR THAT CONTAINS ALL THE RADIAL DISTANCES
 C FROM THE AXIS TO THE CENTER OF EVERY GRID BLOCK.
 C ARBITRARY VALUES FOR THE RADIAL DISTANCES TO THE
 C CENTERS OF THE INNERMOST AND OUTERMOST PHANTOM GRID
 C BLOCKS ARE LOCATED IN R(0) AND R(NR1).
 C DELR(0:NR1) - VECTOR THAT CONTAINS ALL RADIAL GRID BLOCK
 C DIMENSIONS. ARBITRARY RADIAL GRID BLOCK DIMENSIONS FOR
 C THE INNERMOST AND OUTERMOST PHANTOM GRID BLOCKS ARE
 C LOCATED IN DELR(0) AND DELR(NR1).
 C DELZ(0:NZ1) - VECTOR THAT CONTAINS ALL AXIAL GRID BLOCK
 C DIMENSIONS. ARBITRARY AXIAL GRID BLOCK DIMENSION FOR
 C THE PHANTOM GRID BLOCKS NEAREST AND FURTHEST FROM
 C THE ORIGIN ARE LOCATED IN DELZ(0) AND DELZ(NZ1).
 C RS(0:NR1,0:NZ1) - ARRAY CONTAINING THE RESISTANCE OF EACH
 C DOMAIN GRID BLOCK USED CALCULATING THE CONDUCTING
 C SURFACE'S RESISTANCE
 C WED(NR,NZ) - ARRAY CONTAINING $W \cdot \text{IMAG}(\epsilon)$ OF EVERY
 C DOMAIN GRID BLOCK WHERE $\text{IMAG}(\epsilon)$ IS THE IMAGINARY
 C PART OF THE COMPLEX PERMITTIVITY
 C WMU(NR,NZ) - ARRAY CONTAINING $W \cdot \mu$ OF EVERY DOMAIN
 C GRID BLOCK, WHERE μ IS THE ABSOLUTE COMPLEX
 C PERMEABILITY
 C
 C----- OUTPUT VARIABLES
 C
 C POW - THE TOTAL POWER DISSIPATED IN THE CAVITY
 C POWER(NR,NZ) - ARRAY CONTAINING THE POWER DISSIPATED IN
 C EACH DOMAIN GRID BLOCK

 C
 C
 C INTEGER NR,NZ,NR1,NZ1
 C REAL ERMAG(NR,NZ),EZMAG(NR,NZ),HMAG(NR,NZ),
 C REAL R(0:NR1),DELZ(0:NZ1),DELR(0:NR1)
 C REAL WED(NR,NZ),POWER(NR,NZ),RS(0:NR1,0:NZ1)
 C REAL PO1(NR,NZ),PO2(NR,NZ),PO3(NR,NZ),PO4(NR,NZ)
 C REAL POW,FREQ, POW1(NR,NZ)
 C COMPLEX SIGJWE(0:NR1,0:NZ1),WMU(NR,NZ)
 C
 C----- SETTING THE INITIAL POWER DISSIPATION TO ZERO

```
POW=0.0
PI=3.141592654
SUM1=0.0
SUM=0.0
```

```
C
C----- CALCULATING THE RESISTANCE OF EACH GRID BLOCK
C
```

```
CON=1.1E+7
DO 40 I=1,NR
    RS(I,0)=SQRT(REAL(WMU(I,1))/(2*CON))
    RS(I,NZ1)=SQRT(REAL(WMU(I,NZ))/(2*CON))
40 CONTINUE

DO 45 J=1,NZ
    RS(NR1,J)=SQRT(REAL(WMU(NR,J))/(2*CON))
45 CONTINUE

DO 10 J=1,NZ
    DO 20 I=1,NR
        IF (REAL(SIGJWE(I,J)).GT.1.0e5) THEN
            RS(I,J)=SQRT(REAL(WMU(I,J))/(2*CON))
        ELSE
            RS(I,J)=0.0
        END IF
    20 CONTINUE
10 CONTINUE
```

```
C
C----- CALCULATING THE POWER DISSIPATED
C
```

```
DO 50 J=1,NZ
    DO 60 I=1,NR
```

```
C
C----- CALCULATING THE POWER DISSIPATED IN THE DIELECTRIC
C
```

```

C      IF ((REAL(SIGJWE(I,J)).LT.1.0e5).AND.
        (REAL(SIGJWE(I,J)).GT.0.0)) THEN

C      POWER(I,J)=WED(I,J)*(ERMAG(I,J)**2+EZMAG(I,J)**2)*
        2*PI*FREQ*R(I)*PI*DELZ(J)*DELR(I)

        ELSE
        END IF

C
C----- CALCULATING THE POWER DISSIPATED IN THE BOUNDARY
C      WALLS

C      IF (REAL(SIGJWE(I-1,J)).GT.1.0E5) THEN
        PO1(I,J)=HMAG(I,J)**2*PI*DELZ(J)*(R(I)-DELR(I)/2.0)*
        RS(I-1,J)*(R(I)/(R(I)-DELR(I)/2.0))**2
        ELSE
        END IF

C      IF (REAL(SIGJWE(I+1,J)).GT.1.0E5) THEN
        PO2(I,J)=HMAG(I,J)**2*PI*DELZ(J)*(R(I)+DELR(I)/2.0)*
        RS(I+1,J)*(R(I)/(R(I)+DELR(I)/2.0))**2
        ELSE
        END IF

        IF (REAL(SIGJWE(I,J-1)).GT.1.0E5) THEN
        PO3(I,J)=HMAG(I,J)**2*PI*R(I)*DELR(I)*RS(I,J-1)
        ELSE
        END IF

        IF (REAL(SIGJWE(I,J+1)).GT.1.0E5) THEN
        PO4(I,J)=HMAG(I,J)**2*PI*R(I)*DELR(I)*RS(I,J+1)
        ELSE
        END IF

        SUM=SUM+POWER(I,J)
        POW1(I,J)=PO1(I,J)+PO2(I,J)+PO3(I,J)+PO4(I,J)

        SUM1=SUM1+POW1(I,J)
60      CONTINUE
50      CONTINUE

        POW=SUM1+SUM
        RETURN

```

END

C=====

SUBROUTINE OUTPUT

C (NR,NZ,NRNZ,NR1,RH,R,Z,HMAG,HANG,ERMAG,ERANG,
C EZMAG,EZANG)

C

C THIS SUBROUTINE WRITES TO NEW FILES 'OUTHZR', 'HCOMR',
C 'HCOMZ','ERCOMR', 'ERCOMZ', 'EZCOMR', 'EZCOMZ', 'HEATR',
C 'HEATZ', 'PROG1','QUAL', 'QUAL1'

C

C----- INPUT VARIABLES

C ND - THE NUMBER OF FREQUENCY INCREMENTS THAT WILL BE
C TESTED

C NR - NUMBER OF RADIAL GRID BLOCKS IN THE PROBLEM DOMAIN

C NZ - NUMBER OF AXIAL GRID BLOCKS IN THE PROBLEM DOMAIN

C NRNZ - NR*NZ

C NR1 - NR+1

C RH(NRNZ) - COMPLEX VECTOR RH WHOSE ELEMENTS ARE THE
C SOLUTION TO $KK \cdot RH = F$. RH IS THE PRODUCT (RADIAL
C DISTANCE)*(MAGNETIC FIELD INTENSITY).

C R(0:NR1) - VECTOR THAT CONTAINS ALL THE RADIAL DISTANCES
C FROM THE AXIS TO THE CENTER OF EVERY GRID BLOCK.

C ARBITRARY VALUES FOR THE RADIAL DISTANCES TO THE
C CENTERS OF THE INNERMOST AND OUTERMOST PHANTOM GRID
C BLOCKS ARE LOCATED IN R(0) AND R(NR1).

C Z(NZ) - VECTOR THAT CONTAINS ALL THE AXIAL DISTANCES FROM
C THE ORIGIN TO THE CENTER OF EVERY DOMAIN GRID BLOCK

C HMAG(NR,NZ) - ARRAY CONTAINING THE MAGNITUDES OF
C MAGNETIC FIELD INTENSITIES AT THE CENTERS OF ALL GRID
C BLOCKS (A/M)

C HANG(NR,NZ) - ARRAY CONTAINING THE ANGLES OF MAGNETIC
C FIELD INTENSITIES AT THE CENTERS OF ALL GRID BLOCKS
C (DEGREES)

C ERMAG(NR,NZ) - ARRAY CONTAINING THE MAGNITUDES OF RADIAL
C ELECTRIC FIELD INTENSITY COMPONENTS AT THE CENTERS OF
C ALL GRID BLOCKS (V/M)

C ERANG(NR,NZ) - ARRAY CONTAINING THE ANGLES OF RADIAL
C ELECTRIC FIELD INTENSITY COMPONENTS AT THE CENTERS OF
C ALL GRID BLOCKS (DEGREES)

C EZMAG(NR,NZ) - ARRAY CONTAINING THE MAGNITUDES OF AXIAL
C ELECTRIC FIELD INTENSITY COMPONENTS AT THE CENTERS OF

C ALL GRID BLOCKS (V/M)
 C EZANG(NR,NZ) - ARRAY CONTAINING THE ANGLES OF AXIAL
 C ELECTRIC FIELD INTENSITY COMPONENTS AT THE CENTERS OF
 C ALL GRID BLOCKS (DEGREES)
 C HTRATE(NR,NZ) - TIME AVERAGE HEATING RATE AT THE CENTERS
 C OF ALL GRID BLOCKS (W/M**3)
 C JOUL(NR,NZ) - ARRAY CONTAINING THE ELECTRICAL STORED
 C ENERGY IN EACH DOMAIN GRID BLOCK
 C JOUL1(NR,NZ) - ARRAY CONTAINING THE MAGNETIC STORED
 C ENERGY IN EACH DOMAIN GRID BLOCK
 C POW - THE TOTAL POWER DISSIPATED IN THE CAVITY
 C POWER(NR,NZ) - ARRAY CONTAINING THE POWER DISSIPATED IN
 C EACH DOMAIN GRID BLOCK
 C QUAL(ND) - VECTOR CONTAINING THE QUALITY FACTOR OF THE
 C CAVITY
 C TOTEN - THE TOTAL ELECTRICAL ENERGY STORED IN THE CAVITY
 C TOTEN1 - THE TOTAL MAGNETIC ENERGY STORED IN THE CAVITY
 C
 C----- DIMENSIONING OF INPUT VARIABLES

INTEGER NR,NZ,NRNZ
 COMPLEX RH(NRNZ)
 REAL R(0:NR1), Z(NZ)
 REAL HMAG(NR,NZ), HANG(NR,NZ), ERMAG(NR,NZ)
 REAL ERANG(NR,NZ), EZMAG(NR,NZ), EZANG(NR,NZ)

CHARACTER*1 TAB
 TAB=CHAR(9)

```

DO 300 J=1,NZ
      DO 310 I=1,NR
        WRITE(4,*) R(I),TAB,Z(J),TAB,HMAG(I,J),TAB,HANG(I,J)
310      CONTINUE
300    CONTINUE

DO 400 I=1,NR
      DO 410 J=1,NZ
        WRITE(14,*) R(I),TAB,Z(J),TAB,HMAG(I,J),TAB,HANG(I,J)
410      CONTINUE
400    CONTINUE

DO 320 J=1,NZ
      DO 330 I=1,NR
        WRITE(7,*) R(I),TAB,Z(J),TAB,ERMAG(I,J),TAB,ERANG(I,J)
  
```



```

330     CONTINUE
320 CONTINUE

      DO 420 I=1,NR
          DO 430 J=1,NZ
              WRITE(17,*) R(I),TAB,Z(J),TAB,ERMAG(I,J),TAB,ERANG(I,J)
430     CONTINUE
420 CONTINUE

      DO 340 J=1,NZ
          DO 350 I=1,NR
              WRITE(8,*) R(I),TAB,Z(J),TAB,EZMAG(I,J),TAB,EZANG(I,J)
350     CONTINUE
340 CONTINUE

      DO 440 I=1,NR
          DO 450 J=1,NZ
              WRITE(18,*) R(I),TAB,Z(J),TAB,EZMAG(I,J),TAB,EZANG(I,J)
450     CONTINUE
440 CONTINUE

DO 500 J=1,NZ
    DO 510 I=1,NR
        WRITE (20,*) R(I), TAB, Z(J), TAB, HTRATE(I,J)
510 CONTINUE
500 CONTINUE
C
DO 600 I=1,NR
    DO 610 J=1,NZ
        WRITE (30,*) R(I), TAB, Z(J), TAB, HTRATE(I,J)
610 CONTINUE
600 CONTINUE
C

```

```

      RETURN
      END

```

```

C=====
*2345678901234567890123456789012345678901234567890123456789012345

```

APPENDIX 2

EVALUATION OF Q-MEASUREMENT AND LOSS TANGENT UNCERTAINTY

This appendix covers the uncertainty analysis of the measured cavity Q-factor, Q_m , determined via the reflectometer. This uncertainty mainly originates from uncertainties in measured return loss. Next, uncertainty in measured loss tangent is analyzed in terms of measured Q-factor shift, $\Delta\left(\frac{1}{Q_0}\right)$, and relative dielectric constant, ϵ_r' .

A2.1 Uncertainty of Measured Q-factor

Measured Q-factor includes losses of the test cavity and the reflectometer.

Measured Q-factor, Q_m , can be analytically represented by

$$Q_m = \alpha \frac{f_0}{\Delta f_{\text{dB}}} \quad (\text{A2.1})$$

where

$$\alpha = \sqrt{\frac{|\Gamma_{pp}|^2 - |\Gamma_o|^2}{1 - |\Gamma_{pp}|^2}} \quad (\text{A2.2})$$

and $|\Gamma_{pp}|$ is the bandwidth reflection coefficient, and Δf_{dB} is the bandwidth between power points of return loss, $RL = -x$ dB. Taking the partial derivative of Eq.(A2.1) with respect to bandwidth reflection coefficient, $|\Gamma_{pp}|$, yields,

$$\frac{\mathcal{Q}_m}{d|\Gamma_{pp}|} = \sqrt{\frac{1-|\Gamma_{pp}|^2}{|\Gamma_{pp}|^2 - |\Gamma_0|^2}} \frac{|\Gamma_{pp}|(1-|\Gamma_0|^2)}{(1-|\Gamma_{pp}|^2)^2} \frac{f_0}{\Delta f_{\text{xdB}}} \quad (\text{A2.3}).$$

Simplifying Eq.(A2.3) in order to utilize the measured Q-factor expression in Eq(A2.1), yields

$$\frac{\mathcal{Q}_m}{d|\Gamma_{pp}|} = \left(\frac{1-|\Gamma_0|^2}{1-|\Gamma_{pp}|^2} \right) \frac{f_0}{\Delta f_{\text{xdB}}} \frac{|\Gamma_{pp}|}{\sqrt{1-|\Gamma_{pp}|^2}} \frac{1}{\sqrt{|\Gamma_{pp}|^2 - |\Gamma_0|^2}} \sqrt{\frac{|\Gamma_{pp}|^2 - |\Gamma_0|^2}{|\Gamma_{pp}|^2 - |\Gamma_0|^2}} \quad (\text{A2.4}).$$

Re-writing Eq.(A2.4) in terms of Eqs.(A2.1) and (A2.2) yields

$$\frac{\mathcal{Q}_m}{d|\Gamma_{pp}|} = \left(\frac{1-|\Gamma_0|^2}{1-|\Gamma_{pp}|^2} \right) \frac{|\Gamma_{pp}|}{(|\Gamma_{pp}|^2 - |\Gamma_0|^2)} Q_m \quad (\text{A2.5}).$$

Which can be re-arranged to give the normalized uncertainty in measured Q-factor,

$$\frac{\Delta Q_m}{Q_m} = \left(\frac{1-|\Gamma_0|^2}{1-|\Gamma_{pp}|^2} \right) \frac{|\Gamma_{pp}| d|\Gamma_{pp}|}{(|\Gamma_{pp}|^2 - |\Gamma_0|^2)} \quad (\text{A2.6}).$$

In practice, return loss, RL, is measured and is related to $|\Gamma|$ by

$$\text{RL} = -20\log(|\Gamma|) \quad (\text{A2.7}).$$

From this definition, uncertainty in return loss is

$$\frac{d\text{RL}}{d|\Gamma|} = -\left(\frac{20}{\ln 10} \right) \frac{1}{|\Gamma|} \quad (\text{A2.8}).$$

Re-writing Eq.(A2.8) so it can be utilized in Eq.(A2.6) in terms of the bandwidth reflection coefficient, $|\Gamma_{pp}|$, yields

$$|\Gamma_{pp}| \left(\frac{d|\Gamma_{pp}|}{|\Gamma_{pp}|} \right) = - \left(\frac{\ln 10}{20} \right) |\Gamma_{pp}|^2 dRL \quad (\text{A2.9}).$$

The return loss uncertainty can be rewritten in terms of the reflectometer's directivity, D , and the bandwidth reflection coefficient, $|\Gamma_{pp}|$, i.e.,

$$dRL = 20 \log \left(1 + \frac{|\Gamma_D|}{|\Gamma_{pp}|} \right) \quad (\text{A2.10})$$

where $|\Gamma_D| = 10^{\frac{-D}{20}}$ [60] (A2.11).

Utilizing Eqs.(A2.9) and (A2.11), Eq.(A2.6) can be written in a format where relative uncertainty in measured Q-factor can be easily calculated from known values of $|\Gamma_0|$, $|\Gamma_{pp}|$, and $|\Gamma_D|$, i.e.

$$\frac{\Delta Q_m}{Q_m} = \left(\frac{1 - |\Gamma_0|^2}{1 - |\Gamma_{pp}|^2} \right) \frac{|\Gamma_{pp}|^2}{(|\Gamma_{pp}|^2 - |\Gamma_0|^2)} \ln \left(1 + \frac{|\Gamma_D|}{|\Gamma_{pp}|} \right) \quad (\text{A2.12}).$$

In Figure A2.1, relative uncertainty in measured Q-factor, $\frac{\Delta Q_m}{Q_m}$, is plotted versus bandwidth reflection coefficient, $|\Gamma_{pp}|$, for different resonant frequency reflection coefficient values, $|\Gamma_0|$. The directional coupler directivity is $D = 30$ dB for this analysis.

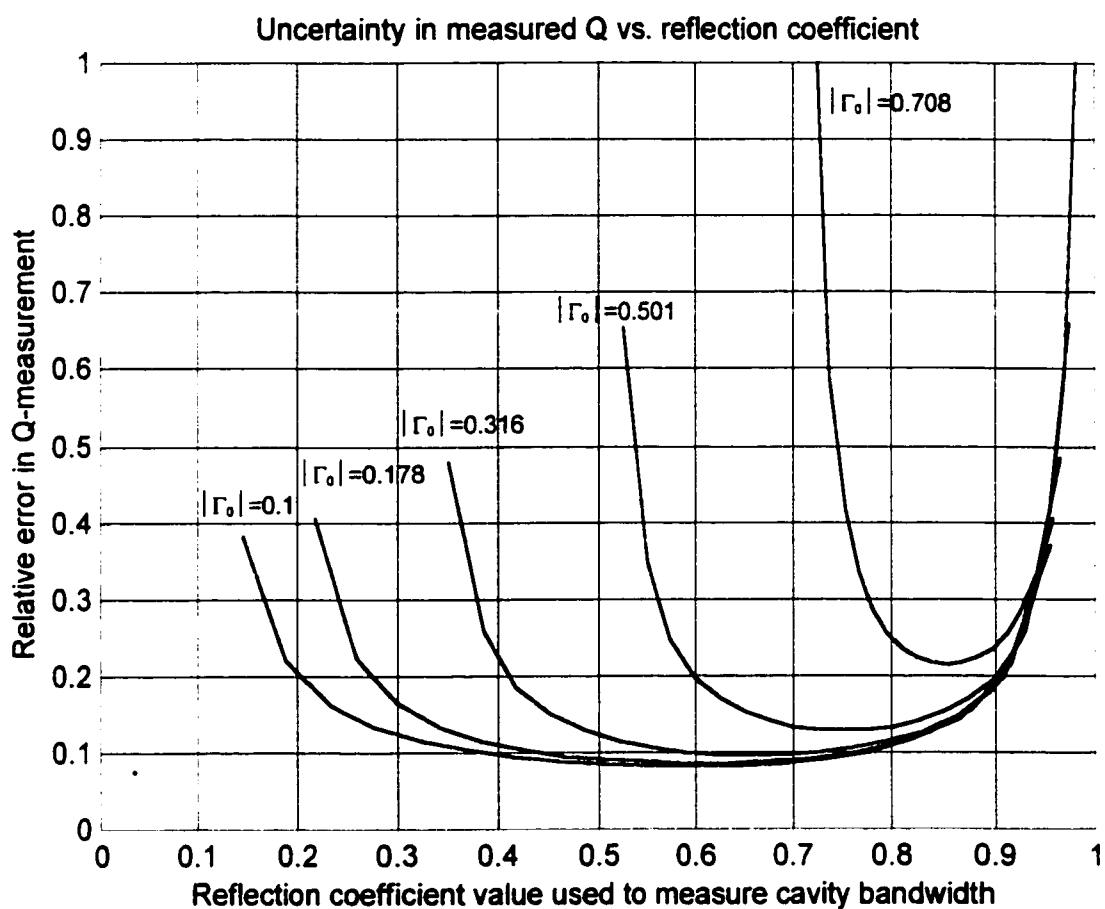


Figure A2.1 Relative uncertainty in measured Q-factor versus the bandwidth reflection coefficient, $|\Gamma_{pp}|$, for various resonant frequency reflection coefficient values, $|\Gamma_0|$, for a reflectometer directivity of $D = 30$ dB [8].

A2.2 Uncertainties in the Loss Tangent Measurement

Uncertainty in measured loss tangent is calculated using Eq.(5.8). Calculating partial derivatives of Eq.(5.8) with respect to the relative dielectric constant, ϵ_r' , and Q-factor shift, $\Delta\left(\frac{1}{Q_0}\right)$, [8],[28] results in

$$\frac{\partial \tan \delta}{\partial \epsilon_r'} = \frac{1}{F_1} \frac{\partial \left(\Delta \left(\frac{1}{Q_0} \right) \right)}{\partial \epsilon_r'} + \frac{\partial \left(\frac{1}{F_1} \right)}{\partial \epsilon_r'} \Delta \left(\frac{1}{Q_0} \right) \quad (\text{A2.13})$$

$$\frac{\partial \tan \delta}{\partial \left(\Delta \left(\frac{1}{Q_0} \right) \right)} = \frac{1}{F_1} \quad (\text{A2.14}).$$

The total uncertainty in loss tangent, $\tan \delta$, is given by the sum of Eqs.(A2.13) and (A2.14), i.e.,

$$\Delta \tan \delta = \frac{1}{F_1} \Delta \left(\Delta \left(\frac{1}{Q_0} \right) \right) + \frac{1}{F_1} \frac{\partial \left(\Delta \left(\frac{1}{Q_0} \right) \right)}{\partial \epsilon_r'} \Delta \epsilon_r' + \frac{\partial \left(\frac{1}{F_1} \right)}{\partial \epsilon_r'} \Delta \left(\frac{1}{Q_0} \right) \Delta \epsilon_r' \quad (\text{A2.15}).$$

Normalizing Eq. (A2.15) to $\tan \delta$ yields

$$\frac{\Delta \tan \delta}{\tan \delta} = \frac{\Delta \left(\Delta \left(\frac{1}{Q_0} \right) \right)}{\Delta \left(\frac{1}{Q_0} \right)} + \frac{1}{\Delta \left(\frac{1}{Q_0} \right)} \frac{\partial \left(\Delta \left(\frac{1}{Q_0} \right) \right)}{\partial \epsilon_r'} \Delta \epsilon_r' + \frac{\partial \left(\frac{1}{F_1} \right)}{\partial \epsilon_r'} \frac{1}{\left(\frac{1}{F_1} \right)} \Delta \epsilon_r' \quad (\text{A2.16}).$$

This equation indicates that the relative uncertainty in measured $\tan \delta$ is composed of three parts, the part caused by the uncertainty in the Q-measurement

$$\left[\frac{\Delta \tan \delta}{\tan \delta} \right]_Q = \frac{\Delta \left(\Delta \left(\frac{1}{Q_0} \right) \right)}{\Delta \left(\frac{1}{Q_0} \right)} = \frac{\Delta Q_0 Q_L^2 - \Delta Q_L Q_0^2}{Q_L Q_0 (Q_0 - Q_L)} \quad (\text{A2.17})$$

and two parts caused by uncertainty in measured relative dielectric constant

$$\left[\frac{\Delta \tan \delta}{\tan \delta} \right]_{\varepsilon_r'} = \frac{1}{\Delta \left(\frac{1}{Q_0} \right)} \frac{\partial \left(\Delta \left(\frac{1}{Q_0} \right) \right)}{\partial \varepsilon_r'} \Delta \varepsilon_r' + \frac{\partial \left(\frac{1}{F_1} \right)}{\partial \varepsilon_r'} \frac{1}{\left(\frac{1}{F_1} \right)} \Delta \varepsilon_r' \quad (\text{A2.18}).$$

In analyzing Eq.(A2.17), if the approximation is made that $\bar{Q} \approx \frac{(Q_L + Q_0)}{2}$

and that $\Delta Q_L \approx \Delta Q_0 \approx \Delta \bar{Q}$, Eq.(A2.17) becomes

$$\left[\frac{\Delta \tan \delta}{\tan \delta} \right]_Q = - \frac{2 \Delta \bar{Q} \bar{Q}}{Q_L Q_0} \quad (\text{A2.19})$$

and hence

$$\left[\frac{\Delta \tan \delta}{\tan \delta} \right]_Q = -2 \frac{\Delta \bar{Q}}{\bar{Q}} \quad (\text{A2.20})$$

provided that $\frac{Q_0}{2} < Q_L$. $\frac{\Delta \bar{Q}}{\bar{Q}}$ can be treated as an average relative uncertainty in

Q measurements.

Evaluating the partial derivative in the first term on the right hand side of Eq.(A2.18) yields

$$\frac{\partial}{\partial \varepsilon_r'} \left(\Delta \left(\frac{1}{Q_0} \right) \right) = \frac{\partial}{\partial \varepsilon_r'} \left(\left(\frac{1}{Q_L} \right)_{\text{meas}} - \left(\frac{1}{Q_C(\varepsilon_r')} \right) \right) = \frac{1}{(Q_C(\varepsilon_r'))^2} \frac{\partial Q_C(\varepsilon_r')}{\partial \varepsilon_r'} \quad (\text{A2.21})$$

where $\frac{\partial}{\partial \epsilon_r'} \left(\left(\frac{1}{Q_L} \right)_{\text{meas}} \right) = 0$, and $Q_C(\epsilon_r')$ is the cavity Q-factor dependent upon

test specimen dielectric constant. Substituting for $Q_C(\epsilon_r')$ from Eq.(5.7) in the derivative term of the right-hand side of Eq.(A2.21) yields

$$\frac{\partial Q_C(\epsilon_r')}{\partial \epsilon_r'} = \left(c_1 + 2c_2(\epsilon_r') + 3c_3(\epsilon_r')^2 + 4c_4(\epsilon_r')^3 + \dots \right) \quad (\text{A2.22})$$

where c_i are polynomial coefficients of Eq.(5.7) as listed in Chapter 5.

Re-writing the partial derivative of the second term on the right hand side of Eq.(A2.18), utilizing Eq.(5.6) yields

$$\frac{\partial}{\partial \epsilon_r'} \left(\frac{1}{F_1} \right) = \left(b_1 + 2b_2(\epsilon_r') + 3b_3(\epsilon_r')^2 + 4b_4(\epsilon_r')^3 + \dots \right) \quad (\text{A2.23})$$

where b_i are polynomial coefficients of Eq.(5.6) as listed in Chapter 5.

At this point, the two terms on the right hand side of Eq.(A2.18) can be re-written in terms of Eqs.(A2.22) and (A2.23), as

$$\frac{1}{\Delta \left(\frac{1}{Q_0} \right)} \frac{\partial \left(\Delta \left(\frac{1}{Q_0} \right) \right)}{\partial \epsilon_r'} \Delta \epsilon_r' = \frac{\Delta \epsilon_r'}{\Delta \left(\frac{1}{Q_0} \right)} \frac{\left(c_1 + 2c_2(\epsilon_r') + 3c_3(\epsilon_r')^2 + \dots \right)}{\left(Q_C(\epsilon_r') \right)^2} \quad (\text{A2.24})$$

and

$$\frac{\partial \left(\frac{1}{F_1} \right)}{\partial \epsilon_r'} \frac{1}{\left(\frac{1}{F_1} \right)} \Delta \epsilon_r' = \frac{\Delta \epsilon_r'}{\Delta \left(\frac{1}{F_1} \right)} \left(b_1 + 2b_2(\epsilon_r') + 3b_3(\epsilon_r')^2 + \dots \right) \quad (\text{A2.25}).$$

In order to estimate the worst case uncertainty in Eq.(A2.24) the minimum value of Q-factor shift, $\Delta\left(\frac{1}{Q_0}\right)_{\min}$, must be used. In Chapter 6, minimum Q-factor

shift values were determined and an analytical expression is given by

$$\Delta\left(\frac{1}{Q_0}\right)_{\min} = \frac{\Delta Q}{Q} \frac{1}{Q_c(\varepsilon_r')} \quad (\text{A2.26})$$

where $\frac{\Delta Q}{Q}$ is the relative uncertainty in measured Q-factor as determined in the

last section. Typical values are $\left(\frac{\Delta Q}{Q}\right)_{\min} = 0.09$ when $D=30\text{dB}$, $|\Gamma_{pp}| = 0.707$ and

$|\Gamma_0| < 0.25$ and $\left(\frac{\Delta Q}{Q}\right)_{\min} = 0.025$ when $D=40\text{dB}$, $|\Gamma_{pp}| = 0.707$ and $|\Gamma_0| < 0.25$.

Re-writing Eq.(A2.25) in a more usable form, first replace the filling factor, F_l , with the expression given in Eq.(5.6), i.e.

$$\left(\frac{1}{F_l}\right) = b_0 + b_1(\varepsilon_r') + b_2(\varepsilon_r')^2 + b_3(\varepsilon_r')^3 + \dots \quad (\text{A2.27}).$$

Now Eq.(A2.25) can be re-written as

$$\frac{\partial\left(\frac{1}{F_l}\right)}{\partial\varepsilon_r'} \frac{1}{\left(\frac{1}{F_l}\right)} \Delta\varepsilon_r' = \Delta\varepsilon_r' \left(\frac{b_1 + 2b_2(\varepsilon_r') + 3b_3(\varepsilon_r')^2 + 4b_4(\varepsilon_r')^3 + \dots}{b_0 + b_1(\varepsilon_r') + b_2(\varepsilon_r')^2 + b_3(\varepsilon_r')^3 + \dots} \right) \quad (\text{A2.28}).$$

In the literature, the polynomial ratio on the right hand side, of Eq(A3.16) is commonly referred to as the error transfer function, ζ , i.e.

$$\zeta = \left(\frac{b_1 + 2b_2(\epsilon_r') + 3b_3(\epsilon_r')^2 + 4b_4(\epsilon_r')^3 + \dots}{b_0 + b_1(\epsilon_r') + b_2(\epsilon_r')^2 + b_3(\epsilon_r')^3 + \dots} \right) \quad (\text{A2.29}).$$

In Figures A2.2 and A2.3, the error transfer function, ζ , is plotted as a function of relative dielectric constant for both modes of cavity operation.

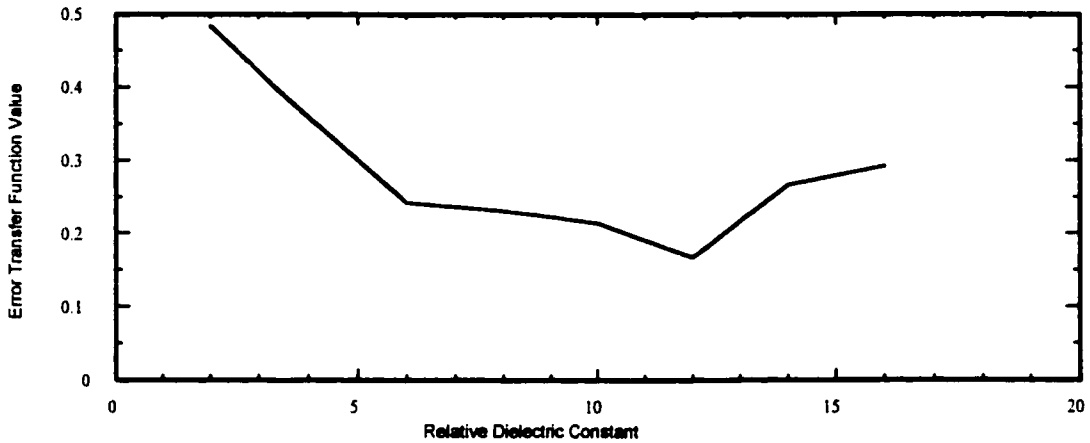


Figure A2.2 Error transfer function, i.e. the relative error in the loss tangent measurement resulting for an error of $\Delta\epsilon_r' = 1.0$ in the measured dielectric constant for the contact mode.

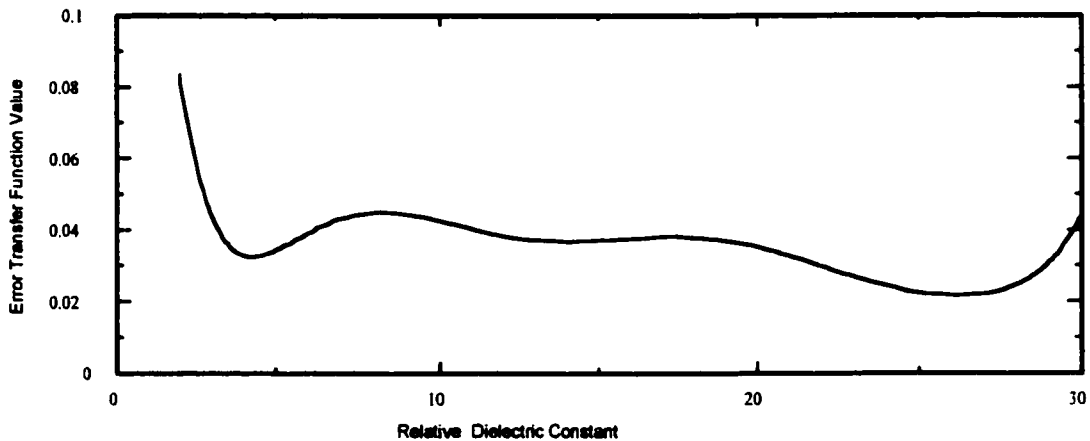


Figure A2.3 Error transfer function, i.e. the relative error in the loss tangent measurement resulting for an error of $\Delta\epsilon_r' = 1.0$ in the measured dielectric constant for the partial contact mode.

At this point the uncertainties given in Eqs.(A2.20), (A2.24) and (A2.25) can be summed to find the total relative uncertainty in loss tangent, i.e.,

$$\left| \frac{\Delta \tan \delta}{\tan \delta} \right| = 2 \left| \frac{\Delta \bar{Q}}{\bar{Q}} \right| + \left| \frac{\Delta \varepsilon_r'}{\Delta \left(\frac{1}{Q_0} \right)} \frac{(c_1 + 2c_2(\varepsilon_r') + 3c_3(\varepsilon_r')^2 + \dots)}{(Q_c(\varepsilon_r'))^2} \right| + |\Delta \varepsilon_r' \zeta| \quad (\text{A2.30}).$$

APPENDIX 3

MEASUREMENT UNCERTAINTY ATTRIBUTABLE TO THE TEST SPECIMEN AND CAVITY HEATING

In Chapter 8, an uncertainty analysis of the reflectometer was performed. However to analyze the measurement accuracy of the entire test setup, the uncertainty in the dielectric measurement attributable to test specimen dimensional uncertainty and cavity heating must also be analyzed.

A3.1 Variation in Test Specimen Dimensions

In any dielectric measurement system, dimensional variations of the test specimen cause uncertainty in the test specimen's measured complex dielectric constant. Because the plate separation of the parallel plate waveguide is essentially constant, the uncertainty in measured thickness of the test specimen must be considered in analyzing the measurement accuracy of this dielectrometer. For this measurement technique, uncertainty in measured thickness contributes significantly to ϵ_r' uncertainty while measured diameter uncertainty is comparatively negligible. Consider for example, the case when uncertainty in the test specimen thickness is $\Delta t = -0.01$ mm. Suppose the test specimen has a complex dielectric constant, ϵ^* , and a radius of $r = 5.0$ mm. Now to determine the thickness dependent uncertainty in the dielectric constant measurement, a specimen with a reduced thickness of $t = 1.99$ mm, $r = 5.0$ mm

and complex dielectric constant, ϵ^* , is modeled using the HERZ program. Obviously the resonant frequency shift caused by this smaller specimen will be less than of the larger ($t = 2.0$ mm) specimen. In order to appreciate the full effects of dimensional uncertainty in the dielectric constant measurement, Figures A3.1 and A3.2 display the relative difference between the dielectric constant predicted assuming a test specimen with $t = 2.00$ mm and $r = 5.0$ mm and the dielectric constant predicted assuming a test specimen with $t = 1.99$ mm and $r = 5.0$ mm. Figures A3.1 and A3.2 display uncertainty in measured dielectric constant for both the contact and partial contact modes respectively.

In comparing data from Figures A3.1 and A3.2 to that given in Tables 8.1 and 8.2, variations in test specimen dimensions have a far more significant effect on dielectric constant measurement accuracy than uncertainty caused by the reflectometer. When measuring relative dielectric constants that are $\epsilon_r' < 10.0$, the uncertainty of both measurement modes is comparable. However, for $\epsilon_r' > 10.0$, superior relative dielectric constant measurement accuracy is attained using the partial contact mode.

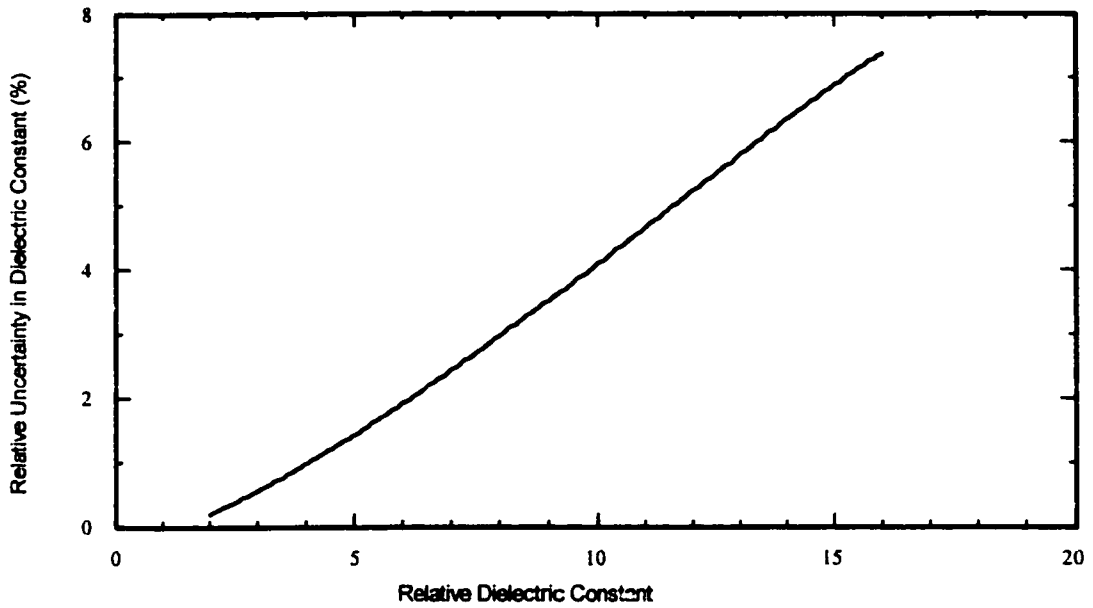


Figure A3.1 Relative uncertainty in measured dielectric constant for a test specimen with a thickness uncertainty of 0.5% and of radius $r = 5.0$ mm (contact mode).

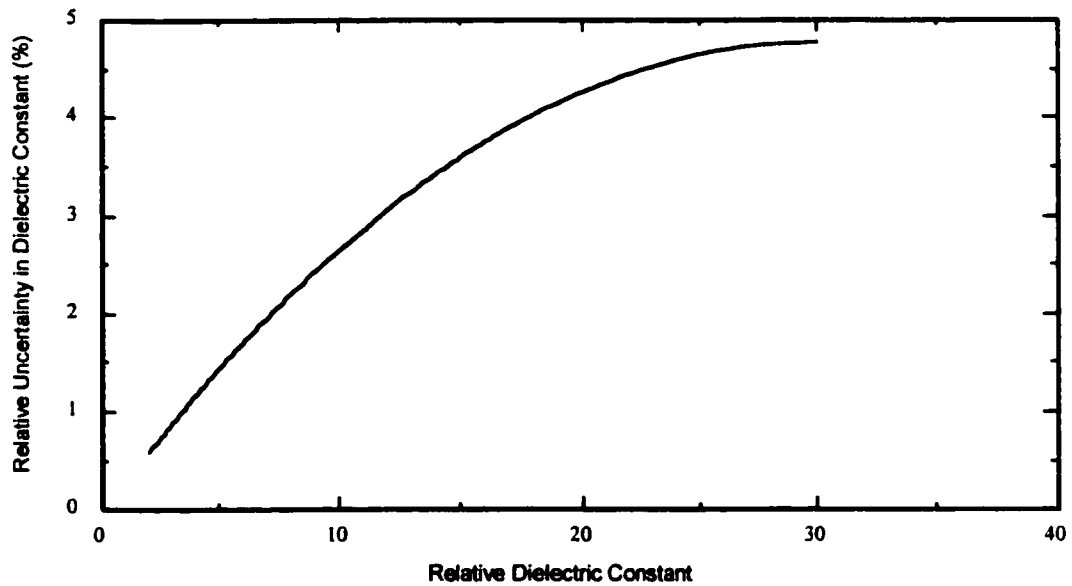


Figure A3.2 Relative uncertainty in measured dielectric constant for a test specimen with a thickness uncertainty of 0.5% and of radius $r = 5.0$ mm (partial contact mode).

A3.2 Measurement Uncertainty Attributable to Cavity Heating

Cavity heating introduces another variable in the dielectric measurement, namely temperature, T . Since unloaded cavity resonant frequency and Q-factor are temperature dependent, temperature measurement uncertainty is introduced to the dielectric determination. At the maximum temperature of 120°C , mechanical changes in the test cavity caused by heating linearly decrease the cavity's resonant frequency by 4 MHz and its unloaded Q-factor by approximately 200 as compared to room temperature values. From the fit of the empirical data (see Chapter 7, Section 6) it was found that the slope of measured resonant frequency versus temperature was $\pm 0.04 \text{ MHz}/^{\circ}\text{C}$ and the slope of measured Q-factor versus temperature was $\pm 2.0 (^{\circ}\text{C})^{-1}$. Below, uncertainty in measured dielectric properties are analyzed as a function of temperature, T .

An estimate in temperature dependent dielectric constant uncertainty is found by taking the partial derivative of the relative dielectric constant function, $\epsilon_r'(\Delta f_0)$, with respect to temperature, T , i.e.

$$|\Delta \epsilon_r'| = \frac{\partial}{\partial T} (\epsilon_r'(\Delta f_0)) \Delta T \quad (\text{A3.1})$$

where ΔT is the uncertainty in measured temperature. Eq.(5.5) gives an expression for the relative dielectric constant function. Taking the partial derivative of Eq.(5.5) with respect to temperature, T , yields

$$\frac{\partial}{\partial T} (\epsilon_r'(\Delta f_0)) = \left(a_1 + 2a_2 |\Delta f_0| + 3a_3 |\Delta f_0|^2 + \dots \right) \frac{\partial}{\partial T} (|\Delta f_0|) \quad (\text{A3.2})$$

where $\frac{\partial}{\partial T}(|\Delta f_0|) = 0.04 \text{ MHz/}^\circ\text{C}$ is the slope of measured resonant frequency per degree Celsius and a_i are polynomial coefficients of Eq.(5.5) as listed in Chapter

5. Replacing the right hand side of Eq.(A3.2) into the partial term, $\frac{\partial}{\partial T}(\epsilon_r'(\Delta f_0))$, of Eq.(A3.1) yields the following

$$|\Delta \epsilon_r'| = \left(a_1 + 2a_2|\Delta f_0| + 3a_3|\Delta f_0|^2 + \dots \right) \frac{\partial}{\partial T}(|\Delta f_0|) \Delta T \quad (\text{A3.3}).$$

In Tables A3.1 and A3.2 tabulated values for Eq.(A3.3) are listed for both modes of cavity operation, temperature uncertainty, ΔT , is set to $\Delta T = 1 \text{ }^\circ\text{C}$ for this analysis.

Table A3.1 Uncertainty in relative dielectric constant as a function of temperature (per $^\circ\text{C}$), contact mode.

ϵ_r'	2.00	4.00	8.00	12.00	14.00	16.00
$ \Delta \epsilon_r' $	0.030	0.025	0.017	0.011	0.0085	0.0066
$\frac{ \Delta \epsilon_r' }{\epsilon_r'} \%$	1.4	0.61	0.21	0.091	0.061	0.022

Table A3.2 Uncertainty in relative dielectric constant as a function of temperature (per $^\circ\text{C}$), partial contact mode.

ϵ_r'	2.00	4.00	8.00	10.00	15.00	20.00	30.00
$ \Delta \epsilon_r' $	0.081	0.12	0.27	0.38	0.75	1.2	1.9
$\frac{ \Delta \epsilon_r' }{\epsilon_r'} \%$	4.1	3.0	3.4	3.8	5.0	5.8	6.3

To estimate temperature dependent loss tangent measurement uncertainty, the partial derivative of the loss tangent function, $\tan\delta\left(\frac{1}{F_1}, \Delta\left(\frac{1}{Q_0}\right)\right)$, is taken with respect to temperature, T, i.e.

$$\Delta \tan\delta = \frac{\partial}{\partial T} \left(\tan\delta\left(\frac{1}{F_1}, \Delta\left(\frac{1}{Q_0}\right)\right) \right) \Delta T \quad (\text{A3.4}).$$

Eq.(5.8) gives an analytical expression for the loss tangent function. Taking the partial derivative of Eq.(5.8) with respect to temperature, the following expression is obtained

$$\frac{\partial}{\partial T} \left(\tan\delta\left(\frac{1}{F_1}, \Delta\left(\frac{1}{Q_0}\right)\right) \right) = \left(\frac{\partial}{\partial T} \left(\frac{1}{F_1} \right) \right) \Delta\left(\frac{1}{Q_0}\right) + \left(\frac{\partial}{\partial T} \left(\Delta\left(\frac{1}{Q_0}\right) \right) \right) \left(\frac{1}{F_1} \right) \quad (\text{A3.5}).$$

To evaluate the first partial derivative term on the right hand side of Eq.(A3.5), $\frac{\partial}{\partial T} \left(\frac{1}{F_1} \right)$, Eq.(5.6) is utilized, i.e.,

$$\frac{\partial}{\partial T} \left(\frac{1}{F_1} \right) = \left(b_1 + 2b_2(\varepsilon_r') + 3b_3(\varepsilon_r')^2 + \dots \right) \frac{\partial \varepsilon_r'}{\partial T} \quad (\text{A3.6})$$

where $\frac{\partial \varepsilon_r'}{\partial T}$ is the slope in relative dielectric constant per degree Celsius, and b_i are polynomial coefficients of Eq.(5.6) as listed in Chapter 5. Values for $\frac{\partial \varepsilon_r'}{\partial T}$ are found utilizing Eq.(A3.2) and $\frac{\partial}{\partial T} \left(|\Delta f_0| \right) = 0.04 \text{ MHz}/^\circ\text{C}$.

To evaluate the second partial derivative term on the right hand side of

Eq.(A3.5), $\frac{\partial}{\partial T} \left(\Delta \left(\frac{1}{Q_0} \right) \right)$, utilize the partial derivative of Eq.(5.7) with respect to

temperature, T , as follows

$$\frac{\partial}{\partial T} \left(\Delta \left(\frac{1}{Q_0} \right) \right) = \frac{\partial}{\partial T} \left(\frac{1}{Q_m} - \frac{1}{Q_c(\varepsilon_r')} \right) = \frac{1}{(Q_c(\varepsilon_r'))^2} \frac{\partial Q_c(\varepsilon_r')}{\partial T} \quad (\text{A3.7})$$

where $\frac{\partial Q_c(\varepsilon_r')}{\partial T}$ is the slope in unloaded cavity Q-factor, as a function of relative

dielectric constant, ε_r' , per degree Celsius. Re-writing the partial derivative of the

last term of Eq.(A3.7) utilizing Eq.(5.7) yields

$$\frac{\partial Q_c(\varepsilon_r')}{\partial T} = \left(\frac{\partial}{\partial T} (c_0(T)) \right) + (c_1 + 2c_2(\varepsilon_r') + 3c_3(\varepsilon_r')^2 + \dots) \frac{\partial \varepsilon_r'}{\partial T} \quad (\text{A3.8})$$

where $\frac{\partial}{\partial T} (c_0(T)) = 2.0 \text{ (}^\circ\text{C)}^{-1}$ is the slope of the empty cavity Q-factor per degree

Celsius and c_i are polynomial coefficients of Eq.(5.8) as listed in Chapter 5.

Replacing the expressions found in Eqs.(A3.6) and (A3.8) into Eq.(A3.4)

yields

$$\Delta \tan \delta = \left((b_1 + 2b_2(\varepsilon_r') + 3b_3(\varepsilon_r')^2 + \dots) \frac{\partial \varepsilon_r'}{\partial T} \left(\Delta \frac{1}{Q_0} \right) \right) \Delta T +$$

$$+ \left(\left(\frac{(c_1 + 2c_2(\varepsilon_r') + 3c_3(\varepsilon_r')^2 + \dots) + \frac{\partial c_0(T)}{\partial T}}{(Q_c(\varepsilon_r'))^2} \right) \left(\frac{1}{F_1} \right) \frac{\partial \varepsilon_r'}{\partial T} \right) \Delta T \quad (\text{A3.9})$$

normalizing Eq.(A3.9) with respect to loss tangent, $\tan \delta$, yields

$$\begin{aligned} \left| \frac{\Delta \tan \delta}{\tan \delta} \right| = & \left(\frac{1}{\left(\frac{1}{F_1} \right)} \left(b_1 + 2b_2(\epsilon_r') + 3b_3(\epsilon_r')^2 + \dots \right) \frac{\partial \epsilon_r'}{\partial T} \right) \Delta T + \\ & + \left(\frac{1}{\Delta \left(\frac{1}{Q_0} \right)} \left(\frac{c_1 + 2c_2(\epsilon_r') + 3c_3(\epsilon_r')^2 + \dots + \frac{\partial c_0(T)}{\partial T}}{(Q_c(\epsilon_r'))^2} \right) \frac{\partial \epsilon_r'}{\partial T} \right) \Delta T \end{aligned} \quad (\text{A3.10}).$$

In Tables A3.3 and A3.4, temperature dependent uncertainty in the loss tangent measurement is listed as a function of directivity for both modes of cavity operation. For this analysis, temperature uncertainty is set to $\Delta T = 1.0 \text{ }^\circ\text{C}$.

Table A3.3 Temperature dependent loss tangent measurement uncertainty (per $^\circ\text{C}$) listed as a function of directivity and relative dielectric constant, contact mode.

ϵ_r'		2.00	4.00	8.00	12.00	14.00	16.00
$\left \frac{\Delta \tan \delta}{\tan \delta} \right _{D=30\text{dB}}$	%	2.0	1.5	1.2	1.2	0.8	0.9
$\left \frac{\Delta \tan \delta}{\tan \delta} \right _{D=40\text{dB}}$	%	3.6	2.9	2.4	2.4	2.2	2.6

Table A3.4 Temperature dependent loss tangent measurement uncertainty (per $^\circ\text{C}$) listed as a function of directivity and relative dielectric constant, partial contact mode.

ϵ_r'		2.00	4.00	8.00	10.00	15.00	20.00	30.00
$\left \frac{\Delta \tan \delta}{\tan \delta} \right _{D=30\text{dB}}$	%	0.8	0.2	0.8	1.8	3.1	4.3	13.7
$\left \frac{\Delta \tan \delta}{\tan \delta} \right _{D=40\text{dB}}$	%	1.2	0.6	1.4	2.2	3.8	4.5	26.9

From the data presented in Tables A3.4 and A3.5, it is apparent that quite accurate loss tangent measurements can be made over temperature. The exception being dielectric materials tested in the partial contact mode that have a relative dielectric constant approaching $\epsilon_r' \Rightarrow 30.0$.